Component-based coupling of first-principles and data-driven models

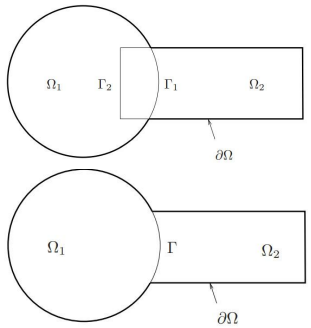

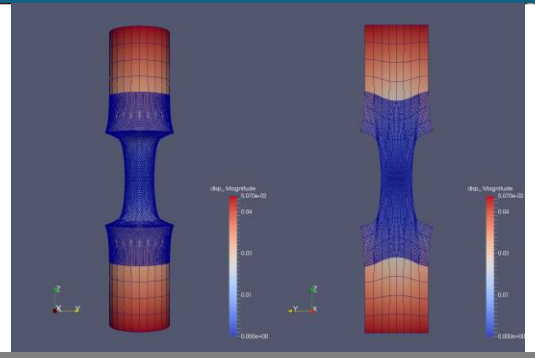

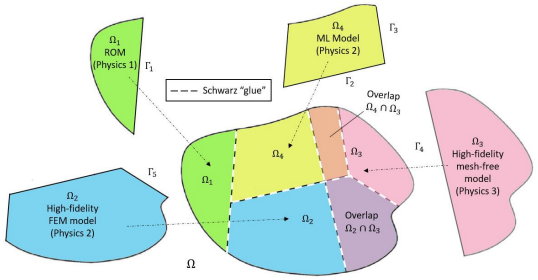

Irina Tezaur[1], Joshua Barnett[1,2], Alejandro Mota[1], Amy De Castro[1,3], Paul Kuberry[1], Pavel Bochev[1]

[1]Sandia National Laboratories, [2]Stanford University, [3]Clemson University

ARIA Workshop on Reduced Order Models
University of Bordeaux, March 8-10, 2023

SAND2023-12631C

Motivation

The past decades have seen tremendous investment in **simulation frameworks** for **coupled multi-scale** and **multi-physics** problems.

- Frameworks rely on **established mathematical theories** to couple physics components.
- Most existing coupling frameworks are based on **traditional discretization methods**.

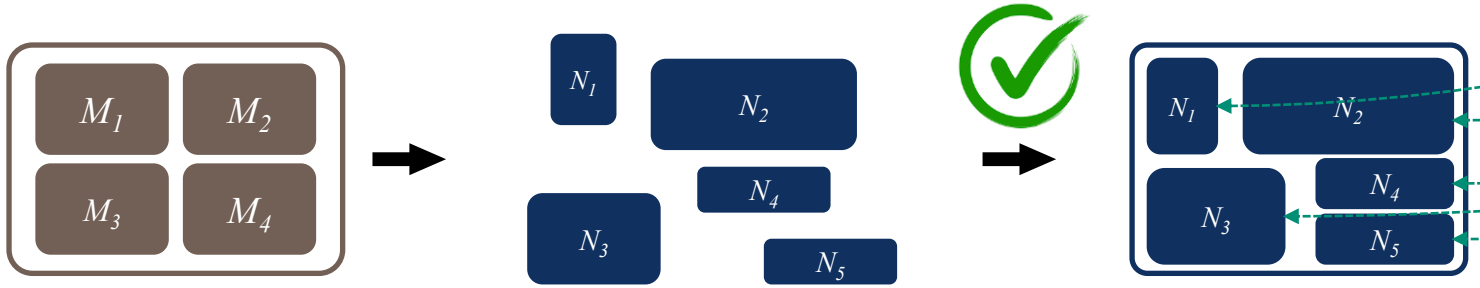

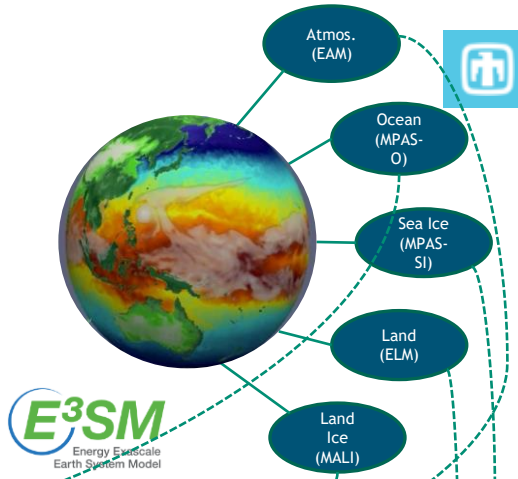

Complex System Model

- PDEs, ODEs
- Nonlocal integral
- Classical DFT
- Atomistic, …

Traditional Methods

- Mesh-based (FE, FV, FD)
- Meshless (SPH, MLS)
- Implicit, explicit
- Eulerian, Lagrangian…

Coupled Numerical Model

- Monolithic (Lagrange multipliers)
- Partitioned (loose) coupling
- Iterative (Schwarz, optimization)

Motivation

The past decades have seen tremendous investment in **simulation frameworks** for **coupled multi-scale** and **multi-physics** problems.

- Frameworks rely on **established mathematical theories** to couple physics components.
- Most existing coupling frameworks are based on **traditional discretization methods**.

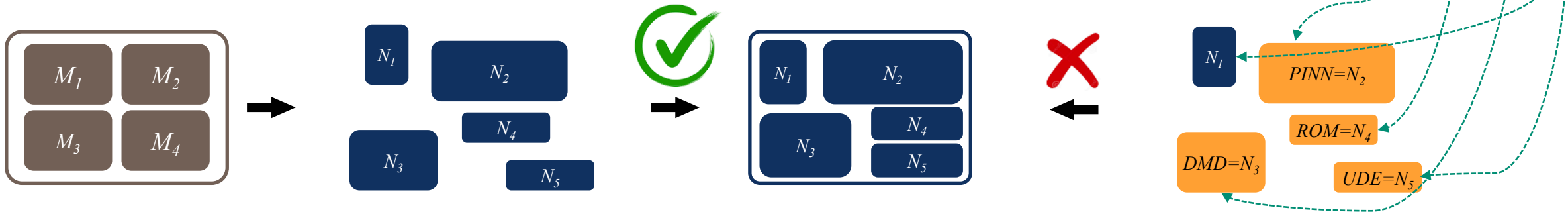

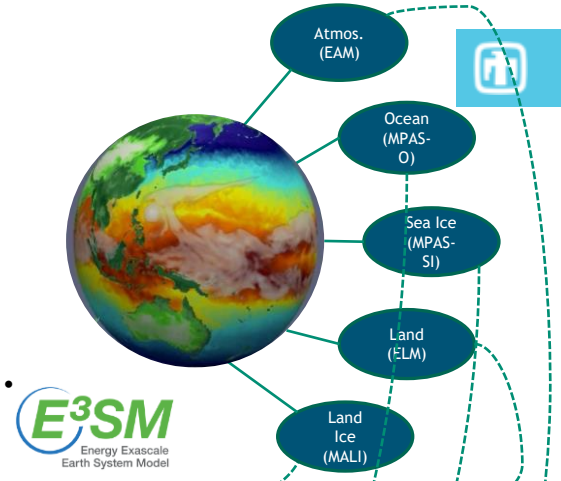

Complex System Model

- PDEs, ODEs
- Nonlocal integral
- Classical DFT
- Atomistic, …

Traditional Methods

- Mesh-based (FE, FV, FD)
- Meshless (SPH, MLS)
- Implicit, explicit
- Eulerian, Lagrangian, …

Coupled Numerical Model

- Monolithic (Lagrange multipliers)
- Partitioned (loose) coupling
- Iterative (Schwarz, optimization)

Traditional + Data-Driven Methods

- PINNs
- Neural ODEs
- Projection-based ROMs, …

- There is currently a big push to integrate **data-driven methods** into modeling & simulation toolchains.

Unfortunately, existing algorithmic and software infrastructures are **ill-equipped** to handle plug-and-play integration of **non-traditional, data-driven models**!

Current Projects on Coupling for Predictive Heterogeneous Models

fHNM: flexible Heterogeneous Numerical Methods

- **Sandia Laboratory Directed Research & Development (LDRD)** project (FY22-FY24)
  - Co-PIs: Pavel Bochev & Irina Tezaur; Team: 5 staff, 2 post docs, 3 students, 2 consultants
  - Academic Alliance: Prof. Arif Masud (UIUC)
- *Primary research objective:* discover the **mathematical principles** guiding the **assembly** of **standard** and **data-driven numerical models** in stable, accurate and physically consistent ways

M2dt: Multi-faceted Mathematics for Predictive Digital Twins

$$\int \mathcal{M}^2 \mathrm{d}t$$

- Funded by DOE's **Advanced Scientific Computing Research (ASCR) Mathematical Multifaceted Integrated Capability Centers (MMICC)** Program (FY23-FY27)
- **Partnership** between UT Austin (Lead Institution), Sandia National Labs (SNL), Argonne National Lab (ANL), Brookhaven National Lab (BNL) and MIT
  - Directors: Karen Willcox & Omar Ghattas (UT Austin)
  - Sandia co-PIs: Irina Tezaur & Pavel Bochev; Sandia team: 6 staff, 1 post doc
- *Primary research objective:* establish a center for research and education on multifaceted **mathematical foundations** for **predictive digital twins (DTs)** for complex energy systems
  - Central to DTs is: (1) tight **two-way coupling** of data and models, (2) **structure preservation** and (3) **dynamic data assimilation**

Coupling Scenarios, Models and Methods

Coupling scenarios:

Scenario I: multi-component coupling with a given domain/component decomposition (for reuse of single-component codes)

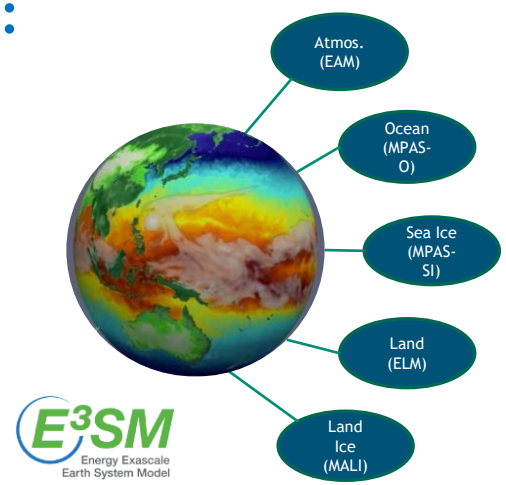

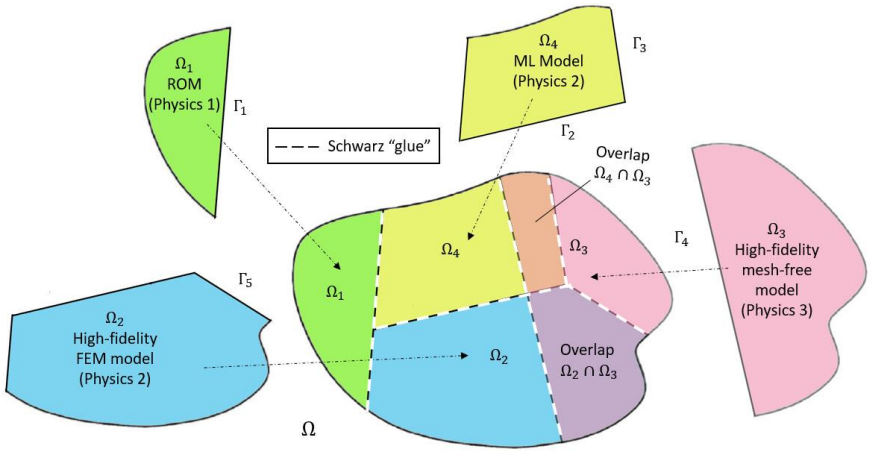

Scenario II: multi-scale coupling where decomposition can be chosen to maximize accuracy, robustness & efficiency of coupled model

Data-driven models: to be "mixed-and-matched" with each other and first-principles models

- *Class A:* projection-based reduced order models (ROMs)
- *Class B:* machine-learned models, i.e., Physics-Informed Neural Networks (PINNs)
- *Class C:* flow map approximation models, i.e., dynamic model decomposition (DMD) models

Coupling methods:

- *Method 1:* Alternating Schwarz-based coupling
- *Method 2:* Optimization-based coupling
- *Method 3:* Coupling via generalized mortar methods (GMMs)

Coupling Scenarios, Models and Methods

Coupling scenarios:

Scenario I: multi-component coupling with a given domain/component decomposition (for reuse of single-component codes)

This talk

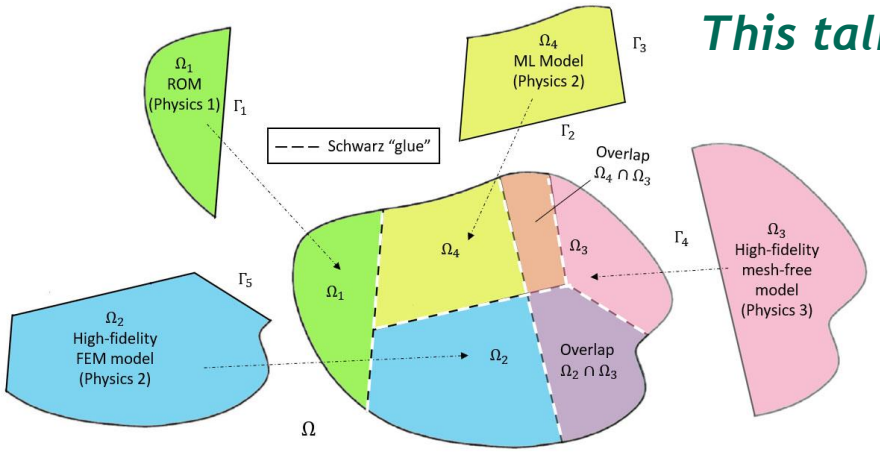

Scenario II: multi-scale coupling where decomposition can be chosen to maximize accuracy, robustness & efficiency of coupled model

Data-driven models: to be "mixed-and-matched" with each other and first-principles models

- *Class A:* projection-based reduced order models (ROMs) — *This talk*
- *Class B:* machine-learned models, i.e., Physics-Informed Neural Networks (PINNs)
- *Class C:* flow map approximation models, i.e., dynamic model decomposition (DMD) models

Coupling methods:

- *Method 1:* Alternating Schwarz-based coupling — *This talk*
- *Method 2:* Optimization-based coupling
- *Method 3:* Coupling via generalized mortar methods (GMMs) — *This talk*

Outline

1. The Alternating Schwarz Method for FOM*-ROM# and ROM-ROM Coupling
   - Method Formulation
   - ROM Construction and Implementation
   - Numerical Example
2. A Lagrange Multiplier-based Partitioned Scheme for FOM-ROM and ROM-ROM Coupling
   - Method Formulation
   - ROM Construction and Implementation
   - Numerical Example
3. Summary and Comparison of Methods
4. Future Work

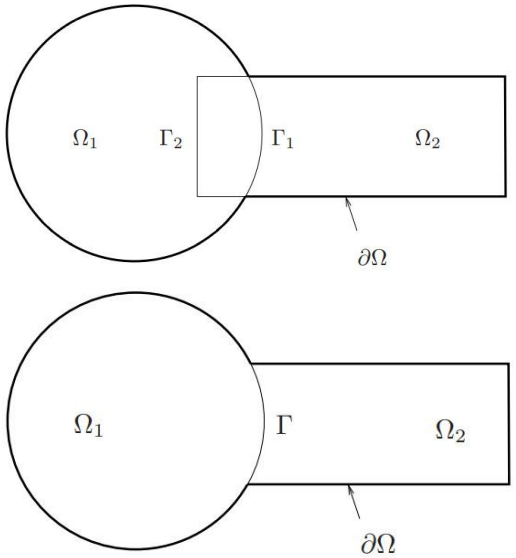

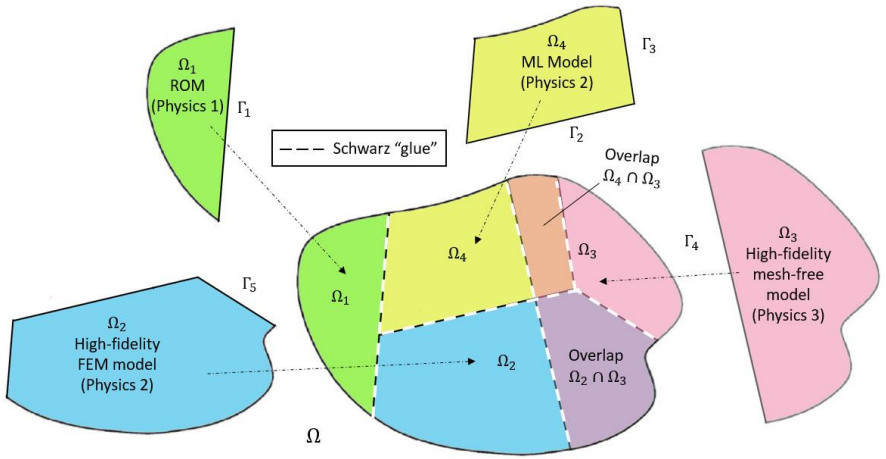

*Full-Order Model. #Reduced Order Model.

Outline

1. **The Alternating Schwarz Method for FOM*-ROM# and ROM-ROM Coupling**
   - **Method Formulation**
   - ROM Construction and Implementation
   - Numerical Example
2. A Lagrange Multiplier-based Partitioned Scheme for FOM-ROM and ROM-ROM Coupling
   - Method Formulation
   - ROM Construction and Implementation
   - Numerical Example
3. Summary and Comparison of Methods
4. Future Work

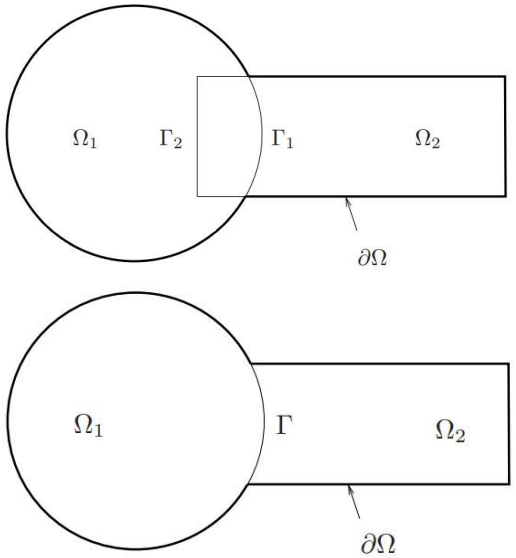

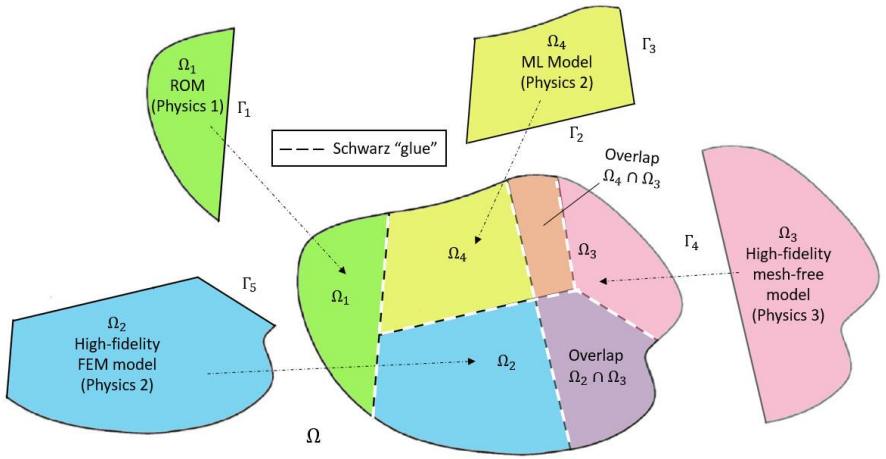

*Full-Order Model. #Reduced Order Model.

Schwarz Alternating Method for Domain Decomposition

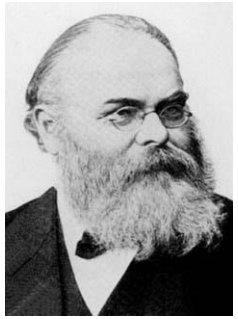

H. Schwarz (1843–1921)

- Proposed in 1870 by H. Schwarz for solving Laplace PDE on irregular domains.

Crux of Method: if the solution is known in regularly shaped domains, use those as pieces to iteratively build a solution for the more complex domain.

Basic Schwarz Algorithm

Initialize:

- Solve PDE by any method on Ω_1 w/ initial guess for transmission BCs on Γ_1.

Iterate until convergence:

- Solve PDE by any method on Ω_2 w/ transmission BCs on Γ_2 based on values just obtained for Ω_1.
- Solve PDE by any method on Ω_1 w/ transmission BCs on Γ_1 based on values just obtained for Ω_2.

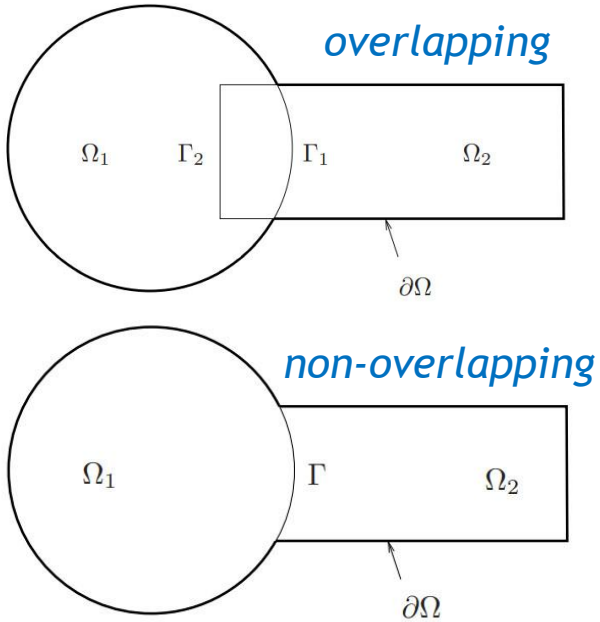

- Schwarz alternating method most commonly used as a ***preconditioner*** for Krylov iterative methods to solve linear algebraic equations.

<u>Idea behind this work</u>: using the Schwarz alternating method as a ***discretization method*** for solving multi-scale or multi-physics partial differential equations (PDEs).

How We Use the Schwarz Alternating Method

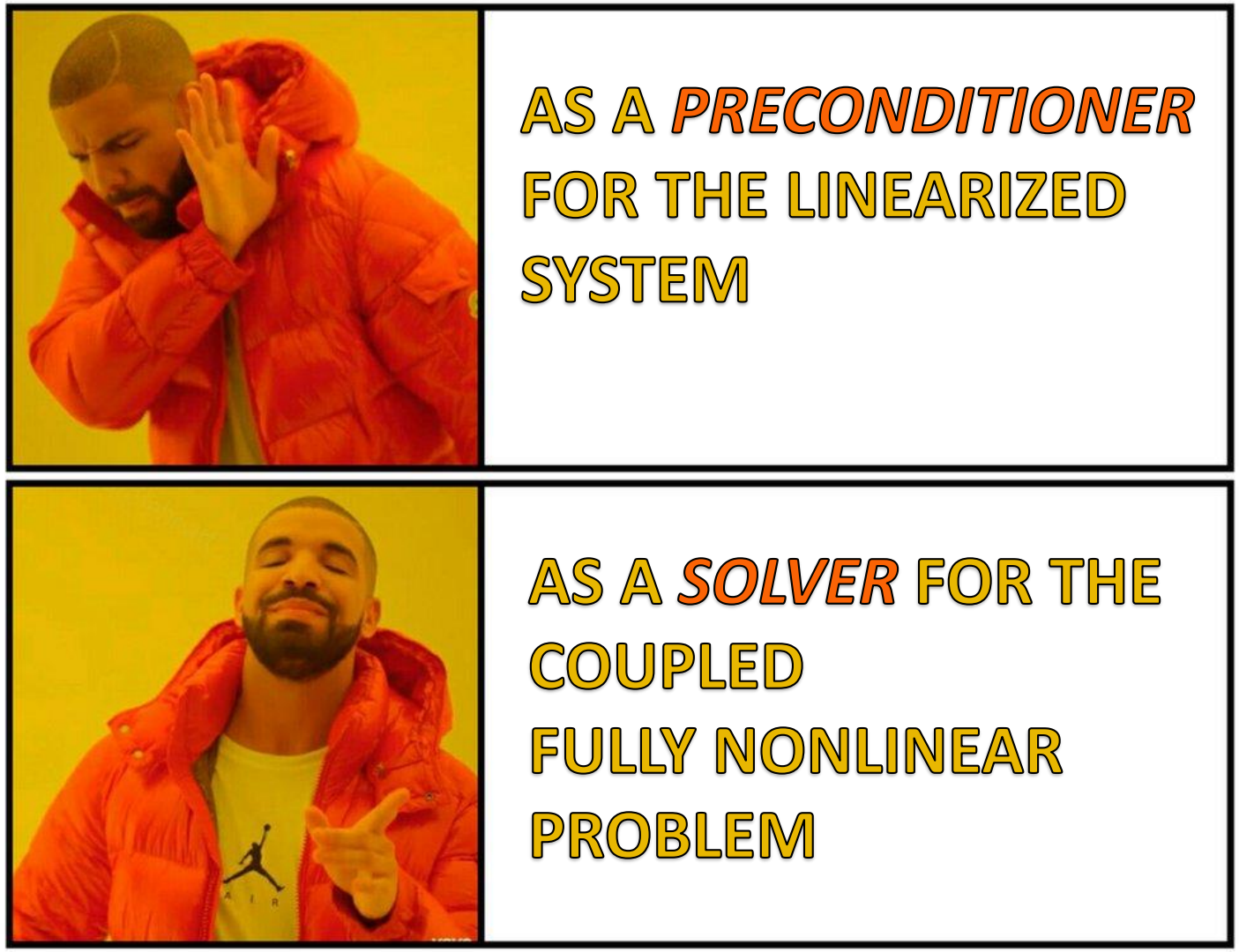

Spatial Coupling via Alternating Schwarz

Model PDE: $\begin{cases} N(\boldsymbol{u}) = \boldsymbol{f}, & \text{in } \Omega \\ \boldsymbol{u} = \boldsymbol{g}, & \text{on } \partial\Omega \end{cases}$

Overlapping Domain Decomposition

$$\begin{cases} N\left(\boldsymbol{u}_1^{(n+1)}\right) = f\ , \text{ in } \Omega_1 \\ \boldsymbol{u}_1^{(n+1)} = \boldsymbol{g}, \text{ on } \partial\Omega_1 \backslash \Gamma_1 \\ \boldsymbol{u}_1^{(n+1)} = \boldsymbol{u}_2^{(n)} \quad \text{on } \Gamma_1 \end{cases}$$

$$\begin{cases} N\left(\boldsymbol{u}_2^{(n+1)}\right) = f\ , \text{ in } \Omega_2 \\ \boldsymbol{u}_2^{(n+1)} = \boldsymbol{g}, \text{ on } \partial\Omega_2 \backslash \Gamma_2 \\ \boldsymbol{u}_2^{(n+1)} = \boldsymbol{u}_1^{(n+1)} \quad \text{on } \Gamma_2 \end{cases}$$

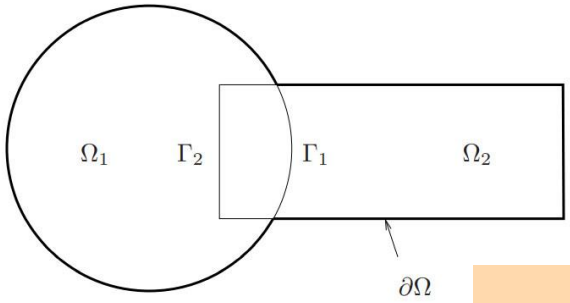

- Dirichlet-Dirichlet transmission BCs [Schwarz 1870; Lions 1988; Mota *et al.* 2017; Mota *et al.* 2022]

This talk: sequential subdomain solves (***multiplicative Schwarz***). Parallel subdomain solves (***additive Schwarz***) also possible.

Non-overlapping Domain Decomposition

$$\begin{cases} N\left(\boldsymbol{u}_1^{(n+1)}\right) = f, & \text{in } \Omega_1 \\ \boldsymbol{u}_1^{(n+1)} = \boldsymbol{g}, & \text{on } \partial\Omega_1 \backslash \Gamma \\ \boldsymbol{u}_1^{(n+1)} = \boldsymbol{\lambda}_{n+1}, & \text{on } \Gamma \end{cases}$$

$$\begin{cases} N\left(\boldsymbol{u}_2^{(n+1)}\right) = f\ , & \text{in } \Omega_2 \\ \boldsymbol{u}_2^{(n+1)} = \boldsymbol{g}, & \text{on } \partial\Omega_2 \backslash \Gamma \\ \boldsymbol{\nabla u}_2^{(n+1)} \cdot \boldsymbol{n} = \boldsymbol{\nabla u}_1^{(n+1)} \cdot \boldsymbol{n}, & \text{on } \Gamma \end{cases}$$

$$\boldsymbol{\lambda}_{n+1} = \theta \boldsymbol{\varphi}_2^{(n)} + (1-\theta)\boldsymbol{\lambda}_n, \text{on } \Gamma, \text{for } n \geq 1$$

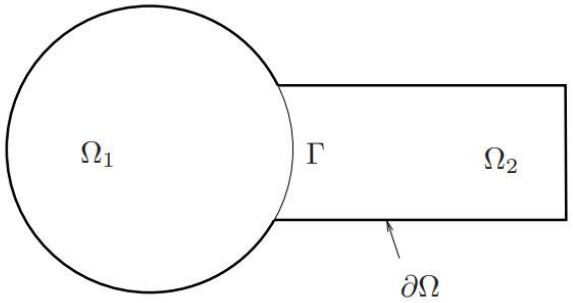

- Relevant for multi-material and multi-physics coupling
- Alternating Dirichlet-Neumann transmission BCs [Zanolli *et al.* 1987]
- Robin-Robin transmission BCs also lead to convergence [Lions 1990]
- $\theta \in [0,1]$: relaxation parameter (can help convergence)

Time-Advancement Within the Schwarz Framework

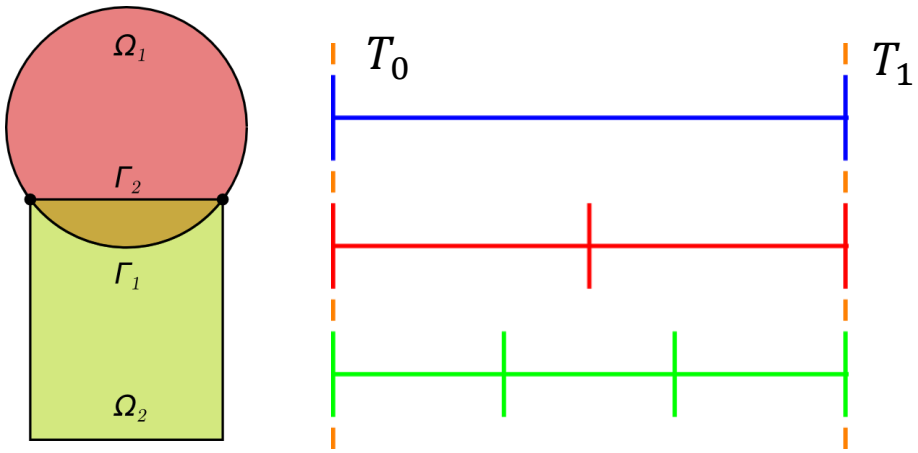

Controller time stepper

Time integrator for Ω_1

Time integrator for Ω_2

Step 0: Initialize $i = 0$ (controller time index).

Model PDE:

$$\begin{cases} \dot{\boldsymbol{u}} + N(\boldsymbol{u}) = \boldsymbol{f}, & \text{in } \Omega \\ \boldsymbol{u}(\boldsymbol{x}, t) = \boldsymbol{g}(t), & \text{on } \partial\Omega \\ \boldsymbol{u}(\boldsymbol{x}, 0) = \boldsymbol{u}_0, & \text{in } \Omega \end{cases}$$

Time-Advancement Within the Schwarz Framework

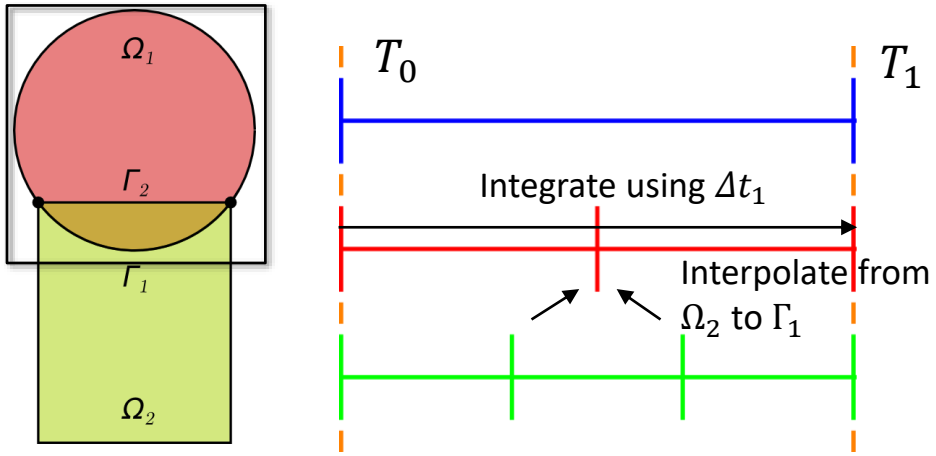

Controller time stepper

Time integrator for Ω_1

Time integrator for Ω_2

Step 0: Initialize $i = 0$ (controller time index).

Step 1: Advance Ω_1 solution from time T_i to time T_{i+1} using time-stepper in Ω_1 with time-step Δt_1, using solution in Ω_2 interpolated to Γ_1 at times $T_i + n\Delta t_1$.

Model PDE:

$$\begin{cases} \dot{\boldsymbol{u}} + N(\boldsymbol{u}) = \boldsymbol{f}, & \text{in } \Omega \\ \boldsymbol{u}(\boldsymbol{x}, t) = \boldsymbol{g}(t), & \text{on } \partial\Omega \\ \boldsymbol{u}(\boldsymbol{x}, 0) = \boldsymbol{u}_0, & \text{in } \Omega \end{cases}$$

Time-Advancement Within the Schwarz Framework

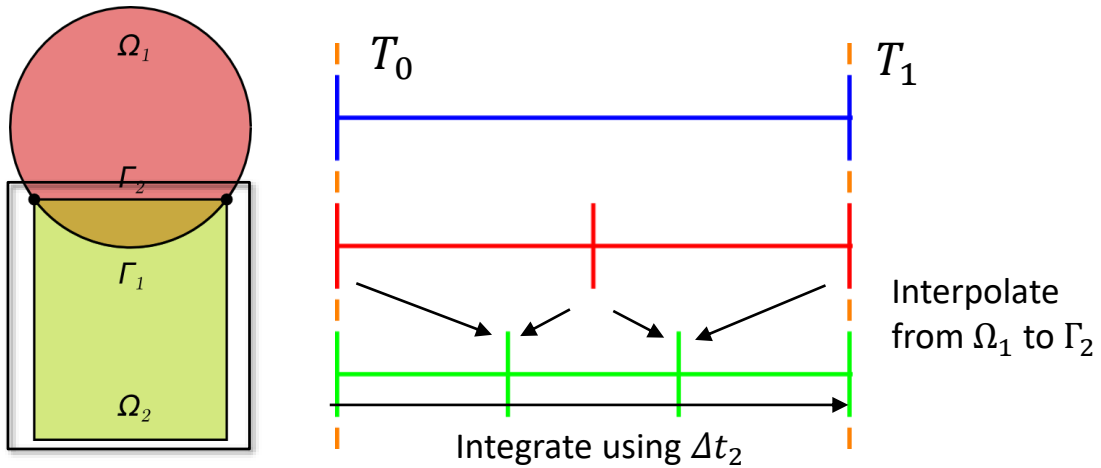

Controller time stepper

Time integrator for Ω_1

Time integrator for Ω_2

Step 0: Initialize $i = 0$ (controller time index).

Step 1: Advance Ω_1 solution from time T_i to time T_{i+1} using time-stepper in Ω_1 with time-step Δt_1, using solution in Ω_2 interpolated to Γ_1 at times $T_i + n\Delta t_1$.

Step 2: Advance Ω_2 solution from time T_i to time T_{i+1} using time-stepper in Ω_2 with time-step Δt_2, using solution in Ω_1 interpolated to Γ_2 at times $T_i + n\Delta t_2$.

Model PDE:

$$\begin{cases} \dot{\boldsymbol{u}} + N(\boldsymbol{u}) = \boldsymbol{f}, & \text{in } \Omega \\ \boldsymbol{u}(\boldsymbol{x}, t) = \boldsymbol{g}(t), & \text{on } \partial\Omega \\ \boldsymbol{u}(\boldsymbol{x}, 0) = \boldsymbol{u}_0, & \text{in } \Omega \end{cases}$$

Time-Advancement Within the Schwarz Framework

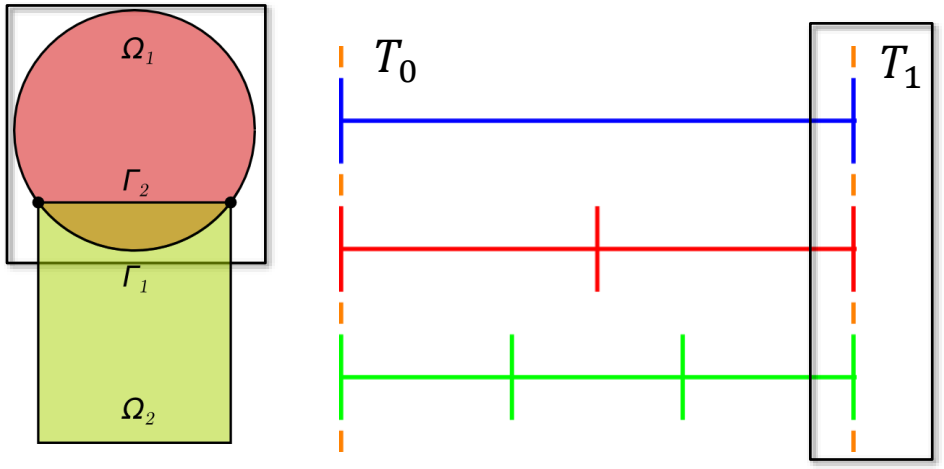

Controller time stepper

Time integrator for Ω_1

Time integrator for Ω_2

Step 0: Initialize $i = 0$ (controller time index).

Step 1: Advance Ω_1 solution from time T_i to time T_{i+1} using time-stepper in Ω_1 with time-step Δt_1, using solution in Ω_2 interpolated to Γ_1 at times $T_i + n\Delta t_1$.

Step 2: Advance Ω_2 solution from time T_i to time T_{i+1} using time-stepper in Ω_2 with time-step Δt_2, using solution in Ω_1 interpolated to Γ_2 at times $T_i + n\Delta t_2$.

Step 3: Check for convergence at time T_{i+1}.

Model PDE:

$$\begin{cases} \dot{\boldsymbol{u}} + N(\boldsymbol{u}) = \boldsymbol{f}, & \text{in } \Omega \\ \boldsymbol{u}(\boldsymbol{x}, t) = \boldsymbol{g}(t), & \text{on } \partial\Omega \\ \boldsymbol{u}(\boldsymbol{x}, 0) = \boldsymbol{u}_0, & \text{in } \Omega \end{cases}$$

Time-Advancement Within the Schwarz Framework

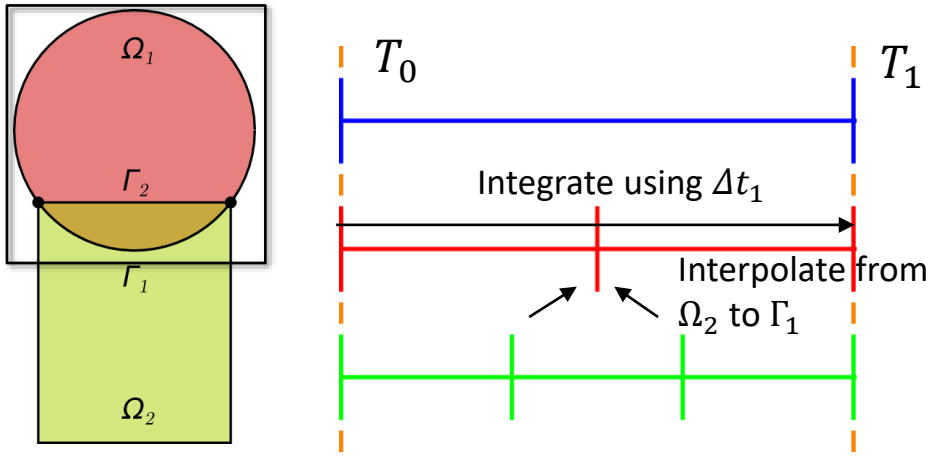

Controller time stepper

Time integrator for Ω_1

Time integrator for Ω_2

Step 0: Initialize $i = 0$ (controller time index).

Step 1: Advance Ω_1 solution from time T_i to time T_{i+1} using time-stepper in Ω_1 with time-step Δt_1, using solution in Ω_2 interpolated to Γ_1 at times $T_i + n\Delta t_1$.

Step 2: Advance Ω_2 solution from time T_i to time T_{i+1} using time-stepper in Ω_2 with time-step Δt_2, using solution in Ω_1 interpolated to Γ_2 at times $T_i + n\Delta t_2$.

Step 3: Check for convergence at time T_{i+1}.

- If unconverged, return to Step 1.

Model PDE:

$$\begin{cases} \dot{\boldsymbol{u}} + N(\boldsymbol{u}) = \boldsymbol{f}, & \text{in } \Omega \\ \boldsymbol{u}(\boldsymbol{x}, t) = \boldsymbol{g}(t), & \text{on } \partial\Omega \\ \boldsymbol{u}(\boldsymbol{x}, 0) = \boldsymbol{u}_0, & \text{in } \Omega \end{cases}$$

Time-Advancement Within the Schwarz Framework

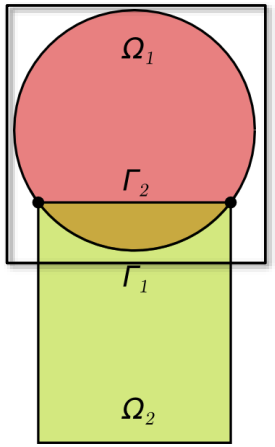

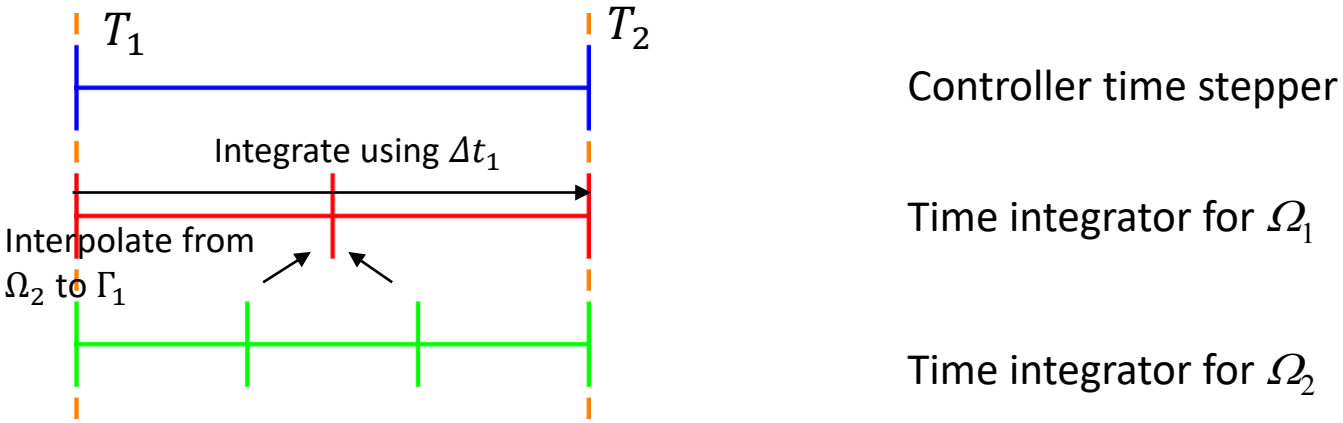

Can use ***different integrators*** with ***different time steps*** within each domain!

Step 0: Initialize $i = 0$ (controller time index).

Step 1: Advance Ω_1 solution from time T_i to time T_{i+1} using time-stepper in Ω_1 with time-step Δt_1, using solution in Ω_2 interpolated to Γ_1 at times $T_i + n\Delta t_1$.

Step 2: Advance Ω_2 solution from time T_i to time T_{i+1} using time-stepper in Ω_2 with time-step Δt_2, using solution in Ω_1 interpolated to Γ_2 at times $T_i + n\Delta t_2$.

Step 3: Check for convergence at time T_{i+1}.

- If unconverged, return to Step 1.
- If converged, set $i = i + 1$ and return to Step 1.

Model PDE:

$$\begin{cases} \dot{\boldsymbol{u}} + N(\boldsymbol{u}) = \boldsymbol{f}, & \text{in } \Omega \\ \boldsymbol{u}(\boldsymbol{x}, t) = \boldsymbol{g}(t), & \text{on } \partial\Omega \\ \boldsymbol{u}(\boldsymbol{x}, 0) = \boldsymbol{u}_0, & \text{in } \Omega \end{cases}$$

Time-Advancement Within the Schwarz Framework

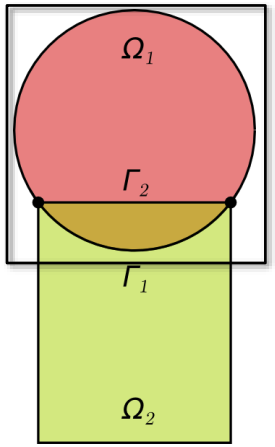

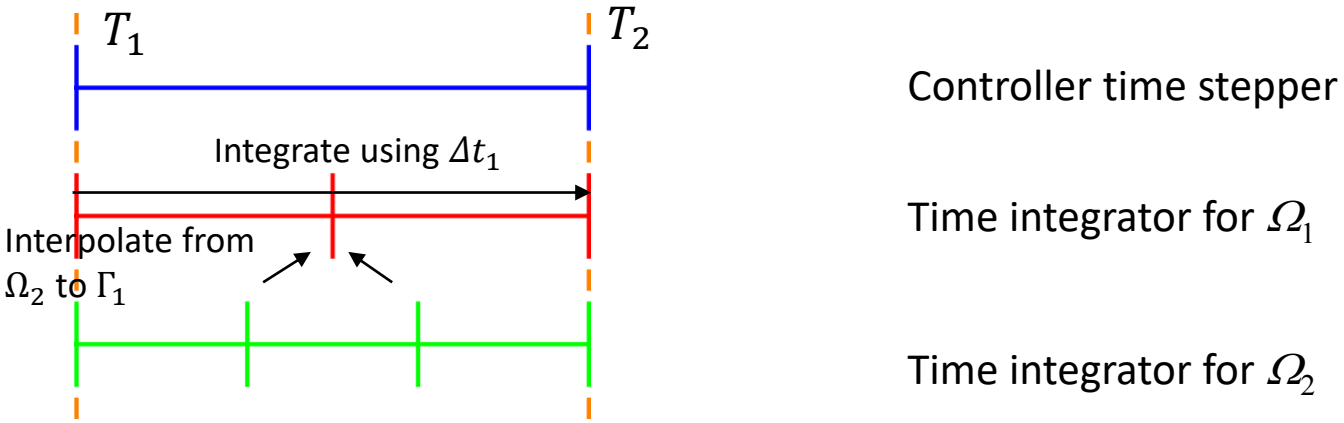

Time-stepping procedure is **equivalent** to doing Schwarz on **space-time domain** [Mota *et al.* 2022].

Step 0: Initialize $i = 0$ (controller time index).

Step 1: Advance Ω_1 solution from time T_i to time T_{i+1} using time-stepper in Ω_1 with time-step Δt_1, using solution in Ω_2 interpolated to Γ_1 at times $T_i + n\Delta t_1$.

Step 2: Advance Ω_2 solution from time T_i to time T_{i+1} using time-stepper in Ω_2 with time-step Δt_2, using solution in Ω_1 interpolated to Γ_2 at times $T_i + n\Delta t_2$.

Step 3: Check for convergence at time T_{i+1}.

- If unconverged, return to Step 1.
- If converged, set $i = i + 1$ and return to Step 1.

Model PDE:

$$\begin{cases} \dot{\boldsymbol{u}} + N(\boldsymbol{u}) = \boldsymbol{f}, & \text{in } \Omega \\ \boldsymbol{u}(\boldsymbol{x}, t) = \boldsymbol{g}(t), & \text{on } \partial\Omega \\ \boldsymbol{u}(\boldsymbol{x}, 0) = \boldsymbol{u}_0, & \text{in } \Omega \end{cases}$$

Schwarz for Multiscale FOM-FOM Coupling in Solid Mechanics[1]

Model Solid Mechanics PDEs:

Quasistatic: $\mathrm{Div}\,\boldsymbol{P} + \rho_0 \boldsymbol{B} = \boldsymbol{0} \quad \text{in} \quad \Omega$

Dynamic: $\mathrm{Div}\,\boldsymbol{P} + \rho_0 \boldsymbol{B} = \rho_0 \ddot{\boldsymbol{\varphi}} \quad \text{in} \quad \Omega \times I$

- Coupling is ***concurrent*** (two-way).
- ***Ease of implementation*** into existing massively-parallel HPC codes.
- ***Scalable, fast, robust*** (we target ***real*** engineering problems, e.g., analyses involving failure of bolted components!).
- Coupling does not introduce ***nonphysical artifacts***.
- ***Theoretical*** convergence properties/guarantees[1].
- ***"Plug-and-play" framework***:
  - Ability to couple regions with ***different non-conformal meshes***, ***different element types*** and ***different levels of refinement*** to simplify task of ***meshing complex geometries***.
  - Ability to use ***different solvers/time-integrators*** in different regions.

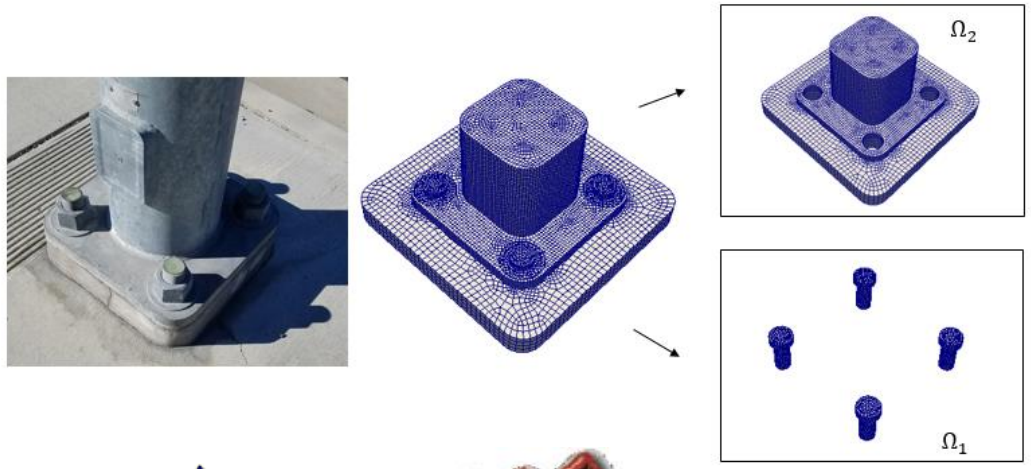

Albany[2] SIERRA

[1] Mota *et al*. 2017; Mota *et al*. 2022. [2] https://github.com/sandialabs/LCM.

Schwarz for Multiscale FOM-FOM Coupling in Solid Mechanics[1]

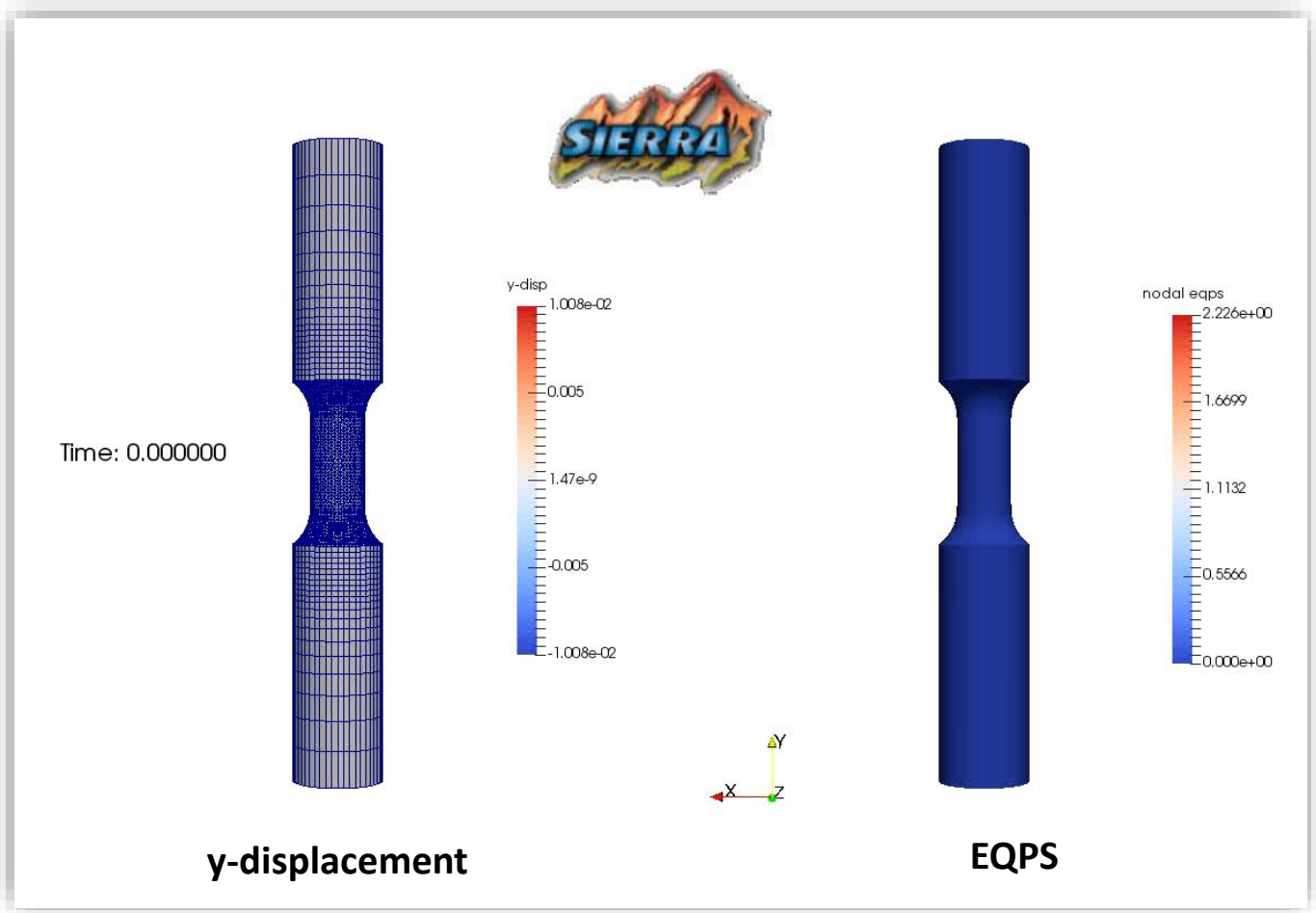

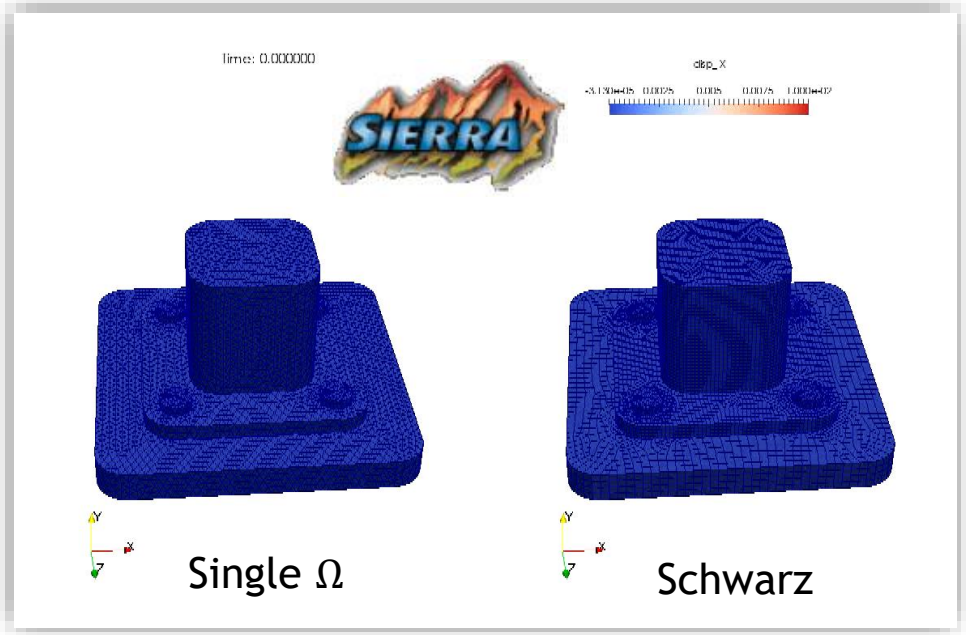

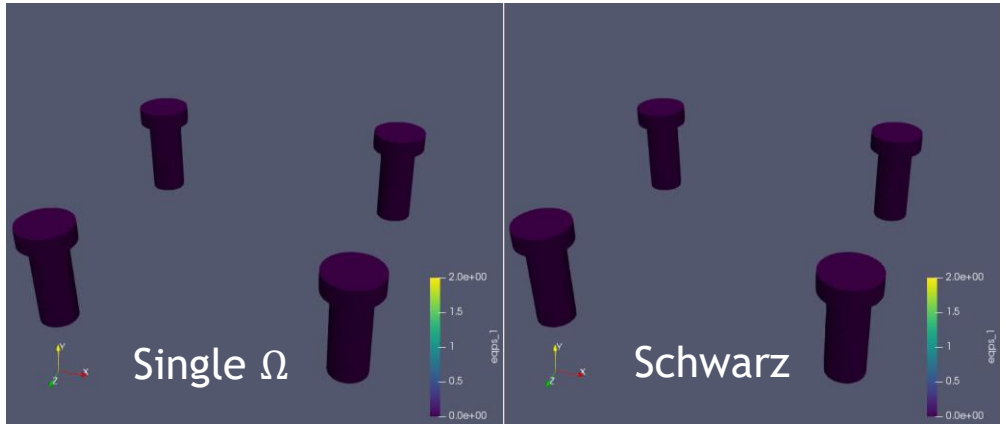

Figure above: tension specimen simulation coupling composite TET10 elements with HEX elements in Sierra/SM.

Figures right: bolted joint simulation coupling composite TET10 elements with HEX elements in Sierra/SM.

[1] Mota *et al.* 2017; Mota *et al.* 2022.

Outline

1. **The Alternating Schwarz Method for FOM*-ROM# and ROM-ROM Coupling**
   - Method Formulation
   - **ROM Construction and Implementation**
   - Numerical Example
2. A Lagrange Multiplier-based Partitioned Scheme for FOM-ROM and ROM-ROM Coupling
   - Method Formulation
   - ROM Construction and Implementation
   - Numerical Example
3. Summary and Comparison of Methods
4. Future Work

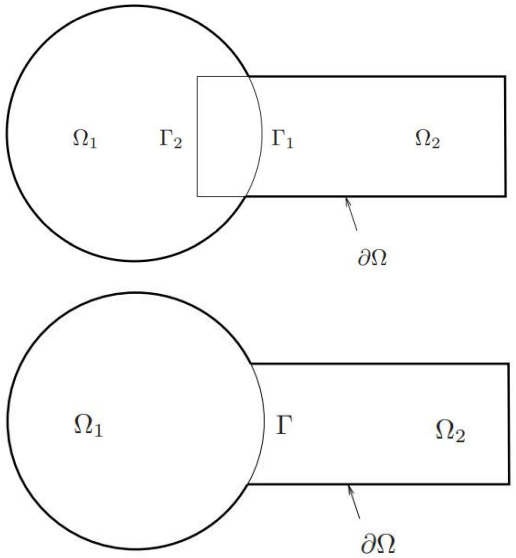

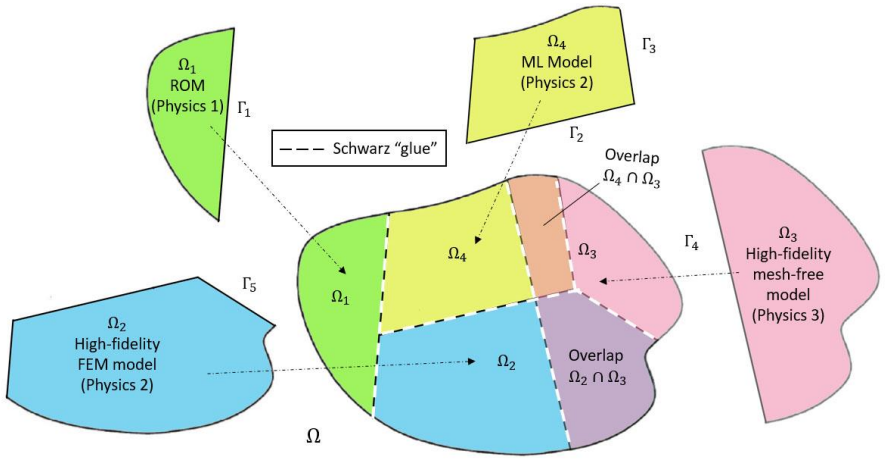

*Full-Order Model. #Reduced Order Model.

Dynamic Solid Mechanics Formulation

- Kinetic energy: $T(\dot{\boldsymbol{\varphi}}) := \frac{1}{2}\int_{\Omega} \rho\dot{\boldsymbol{\varphi}} \cdot \dot{\boldsymbol{\varphi}}\, dV$
- Potential Energy: $V(\boldsymbol{\varphi}) := \int_{\Omega} A(\boldsymbol{F}, \boldsymbol{Z}) dV - \int_{\Omega} \rho\boldsymbol{B} \cdot \boldsymbol{\varphi}\, dV$
- Lagrangian: $L(\boldsymbol{\varphi}, \dot{\boldsymbol{\varphi}}) := T(\dot{\boldsymbol{\varphi}}) - V(\boldsymbol{\varphi})$
- Action functional: $S[\boldsymbol{\varphi}] := \int_{I} L(\boldsymbol{\varphi}, \dot{\boldsymbol{\varphi}})\, dt$
- Euler-Lagrange equations:

$$\begin{cases} \mathrm{Div}\, \boldsymbol{P} + \rho\boldsymbol{B} = \rho\ddot{\boldsymbol{\varphi}}, & \text{in } \Omega \times I \\ \boldsymbol{\varphi}(\boldsymbol{X}, t_0) = \boldsymbol{x}_0, & \text{in } \Omega \\ \dot{\boldsymbol{\varphi}}(\boldsymbol{X}, t_0) = \boldsymbol{v}_0, & \text{in } \Omega \\ \boldsymbol{\varphi}(\boldsymbol{X}, t) = \boldsymbol{\chi}, & \text{on } \partial\Omega \times I \end{cases}$$

- Semi-discrete problem following FEM discretization in space:

$$\boldsymbol{M}\ddot{\boldsymbol{u}} + \boldsymbol{f}_{\mathrm{int}}(\boldsymbol{u}, \dot{\boldsymbol{u}}) = \boldsymbol{f}_{\mathrm{ext}}$$

- $A(\boldsymbol{F}, \boldsymbol{Z})$: Helmholtz free-energy density
- $\boldsymbol{F} := \nabla\boldsymbol{\varphi}$: deformation gradient
- $\boldsymbol{Z}$: collection of internal variables (for plastic materials)
- ρ: density, $\boldsymbol{B}$: body force

$t = 0$

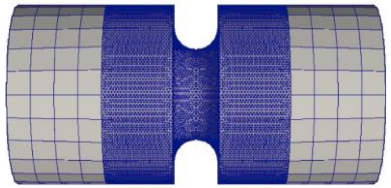

$t = T$

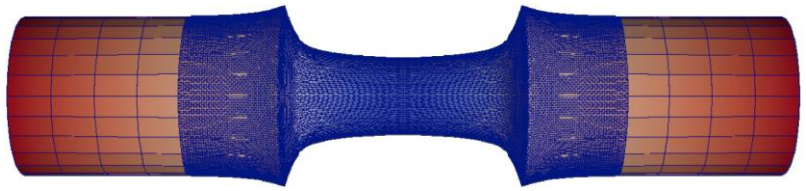

Projection-Based Model Order Reduction via the POD/Galerkin Method

Full Order Model (FOM): $\boldsymbol{M}\frac{d^2\boldsymbol{u}}{dt^2} + \boldsymbol{f}_{\text{int}}(\boldsymbol{u}) = \boldsymbol{f}_{\text{ext}}$

1. Acquisition

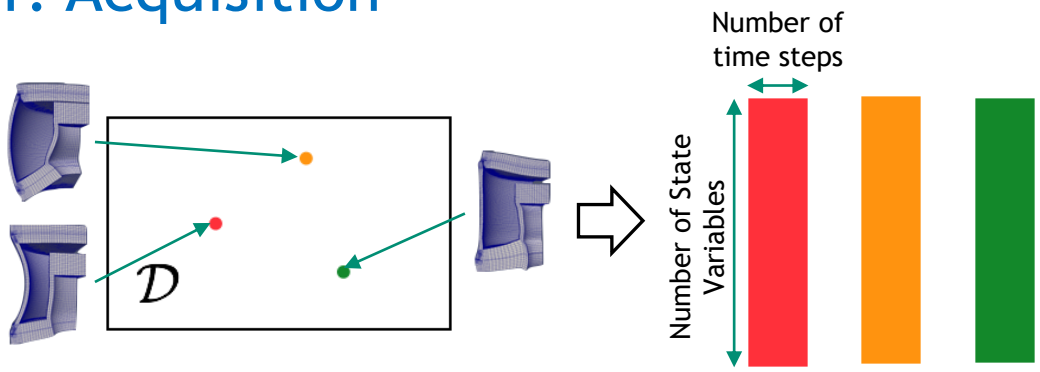

Solve ODE at different design points

Save solution data

2. Learning

Proper Orthogonal Decomposition (POD):

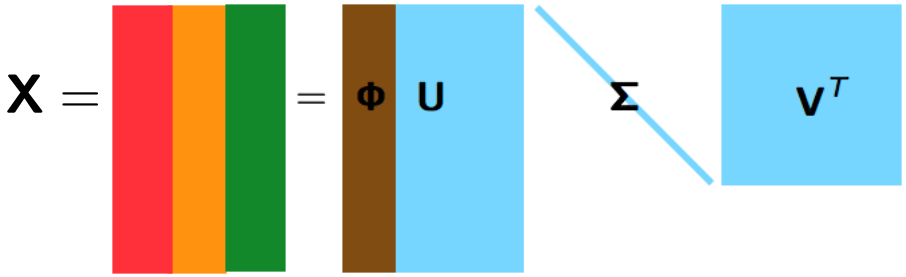

3. Projection-Based Reduction

Reduce the number of unknowns

$$\boldsymbol{u}(t) \approx \tilde{\boldsymbol{u}}(t) = \boldsymbol{\Phi}\hat{\boldsymbol{u}}(t)$$

Perform Galerkin projection

$$\boldsymbol{\Phi}^T\boldsymbol{M}\boldsymbol{\Phi}\frac{d^2\hat{\boldsymbol{u}}}{dt^2} + \boldsymbol{\Phi}^T\boldsymbol{f}_{\text{int}}(\boldsymbol{\Phi}\hat{\boldsymbol{u}}) = \boldsymbol{\Phi}^T\boldsymbol{f}_{\text{ext}}$$

Hyper-reduce nonlinear terms

$$\boldsymbol{f}_{\text{int}}(\boldsymbol{\Phi}\hat{\boldsymbol{u}}) \approx \boldsymbol{A}\,\boldsymbol{f}_{\text{int}}(\boldsymbol{\Phi}\hat{\boldsymbol{u}})$$

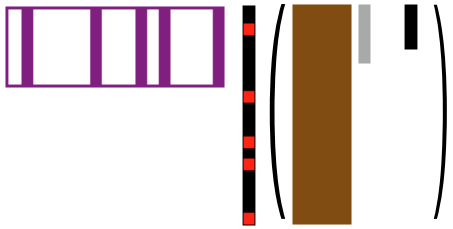

Hyper-reduction/sample mesh

ROM = projection-based Reduced Order Model

HROM = Hyper-reduced ROM

Schwarz Extensions to FOM-ROM and ROM-ROM Couplings

Enforcement of Dirichlet boundary conditions (DBCs) in ROM at indices $\boldsymbol{i}_{\mathrm{Dir}}$

- Method I in [Gunzburger *et al.* 2007] is employed

$$\boldsymbol{u}(t) \approx \bar{\boldsymbol{u}} + \boldsymbol{\Phi}\hat{\boldsymbol{u}}(t), \quad \boldsymbol{v}(t) \approx \bar{\boldsymbol{v}} + \boldsymbol{\Phi}\hat{\boldsymbol{v}}(t), \quad \boldsymbol{a}(t) \approx \bar{\boldsymbol{a}} + \boldsymbol{\Phi}\hat{\boldsymbol{a}}(t)$$

  - POD modes made to satisfy homogeneous DBCs: $\boldsymbol{\Phi}(\boldsymbol{i}_{\mathrm{Dir}}, :) = \boldsymbol{0}$
  - BCs imposed by modifying $\bar{\boldsymbol{u}}$, $\bar{\boldsymbol{v}}$, $\bar{\boldsymbol{a}}$: $\bar{\boldsymbol{u}}(\boldsymbol{i}_{\mathrm{Dir}}) \leftarrow \boldsymbol{\chi}_u$, $\bar{\boldsymbol{v}}(\boldsymbol{i}_{\mathrm{Dir}}) \leftarrow \boldsymbol{\chi}_v$, $\bar{\boldsymbol{a}}(\boldsymbol{i}_{\mathrm{Dir}}) \leftarrow \boldsymbol{\chi}_a$

Choice of domain decomposition

- Error-based indicators that help decide in what region of the domain a ROM can be viable should drive domain decomposition [Bergmann *et al.* 2018] (future work)

Snapshot collection and reduced basis construction

- POD results presented herein use snapshots obtained via FOM-FOM coupling on $\Omega = \bigcup_i \Omega_i$
- *Scenario I:* generate snapshots/bases separately in each Ω_i [Hoang *et al.* 2021, Smetana *et al.* 2022]

For nonlinear solid mechanics, hyper-reduction methods need to preserve Hamiltonian structure

- We employ the Energy-Conserving Sampling & Weighting Method (ECSW) [Farhat *et al.* 2015]
- Boundary points must be included in sample mesh for DBC enforcement

Outline

1. **The Alternating Schwarz Method for FOM*-ROM# and ROM-ROM Coupling**
   - Method Formulation
   - ROM Construction and Implementation
   - **Numerical Example**
2. A Lagrange Multiplier-based Partitioned Scheme for FOM-ROM and ROM-ROM Coupling
   - Method Formulation
   - ROM Construction and Implementation
   - Numerical Example
3. Summary and Comparison of Methods
4. Future Work

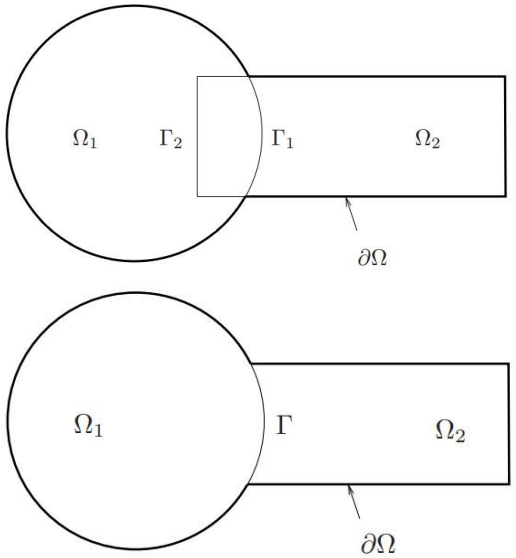

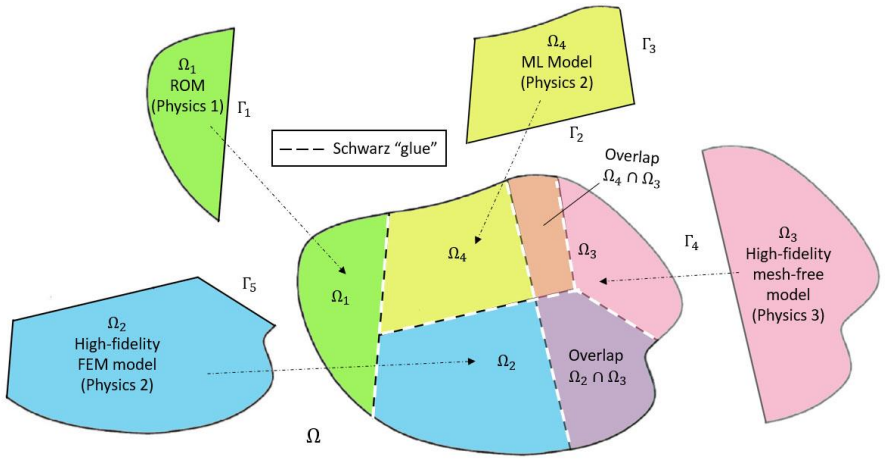

*Full-Order Model. #Reduced Order Model.

Numerical Example: 1D Dynamic Wave Propagation Problem

- ***1D beam*** geometry $\Omega = (0,1)$, clamped at both ends, with prescribed initial condition discretized using FEM + Newmark-β
- Simple problem but very ***stringent test*** for discretization/ coupling methods.
- Two **constitutive models** considered:
  - ➢ Linear elastic (problem has exact analytical solution)
  - ➢ Nonlinear hyperelastic Henky *This talk*

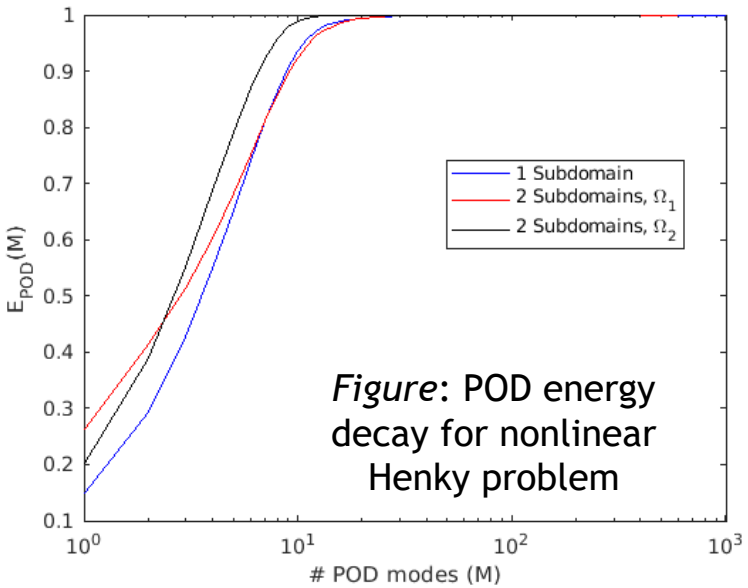

Figure: POD energy decay for nonlinear Henky problem

- ROMs results are ***reproductive*** and ***predictive***, and are based on the ***POD/Galerkin*** method, with POD calculated from FOM-FOM coupled model.
  - ➢ 50 POD modes capture ~100% snapshot energy for linear variant of this problem.
  - ➢ 536 POD modes capture ~100% snapshot energy for Henky variant of this problem.
- Hyper-reduced ROMs (HROMs) perform ***hyper-reduction*** using ECSW [Farhat *et al.*, 2015]
  - ➢ Ensures that ***Lagrangian structure*** of problem is preserved in HROM.
- ***Couplings tested:*** overlapping, non-overlapping, FOM-FOM, FOM-ROM, ROM-ROM, FOM-HROM, HROM-HROM, implicit-explicit, implicit-implicit, explicit-explicit. *This talk*

Numerical Example: 1D Dynamic Wave Propagation Problem

- **Two variants** of problem, with different initial conditions (ICs):
  - Symmetric Gaussian IC (top right)
  - Rounded Square IC (bottom right)
- **Non-overlapping domain decomposition (DD)** of $\Omega = \Omega_1 \cup \Omega_2$, where Ω_1 = [0, 0.6] and Ω_2 = [0.6, 1.0]
  - DD is based on heuristics: during time-interval considered ($0 \leq t \leq 1 \times 10^3$), sharper gradient forms in Ω_1, suggesting FOM or larger ROM is needed there.
- **Reproductive problem**:
  - Displacement snapshots collected using FOM-FOM non-overlapping coupling with **Symmetric Gaussian IC**
  - FOM-ROM, FOM-HROM, ROM-ROM and HROM-HROM run with **Symmetric Gaussian IC**
- **Predictive problem**:
  - Displacement snapshots collected using FOM-FOM non-overlapping coupling with **Symmetric Gaussian IC**
  - FOM-ROM, FOM-HROM, ROM-ROM and HROM-HROM run with **Rounded Square IC**

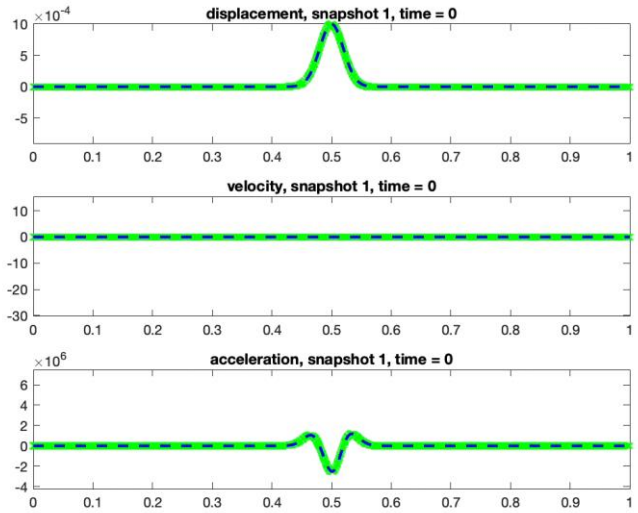

Figure above: Symmetric Gaussian IC problem solution
Figure below: Rounded Square IC problem solution

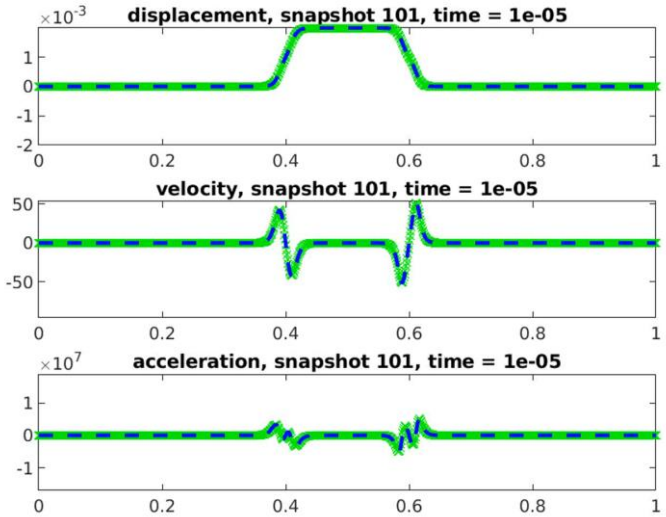

Numerical Example: Reproductive Problem Results

Model	M_1/M_2	$N_{e,1}/N_{e,2}$	CPU time (s)	$\mathcal{E}_{\mathrm{MSE}}(\tilde{\boldsymbol{u}}_1)/\mathcal{E}_{\mathrm{MSE}}(\tilde{\boldsymbol{u}}_2)$	$\mathcal{E}_{\mathrm{MSE}}(\tilde{\boldsymbol{v}}_1)/\mathcal{E}_{\mathrm{MSE}}(\tilde{\boldsymbol{v}}_2)$	$\mathcal{E}_{\mathrm{MSE}}(\tilde{\boldsymbol{a}}_1)/\mathcal{E}_{\mathrm{MSE}}(\tilde{\boldsymbol{a}}_2)$	N_S
FOM	$-/-$	$-/-$	1.871×10^3	$-/-$	$-/-$	$-/-$	$-$
ROM	$60/-$	$-/-$	1.398×10^3	$1.659 \times 10^{-2}/-$	1.037×10^{-1}	$4.681 \times 10^{-1}/-$	$-$
HROM	$60/-$	$155/-$	5.878×10^2	$1.730 \times 10^{-2}/-$	$1.063 \times 10^{-1}/-$	$4.741 \times 10^{-1}/-$	$-$
ROM	$200/-$	$-/-$	1.448×10^3	$2.287 \times 10^{-4}/-$	$4.038 \times 10^{-3}/-$	$4.542 \times 10^{-2}/-$	$-$
HROM	$200/-$	$428/-$	9.229×10^2	$8.396 \times 10^{-4}/-$	$8.947 \times 10^{-3}/-$	$7.462 \times 10^{-2}/-$	$-$
FOM-FOM	$-/-$	$-/-$	2.345×10^3	$-$	$-$	$-$	24,630
FOM-ROM	$-/80$	$-/-$	2.341×10^3	$2.171 \times 10^{-6}/1.253 \times 10^{-5}$	$3.884 \times 10^{-5}/2.401 \times 10^{-4}$	$2.982 \times 10^{-4}/2.805 \times 10^{-3}$	25,227
FOM-HROM	$-/80$	$-/130$	2.085×10^3	$2.022 \times 10^{-4}/5.734 \times 10^{-4}$	$1.723e \times 10^{-3}/5.776 \times 10^{-3}$	$7.421 \times 10^{-3}/3.791 \times 10^{-2}$	29,678
FOM-ROM	$-/200$	$-/-$	2.449×10^3	$4.754 \times 10^{-12}/7.357 \times 10^{-11}$	$1.835 \times 10^{-10}/4.027 \times 10^{-9}$	$5.550 \times 10^{-9}/1.401 \times 10^{-7}$	24,630
FOM-HROM	$-/200$	$-/252$	2.352×10^3	$1.421 \times 10^{-5}/4.563 \times 10^{-4}$	$1.724 \times 10^{-4}/2.243 \times 10^{-3}$	$9.567 \times 10^{-4}/1.364 \times 10^{-2}$	27,156
ROM-ROM	$200/80$	$-/-$	2.778×10^3	$4.861 \times 10^{-5}/3.093 \times 10^{-5}$	$1.219 \times 10^{-3}/4.177 \times 10^{-4}$	$1.586 \times 10^{-2}/3.936 \times 10^{-3}$	27,810
HROM-HROM	$200/80$	$315/130$	1.769×10^3	$3.410 \times 10^{-3}/6.662 \times 10^{-4}$	$4.110 \times 10^{-2}/6.432 \times 10^{-3}$	$2.485 \times 10^{-1}/4.307 \times 10^{-2}$	29,860
ROM-ROM	$300/80$	$-/-$	2.646×10^3	$2.580 \times 10^{-6}/1.292 \times 10^{-5}$	$6.226 \times 10^{-5}/2.483 \times 10^{-4}$	$9.470 \times 10^{-4}/2.906 \times 10^{-3}$	25,059
HROM-HROM	$300/80$	$405/130$	1.938×10^3	$6.960 \times 10^{-3}/7.230 \times 10^{-4}$	$6.328 \times 10^{-2}/7.403 \times 10^{-3}$	$3.137 \times 10^{-1}/4.960 \times 10^{-2}$	29,896

Green shading highlights most competitive coupled models

- All coupled models evaluated converged on average in <**3 Schwarz iterations** per time-step
- Larger FOM-ROM coupling has **same total # Schwarz iters** (N_S) as FOM-FOM coupling
- Other couplings require more Schwarz iters than FOM-FOM coupling to converge
  - **More Schwarz iters** required when coupling **less accurate models**
  - Larger 300/80 mode ROM-ROM takes less wall-clock time than smaller 200/80 mode ROM-ROM
- **FOM-HROM** and **HROM-HROM** couplings **outperform** the **FOM-FOM** coupling in terms of CPU time by 12.5-32.6%
- All couplings involving ROMs/HROMs are **at least as accurate** as single-domain ROMs/HROMs

Numerical Example: Reproductive Problem Results

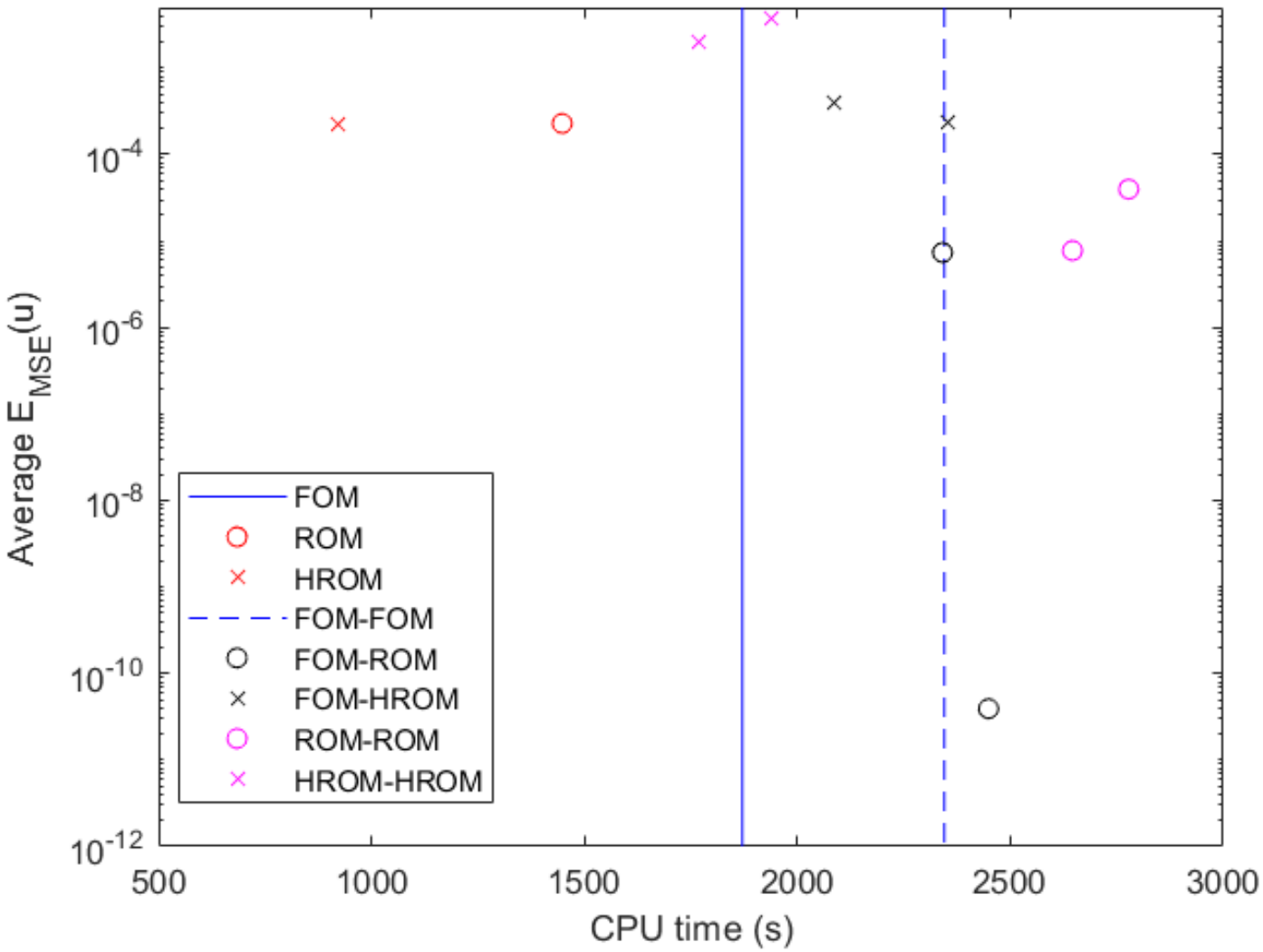

- **Single-domain** ROM and HROM are most **efficient**
- Couplings involving ROMs and HROMs enable one to achieve **smaller errors**
- Benefits of **hyper-reduction** are **limited** on **1D problem**

Numerical Example: Reproductive Problem Results

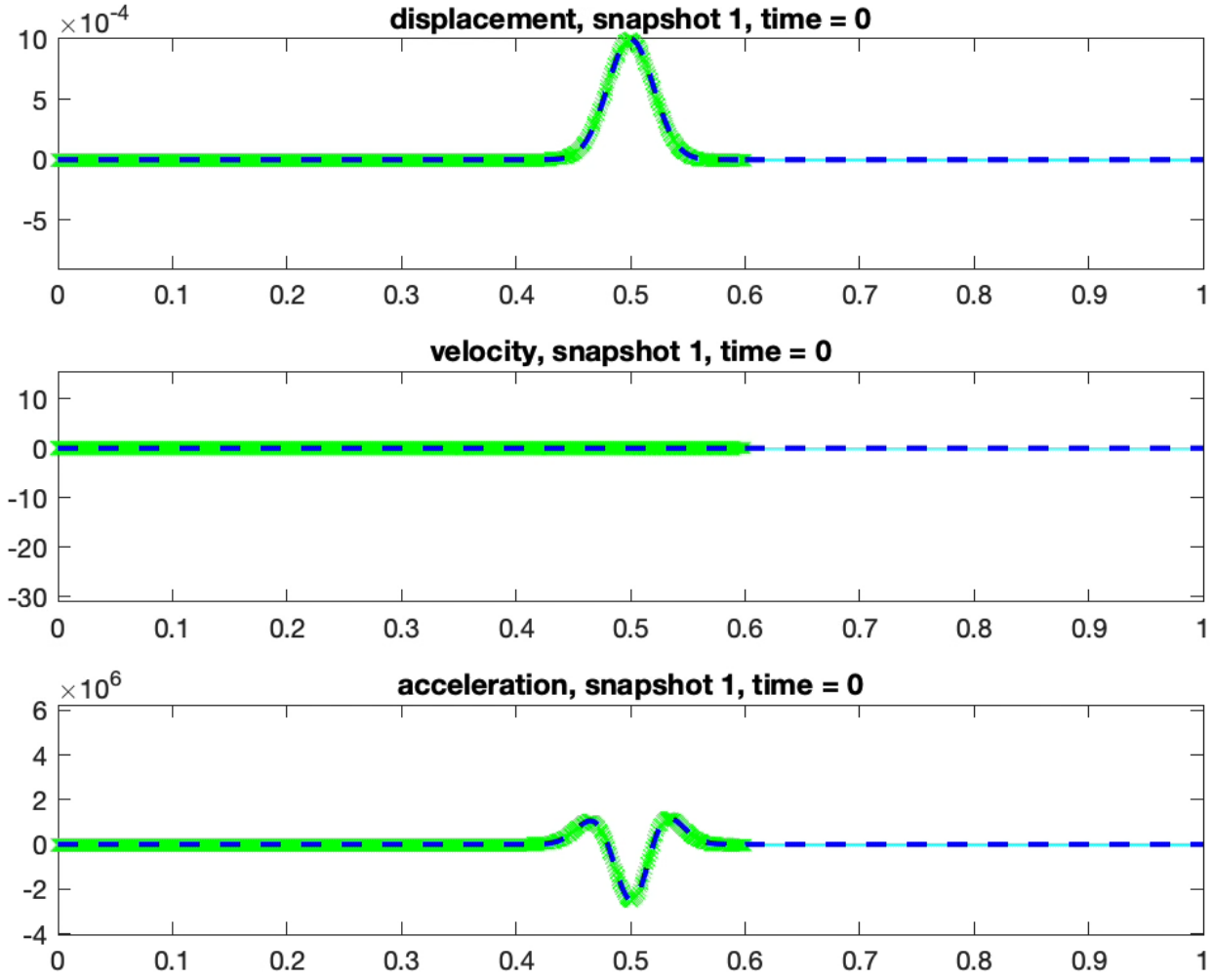

Figure left: FOM (green) – HROM (cyan) coupling compared with single-domain FOM solution (blue). HROM has 200 modes.

Figure below: ECSW algorithm samples 253/400 elements

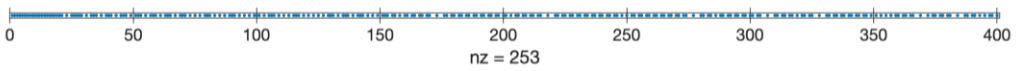

Numerical Example: Predictive Problem Results

- Start by calculating **projection error** for reproductive and predictive version of the Rounded Square IC problem:

$$\mathcal{E}_{\text{proj}}(\boldsymbol{u}, \boldsymbol{\Phi}_M) := \frac{||\boldsymbol{u} - \boldsymbol{\Phi}_M(\boldsymbol{\Phi}_M^T \boldsymbol{\Phi}_M)^{-1}\boldsymbol{\Phi}_M^T \boldsymbol{u}||_2}{||\boldsymbol{u}||_2}$$

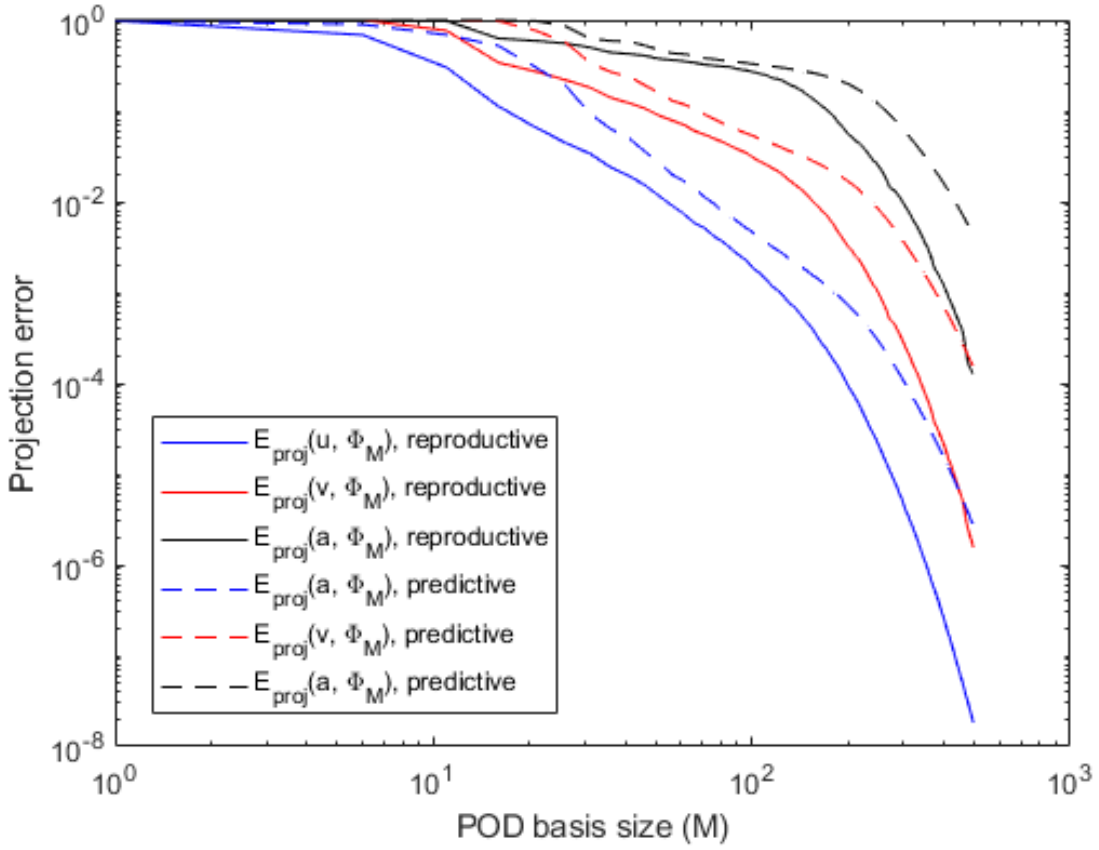

- Projection error suggests **predictive ROM** can achieve **accuracy** and **convergence** with **basis refinement**
- **O(100) modes** are needed to achieve sufficiently accurate ROM
  - Larger ROMs containing O(100) modes considered in our coupling experiments: M_1= 300, M_2= 200

Numerical Example: Predictive Problem Results

Model	CPU time (s)	$N_{e,1}/N_{e,2}$	$\mathcal{E}_{\mathrm{MSE}}(\tilde{\boldsymbol{u}}_1)/\mathcal{E}_{\mathrm{MSE}}(\tilde{\boldsymbol{u}}_2)$	$\mathcal{E}_{\mathrm{MSE}}(\tilde{\boldsymbol{v}}_1)/\mathcal{E}_{\mathrm{MSE}}(\tilde{\boldsymbol{v}}_2)$	$\mathcal{E}_{\mathrm{MSE}}(\tilde{\boldsymbol{a}}_1)/\mathcal{E}_{\mathrm{MSE}}(\tilde{\boldsymbol{a}}_2)$	N_S
FOM	1.288×10^3	$-/-$	$-/-$	$-/-$	$-/-$	$-$
ROM	1.358×10^3	$-/-$	$3.451\times10^{-3}/-$	$6.750 \times 10^{-2}/-$	$3.021 \times 10^{-1}/-$	$-$
HROM	9.759×10^2	$614/-$	$3.463 \times 10^{-3}/-$	$6.750 \times 10^{-2}/-$	$3.021 \times 10^{-1}/-$	$-$
FOM-FOM	2.133×10^3	$-/-$	$-/-$	$-/-$	$-/-$	23,280
FOM-ROM	2.084×10^3	$-/-$	$1.907 \times 10^{-8}/$ 1.170×10^{-6}	$1.461 \times 10^{-6}/$ 9.882×10^{-5}	$3.973 \times 10^{-5}/$ 1.757×10^{-3}	23,288
FOM-HROM	2.219×10^3	$-/253$	1.967×10^{-4} 1.720×10^{-3}	4.986×10^{-3} 4.185×10^{-2}	2.768×10^{-2} 2.388×10^{-1}	29,700
ROM-ROM	2.502×10^3	$-/-$	$5.592 \times 10^{-4}/$ 4.346×10^{-4}	$1.575 \times 10^{-2}/$ 1.001×10^{-2}	$9.197 \times 10^{-2}/$ 5.304×10^{-2}	26,220
HROM-HROM	2.200×10^3	$405/253$	4.802×10^{-3} 1.960×10^{-3}	8.500×10^{-2} 4.630×10^{-2}	3.744×10^{-1} 2.580×10^{-1}	30,067

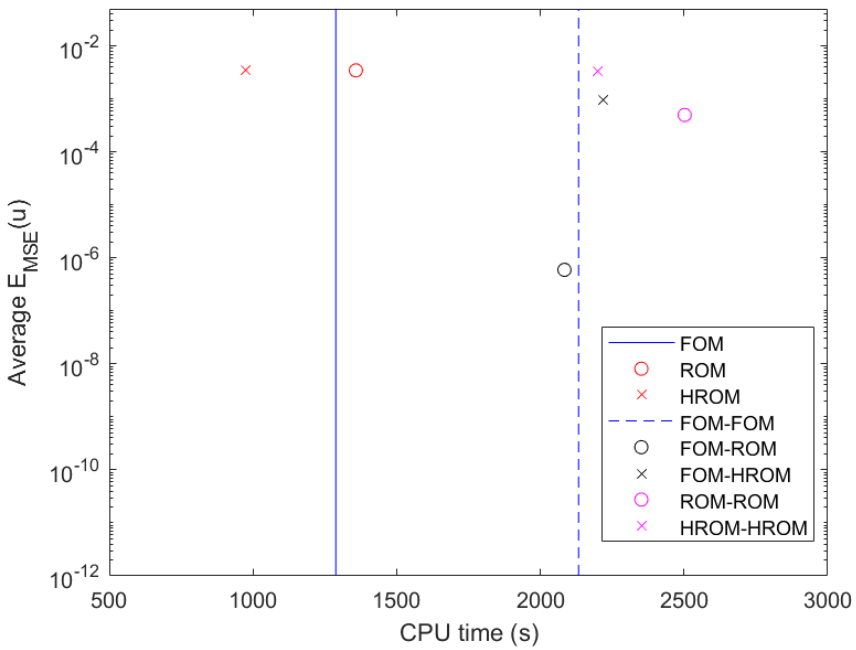

- Results indicate that **predictive accuracy/robustness** can be **improved** by **coupling** ROM or HROM to FOM
  - FOM-ROM coupling is **remarkably accurate**, achieving displacement error $O(1 \times 10^{-8})$
  - FOM-HROM and ROM-ROM couplings are **more accurate** than single-domain ROMs
  - HROM-HROM **on par** with single-domain HROM in terms of accuracy
- **Wall-clock times** of coupled models can be improved
  - FOM-HROM, ROM-ROM and HROM-HROM models are **slower** than FOM-FOM model as **more Schwarz iterations** required to achieve convergence
  - **Hyper-reduction** samples ~60% of total mesh points for this 1D traveling wave problem
    - Greater gains from hyper-reduction anticipated for 2D/3D problems

Numerical Example: Predictive Problem Results

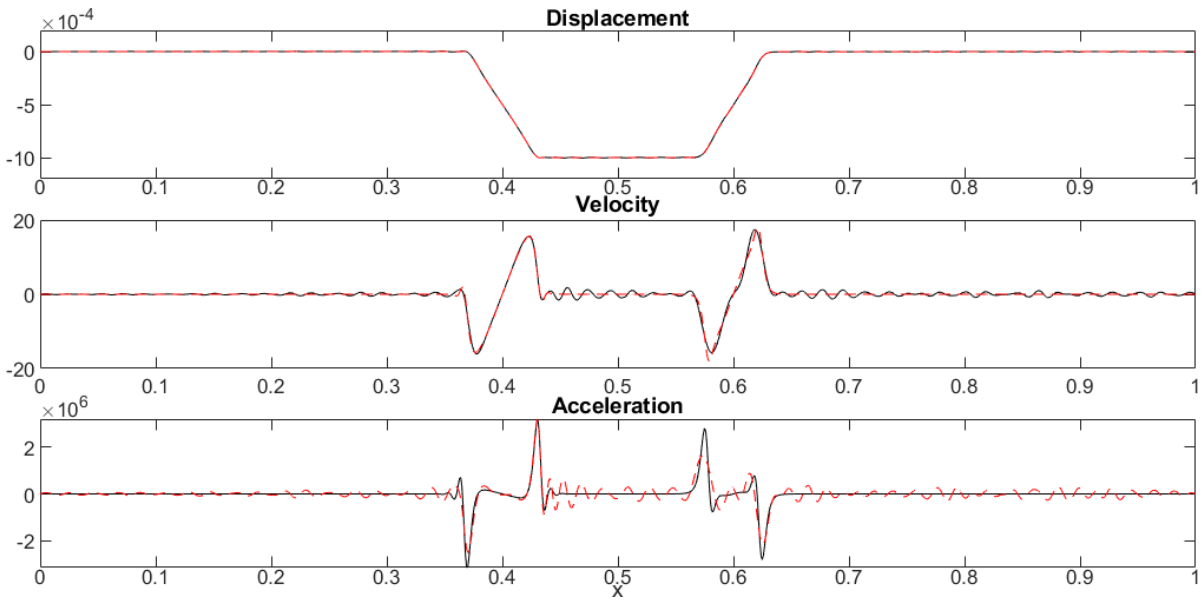

Predictive single-domain ROM (M_1= 300) solution at final time

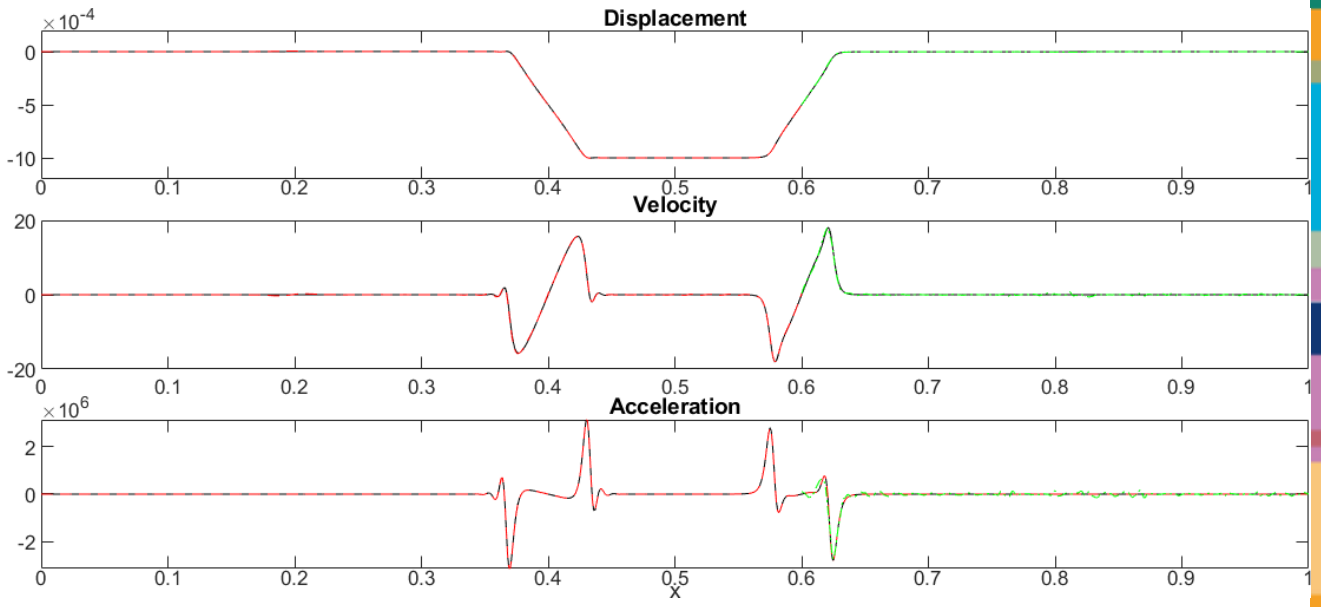

Predictive FOM-HROM (M_2= 200) solution at final time

— Single-domain FOM solution	— Solution in Ω_1	— Solution in Ω_2

- Predictive **single-domain ROM** solution exhibits **spurious oscillations** in velocity and acceleration
- Predictive **FOM-HROM** solution is **smooth** and **oscillation-free**
  - ➢ Highlights coupling method's ability to improve ROM predictive accuracy

Numerical Example: Predictive Problem Results

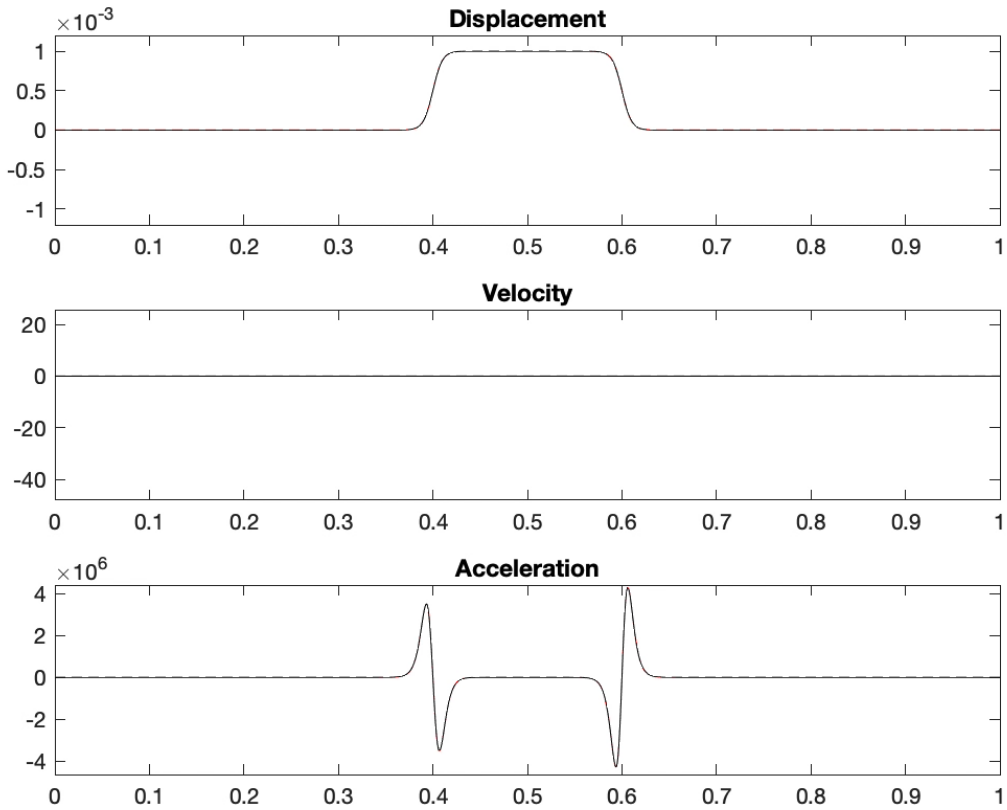

Predictive single-domain ROM (M_1= 300)

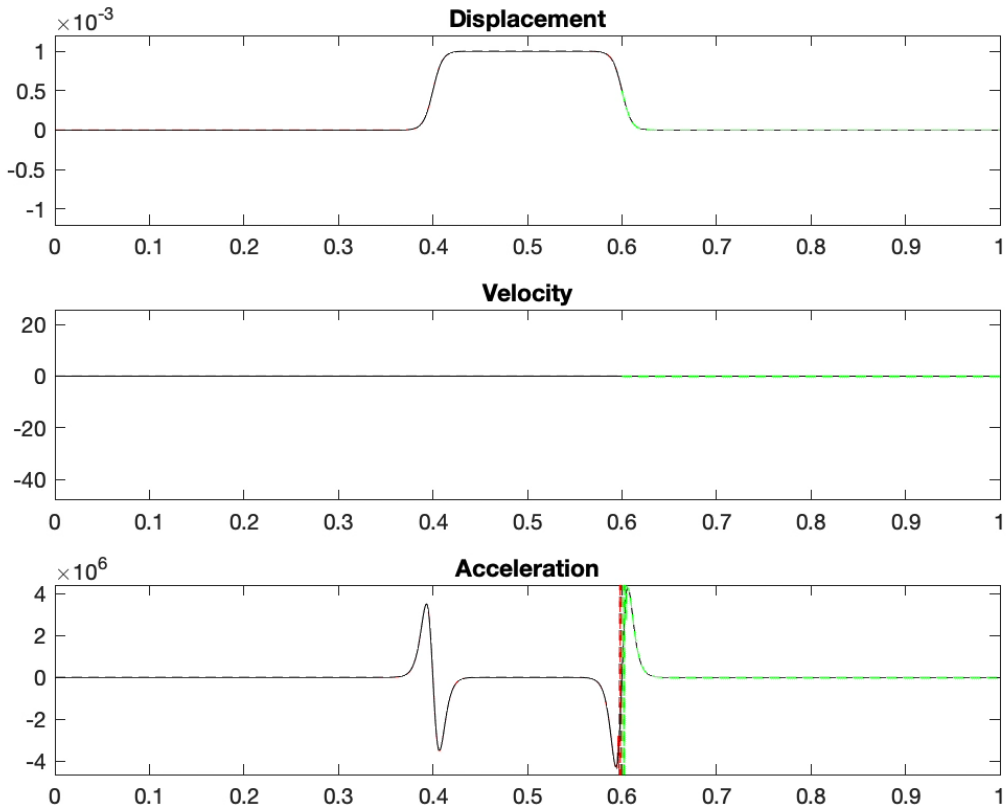

Predictive FOM-HROM (M_2= 200)

— Single-domain FOM solution — Solution in Ω_1 — Solution in Ω_2

Outline

1. The Alternating Schwarz Method for FOM*-ROM# and ROM-ROM Coupling
   - Method Formulation
   - ROM Construction and Implementation
   - Numerical Example
2. **A Lagrange Multiplier-based Partitioned Scheme for FOM-ROM and ROM-ROM Coupling**
   - **Method Formulation**
   - ROM Construction and Implementation
   - Numerical Example
3. Summary and Comparison of Methods
4. Future Work

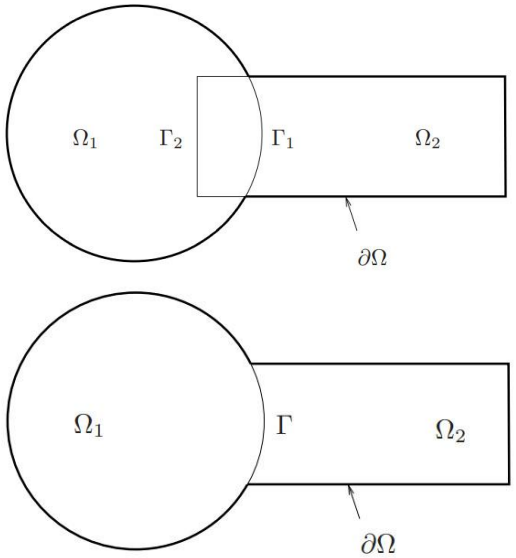

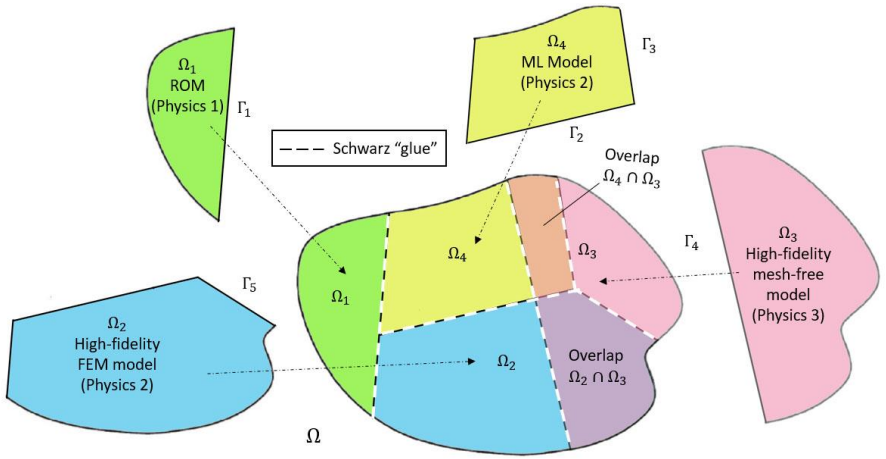

*Full-Order Model. #Reduced Order Model.

Lagrange Multiplier-Based Partitioned Coupling Formulation

Model problem: time-dependent **advection-diffusion** problem on $\Omega = \Omega_1 \cup \Omega_2$ with $\Omega_1 \cap \Omega_2 = \emptyset$

$$\boxed{\begin{array}{lll} \dot{c}_i - \nabla \cdot F_i(c_i) = f_i, & \text{in} & \Omega_i \times [0,T] \\ c_i = g_i, & \text{on} & \Gamma_i \times [0,T] \\ c_i(\boldsymbol{x},0) = c_{i,0}(x), & \text{in} & \Omega_i \end{array}} \quad (1)$$

- $i \in \{1,2\}$
- c_i: unknown scalar solution field
- f_i: body force, g_i: boundary data on Γ_i
- $F_i(c_i) := \kappa_i \nabla c_i - \boldsymbol{u} c_i$: total flux function
- κ_i: non-negative diffusion coefficient
- $\boldsymbol{u}$: given advection velocity field

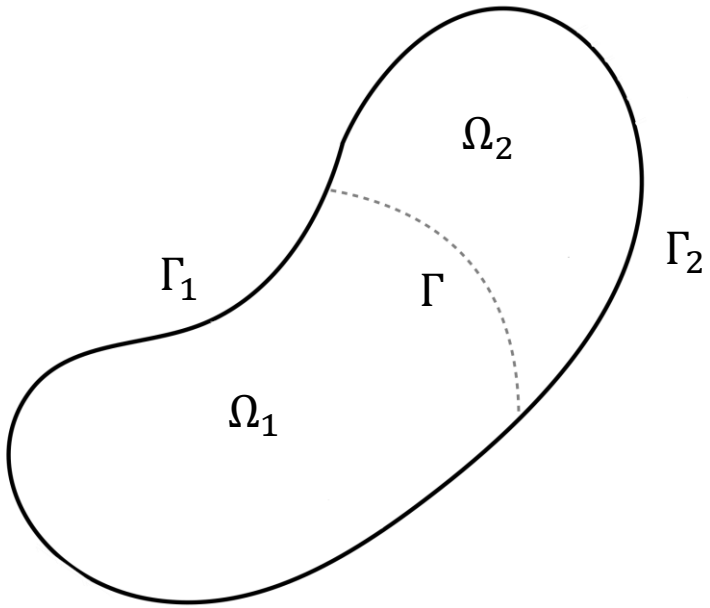

Figure above: example non-overlapping domain decomposition (DD) of $\Omega = \Omega_1 \cup \Omega_2$

Compatibility conditions: on interface $\Gamma \times [0,T]$

- ***Continuity of states***: $c_1(\boldsymbol{x},t) - c_2(\boldsymbol{x},t) = 0$
- ***Continuity of total flux***: $F_1(\boldsymbol{x},t) \cdot \boldsymbol{n}_\Gamma = F_1(\boldsymbol{x},t) \cdot \boldsymbol{n}_\Gamma$

$\Rightarrow$ *Imposed weakly using Lagrange multiplier (LM)* λ

Lagrange Multiplier-Based Partitioned FOM-FOM Coupling

FEM-FEM coupling for high Peclet transport problem

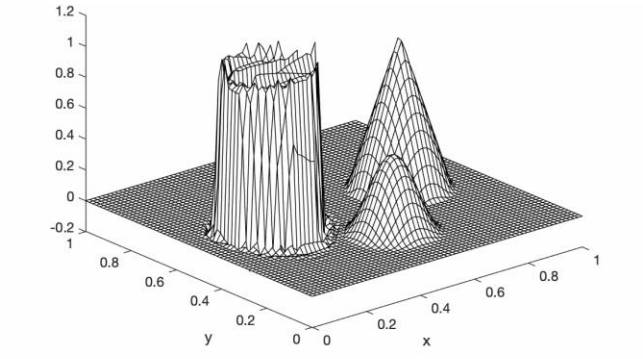

Coupling of nonconforming meshes

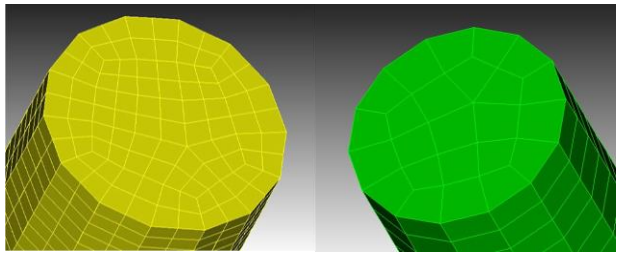

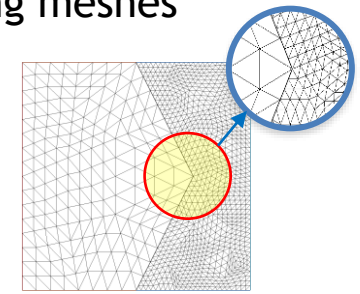

Patch test (ALEGRA-Sierra/SM coupling)

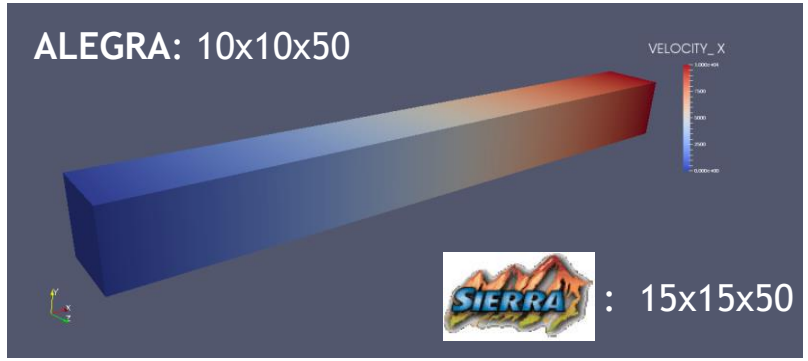

"Plug-and-play" framework:

- Ability to couple regions with ***different non-conformal meshes***, ***different element types*** and ***different levels of refinement*** to simplify task of ***meshing complex geometries***
- Ability to use ***different solvers/time-integrators*** in different regions[1,2]
- Coupling is ***non-iterative*** (single pass)

Method is theoretically rigorous[3]:

- Coupling does not introduce ***nonphysical artifacts***
- ***Theoretical convergence*** properties/guarantees including well-posedness of coupling force system
- ***Preserves*** the ***exact solution*** for conformal meshes

Method has been applied to several application spaces:

- ***Transport*** (unsteady advection-diffusion)
- ***Ocean-atmosphere coupling***
- ***Elasticity*** (e.g., ALEGRA-Sierra/SM coupling)

[1]Connors *et al.* 2022. [2]Sockwell *et al.* 2023. [3]Peterson *et al.* 2019.

A Lagrange Multiplier-Based Partitioned Scheme

Hybrid semi-discrete coupled formulation: obtained by differentiating interface conditions in time and discretizing hybrid problem using FEM in space

$$\begin{pmatrix} \boldsymbol{M}_1 & \boldsymbol{0} & \boldsymbol{G}_1^T \\ \boldsymbol{0} & \boldsymbol{M}_2 & -\boldsymbol{G}_2^T \\ \boldsymbol{G}_1 & -\boldsymbol{G}_2 & \boldsymbol{0} \end{pmatrix} \begin{pmatrix} \dot{\boldsymbol{c}}_1 \\ \dot{\boldsymbol{c}}_2 \\ \boldsymbol{\lambda} \end{pmatrix} = \begin{pmatrix} \boldsymbol{f}_1 - \boldsymbol{K}_1 \boldsymbol{c}_1 \\ \boldsymbol{f}_2 - \boldsymbol{K}_2 \boldsymbol{c}_2 \\ \boldsymbol{0} \end{pmatrix} \qquad (2)$$

- $\boldsymbol{M}_i$: mass matrices
- $\boldsymbol{K}_i := \boldsymbol{D}_i + \boldsymbol{A}_i$: stiffness matrices, where $\boldsymbol{D}_i$ and $\boldsymbol{A}_i$ are matrices for diffusive and advective terms, respectively
- $\boldsymbol{G}_i$: constraints matrices enforcing constraints in weak sense

Decoupling via Schur complement: equation (2) is equivalent to

*Equations **decouple** if using **explicit** or **IMEX** time-integration!*

$$\boxed{\begin{pmatrix} \boldsymbol{M}_1 & \boldsymbol{0} \\ \boldsymbol{0} & \boldsymbol{M}_2 \end{pmatrix} \begin{pmatrix} \dot{\boldsymbol{c}}_1 \\ \dot{\boldsymbol{c}}_2 \end{pmatrix} = \begin{pmatrix} \boldsymbol{f}_1 - \boldsymbol{K}_1 \boldsymbol{c}_1 - \boldsymbol{G}_1^T \boldsymbol{\lambda} \\ \boldsymbol{f}_2 - \boldsymbol{K}_2 \boldsymbol{c}_2 + \boldsymbol{G}_2^T \boldsymbol{\lambda} \end{pmatrix}} \qquad (3)$$

where $(\boldsymbol{G}_1 \boldsymbol{M}_1^{-1} \boldsymbol{G}_1^T + \boldsymbol{G}_2 \boldsymbol{M}_2^{-1} \boldsymbol{G}_2^T)\boldsymbol{\lambda} = \boldsymbol{G}_1 \boldsymbol{M}_1^{-1}(\boldsymbol{f}_1 - \boldsymbol{K}_1 \boldsymbol{c}_1) - \boldsymbol{G}_2 \boldsymbol{M}_2^{-1}(\boldsymbol{f}_2 - \boldsymbol{K}_2 \boldsymbol{c}_2)$ (4)

*Time **integration schemes** and **time-steps** in Ω_1 and Ω_2 can be **different**!*

Implicit Value Recovery (IVR) Algorithm [Peterson *et al.* 2019]

- Pick explicit or IMEX time-integration scheme for Ω_1 and Ω_2
- Approximate LM space as trace of FE space on Ω_1 or Ω_2*
- Compute matrices $\boldsymbol{M}_i, \boldsymbol{K}_i$, $\boldsymbol{G}_i$ and vectors $\boldsymbol{f}_i$
- For each timestep t^n:
  - Solve Schur complement system (4) for the LM $\boldsymbol{\lambda}^n$
  - Update the state variables $\boldsymbol{c}_i^n$ by advancing (3) in time

* Ensures that dual Schur complement of (2) is s.p.d.

Outline

1. The Alternating Schwarz Method for FOM*-ROM# and ROM-ROM Coupling
   - Method Formulation
   - ROM Construction and Implementation
   - Numerical Example
2. **A Lagrange Multiplier-based Partitioned Scheme for FOM-ROM and ROM-ROM Coupling**
   - Method Formulation
   - **ROM Construction and Implementation**
   - Numerical Example
3. Summary and Comparison of Methods
4. Future Work

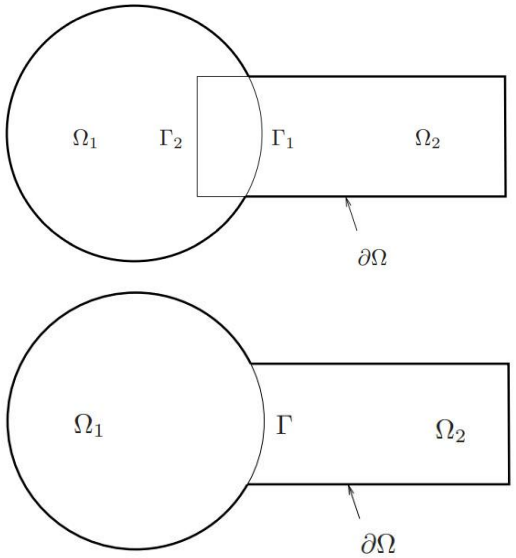

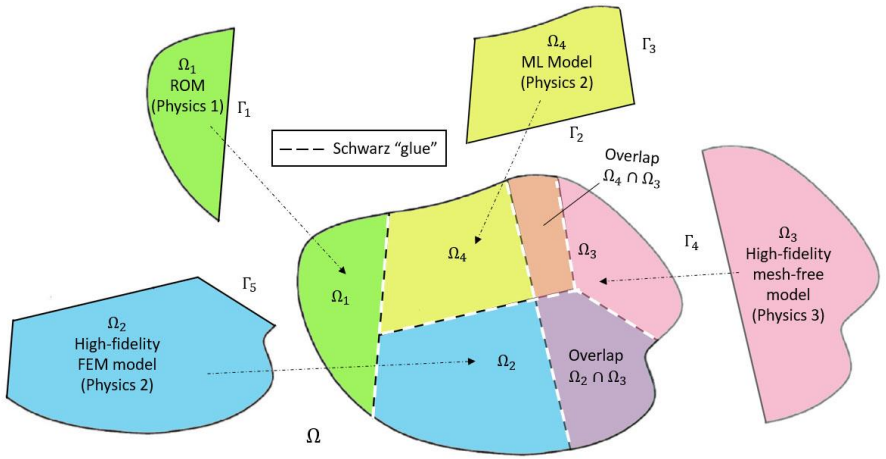

*Full-Order Model. #Reduced Order Model.

ROM-ROM Coupling: Full Subdomain Bases & Full LM Spaces

- Collect **snapshots** using suitable monolithic FOM solve for equation (1) and **subtract DBC data** on $\Gamma_1 \cup \Gamma_2$
- **Partition** modified snapshots into **subdomain snapshot matrices** $\boldsymbol{X}_1$ and $\boldsymbol{X}_2$ on Ω_1 and Ω_2, respectively
- Calculate **"full" subdomain POD bases** $\boldsymbol{\Phi}_1$ and $\boldsymbol{\Phi}_2$ of dimensions M_1 and M_2 from SVD of $\boldsymbol{X}_1$ and $\boldsymbol{X}_2$
- **Approximate** the solution as a **linear combination** of the POD modes in each subdomain:

$$\boldsymbol{c}_1(t) \approx \tilde{\boldsymbol{c}}_1(t) := \bar{\boldsymbol{c}}_1 + \boldsymbol{\Phi}_1 \hat{\boldsymbol{c}}_1(t), \qquad \boldsymbol{c}_2(t) \approx \tilde{\boldsymbol{c}}_2(t) := \bar{\boldsymbol{c}}_2 + \boldsymbol{\Phi}_2 \hat{\boldsymbol{c}}_2(t) \qquad (5)$$

- Substitute (5) into (2) and **project** (3) onto POD modes to obtain system of the form:

$$\begin{pmatrix} \widetilde{\boldsymbol{M}}_1 & \boldsymbol{0} & \widetilde{\boldsymbol{G}}_1^T \\ \boldsymbol{0} & \widetilde{\boldsymbol{M}}_2 & -\widetilde{\boldsymbol{G}}_2^T \\ \widetilde{\boldsymbol{G}}_1 & -\widetilde{\boldsymbol{G}}_2 & \boldsymbol{0} \end{pmatrix} \begin{pmatrix} \dot{\hat{\boldsymbol{c}}}_1 \\ \dot{\hat{\boldsymbol{c}}}_2 \\ \boldsymbol{\lambda} \end{pmatrix} = \begin{pmatrix} \boldsymbol{s}_1 \\ \boldsymbol{s}_2 \\ \boldsymbol{0} \end{pmatrix}$$

where $\widetilde{\boldsymbol{M}}_i := \boldsymbol{\Phi}_i^T \boldsymbol{M}_i \boldsymbol{\Phi}_i$, $\widetilde{\boldsymbol{G}}_i := \boldsymbol{G}_i \boldsymbol{\Phi}_i$,
$\boldsymbol{s}_i := \boldsymbol{\Phi}_i^T \boldsymbol{f}_i - \boldsymbol{\Phi}_i^T \boldsymbol{K}_i \boldsymbol{\Phi}_i \hat{\boldsymbol{c}}_i - \boldsymbol{\Phi}_i^T \boldsymbol{K}_i \bar{\boldsymbol{c}}_i - \boldsymbol{\Phi}_i^T \boldsymbol{M}_i \dot{\bar{\boldsymbol{c}}}_i$ (6)

Online ROM-ROM IVR Solution Algorithm with Full Subdomain Bases & LM Spaces: at each time step t^n

- Use $\hat{\boldsymbol{c}}_1^n$ and $\hat{\boldsymbol{c}}_2^n$ to compute updated RHS $\boldsymbol{s}_1^n$ and $\boldsymbol{s}_2^n$
- Solve the Schur complement system for $\boldsymbol{\lambda}^n$:

$$(\widetilde{\boldsymbol{G}}_1 \widetilde{\boldsymbol{M}}_1^{-1} \widetilde{\boldsymbol{G}}_1^T + \widetilde{\boldsymbol{G}}_2 \widetilde{\boldsymbol{M}}_2^{-1} \widetilde{\boldsymbol{G}}_2^T) \boldsymbol{\lambda}^n = \widetilde{\boldsymbol{G}}_1 \widetilde{\boldsymbol{M}}_1^{-1} \boldsymbol{s}_1^n - \widetilde{\boldsymbol{G}}_2 \widetilde{\boldsymbol{M}}_2^{-1} \boldsymbol{s}_2^n$$

- Advance the following systems forward in time: $\widetilde{\boldsymbol{M}}_1 \dot{\hat{\boldsymbol{c}}}_1^n = \boldsymbol{s}_1^n - \widetilde{\boldsymbol{G}}_1 \boldsymbol{\lambda}^n$ and $\widetilde{\boldsymbol{M}}_2 \dot{\hat{\boldsymbol{c}}}_2^n = \boldsymbol{s}_2^n + \widetilde{\boldsymbol{G}}_2 \boldsymbol{\lambda}^n$

FOM-ROM coupling formulation is similar

ROM-ROM Coupling: What Could Go Wrong?

A provably non-singular dual Schur complement requires:

1. ***Symmetric positive-definite projected mass matrices*** $\widetilde{\boldsymbol{M}}_i$

2. ***Projected constraint matrix*** $\left(\widetilde{\boldsymbol{G}}_1,\ \widetilde{\boldsymbol{G}}_2\right)^{\boldsymbol{T}}$ ***must have full column rank***

ROM-ROM Coupling: What Could Go Wrong?

A provably non-singular dual Schur complement requires:

1. ***Symmetric positive-definite projected mass matrices*** $\widetilde{\boldsymbol{M}}_i$

   ☹ Not guaranteed *a priori* with full subdomain bases $\boldsymbol{\Phi}_1$ and $\boldsymbol{\Phi}_2$

2. ***Projected constraint matrix*** $\left(\widetilde{\boldsymbol{G}}_1,\ \widetilde{\boldsymbol{G}}_2\right)^{\boldsymbol{T}}$ ***must have full column rank***

   ☹ Not guaranteed for "full" LM space, taken as trace of underlying FEM discretization space

ROM-ROM Coupling: What Could Go Wrong?

A provably non-singular dual Schur complement requires:

1. ***Symmetric positive-definite projected mass matrices*** $\widetilde{\boldsymbol{M}}_i$
   - ☹ Not guaranteed *a priori* with full subdomain bases $\boldsymbol{\Phi}_1$ and $\boldsymbol{\Phi}_2$
   - ☺ Remedied by creating separate **"split" reduced bases** $\boldsymbol{\Phi}_{i,\Gamma}$ and $\boldsymbol{\Phi}_{i,0}$, for interface and interior DOFs
     - ➢ Columns of each basis matrix will have full column rank

2. ***Projected constraint matrix*** $\left(\widetilde{\boldsymbol{G}}_1,\ \widetilde{\boldsymbol{G}}_2\right)^{\boldsymbol{T}}$ ***must have full column rank***
   - ☹ Not guaranteed for "full" LM space, taken as trace of underlying FEM discretization space
   - ☺ Remedied by **reducing LM space** to ensure satisfaction of discrete *inf-sup* condition for (6)
     - ➢ Reduce size of LM space to size $N_{R,\Gamma} < N_{R,1\Gamma} + N_{R,2\Gamma}$, where $N_{R,i\Gamma}$ = # POD modes in $\boldsymbol{\Phi}_{i,\Gamma}$
     - ➢ For now, approximate $\boldsymbol{\lambda} \approx \boldsymbol{\Phi}_{\mathrm{LM}}\hat{\boldsymbol{\lambda}}$ where $\boldsymbol{\Phi}_{\mathrm{LM}} = \boldsymbol{\Phi}_{i,\Gamma}$ for $i = 1,2$, so that $N_{R,\Gamma} = N_{R,i\Gamma}$

ROM-ROM Coupling: Split Bases & Reduced LM Spaces

- Consider two **separate expansions** for **interface** and **interior DOFs** for $i = 1,2$:

$$\boldsymbol{c}_{i,0}(t) \approx \tilde{\boldsymbol{c}}_{i,0}(t) := \bar{\boldsymbol{c}}_{i,0} + \boldsymbol{\Phi}_{i,0}\hat{\boldsymbol{c}}_{i,0}(t), \qquad \boldsymbol{c}_{i,\Gamma}(t) \approx \tilde{\boldsymbol{c}}_{i,\Gamma}(t) := \bar{\boldsymbol{c}}_{i,\Gamma} + \boldsymbol{\Phi}_{i,\Gamma}\hat{\boldsymbol{c}}_{i,\Gamma}(t)$$

- Substituting above expansions into (2) and projecting equations onto reduced bases gives system of the form:

Reduced LM space also helps **prevent over-constraining** for **full subdomain basis** implementation.

$$\begin{pmatrix} \widetilde{\boldsymbol{M}}_{1,\Gamma} & \widetilde{\boldsymbol{M}}_{1,\Gamma 0} & \boldsymbol{0} & \boldsymbol{0} & \widetilde{\boldsymbol{G}}_1^T \\ \widetilde{\boldsymbol{M}}_{1,0\Gamma} & \widetilde{\boldsymbol{M}}_{1,0} & \boldsymbol{0} & \boldsymbol{0} & \boldsymbol{0} \\ \boldsymbol{0} & \boldsymbol{0} & \widetilde{\boldsymbol{M}}_{2,\Gamma} & \widetilde{\boldsymbol{M}}_{2,\Gamma 0} & -\widetilde{\boldsymbol{G}}_2^T \\ \boldsymbol{0} & \boldsymbol{0} & \widetilde{\boldsymbol{M}}_{2,0\Gamma} & \widetilde{\boldsymbol{M}}_{2,0} & \boldsymbol{0} \\ \widetilde{\boldsymbol{G}}_1 & \boldsymbol{0} & -\widetilde{\boldsymbol{G}}_2 & \boldsymbol{0} & \boldsymbol{0} \end{pmatrix} \begin{pmatrix} \dot{\hat{\boldsymbol{c}}}_{1,\Gamma} \\ \dot{\hat{\boldsymbol{c}}}_{1,0} \\ \dot{\hat{\boldsymbol{c}}}_{2,\Gamma} \\ \dot{\hat{\boldsymbol{c}}}_{1,0} \\ \hat{\boldsymbol{\lambda}} \end{pmatrix} = \begin{pmatrix} \boldsymbol{s}_{1,\Gamma} \\ \boldsymbol{s}_{1,0} \\ \boldsymbol{s}_{2,\Gamma} \\ \boldsymbol{s}_{2,0} \\ \boldsymbol{0} \end{pmatrix}$$

Split basis + reduced LM space guarantees ROM-ROM coupling has **non-singular dual Schur complement***.

Online ROM-ROM IVR Solution Algorithm with Split Bases & Reduced LM Spaces: at each time step t^n

- Use $\hat{\boldsymbol{c}}_{i,0}^n$ and $\hat{\boldsymbol{c}}_{i,\Gamma}^n$ to compute updated RHS $\boldsymbol{s}_{i,0}^n$ and $\boldsymbol{s}_{i,\Gamma}^n$ for $i = 1,2$.
- Define $\widetilde{\boldsymbol{M}}_{i,jk} := \boldsymbol{\Phi}_{i,j}^T \boldsymbol{M}_{i,jk} \boldsymbol{\Phi}_{i,k}$, $\widetilde{\boldsymbol{G}}_i := \boldsymbol{\Phi}_{\mathrm{LM}}^T \boldsymbol{G}_i \boldsymbol{\Phi}_{i,\Gamma}$, $\widetilde{\boldsymbol{P}}_i := \widetilde{\boldsymbol{M}}_{i,\Gamma} - \widetilde{\boldsymbol{M}}_{i,\Gamma 0}\boldsymbol{M}_{i,0}^{-1}\widetilde{\boldsymbol{M}}_{i,\Gamma 0}$ for $\{j,k\} \in \{0,\Gamma\}$ and solve:

$$(\widetilde{\boldsymbol{G}}_1\widetilde{\boldsymbol{P}}_1^{-1}\widetilde{\boldsymbol{G}}_1^T + \widetilde{\boldsymbol{G}}_2\widetilde{\boldsymbol{P}}_2^{-1}\widetilde{\boldsymbol{G}}_2^T)\hat{\boldsymbol{\lambda}}^n = \widetilde{\boldsymbol{G}}_1\widetilde{\boldsymbol{P}}_1^{-1}\left(\boldsymbol{s}_{1,\Gamma}^n - \widetilde{\boldsymbol{M}}_{1,\Gamma 0}\boldsymbol{M}_{1,0}^{-1}\boldsymbol{s}_{1,0}^n\right) - \widetilde{\boldsymbol{G}}_2\widetilde{\boldsymbol{P}}_2^{-1}\left(\boldsymbol{s}_{2,\Gamma}^n - \widetilde{\boldsymbol{M}}_{2,\Gamma 0}\boldsymbol{M}_{2,0}^{-1}\boldsymbol{s}_{2,0}^n\right)$$

- Advance the following systems forward in time:

$$\begin{pmatrix} \widetilde{\boldsymbol{M}}_{i,\Gamma} & \widetilde{\boldsymbol{M}}_{i,\Gamma 0} \\ \widetilde{\boldsymbol{M}}_{i,\Gamma 0} & \widetilde{\boldsymbol{M}}_{i,\Gamma} \end{pmatrix} \begin{pmatrix} \dot{\hat{\boldsymbol{c}}}_{i,\Gamma}^n \\ \dot{\hat{\boldsymbol{c}}}_{i,0}^n \end{pmatrix} = \begin{pmatrix} \boldsymbol{s}_{i,\Gamma}^n + (-1)^i \widetilde{\boldsymbol{G}}_i^T \hat{\boldsymbol{\lambda}}^n \\ \boldsymbol{s}_{i,0}^n \end{pmatrix}$$

* If conditions in [Peterson *et al.*, 2019] are satisfied for underlying FOM-FOM coupling.

Outline

1. The Alternating Schwarz Method for FOM*-ROM# and ROM-ROM Coupling
   - Method Formulation
   - ROM Construction and Implementation
   - Numerical Example
2. **A Lagrange Multiplier-based Partitioned Scheme for FOM-ROM and ROM-ROM Coupling**
   - Method Formulation
   - ROM Construction and Implementation
   - **Numerical Example**
3. Summary and Comparison of Methods
4. Future Work

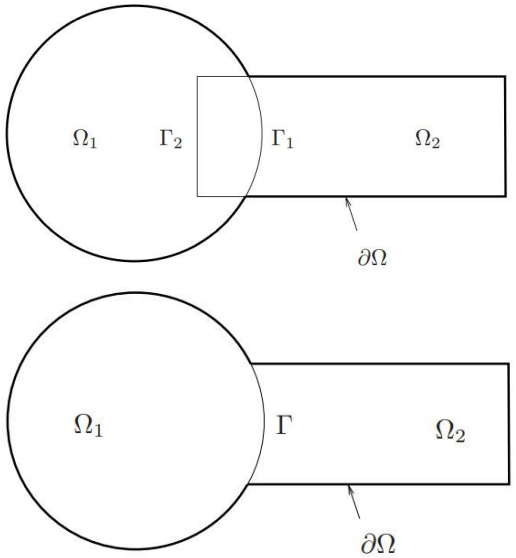

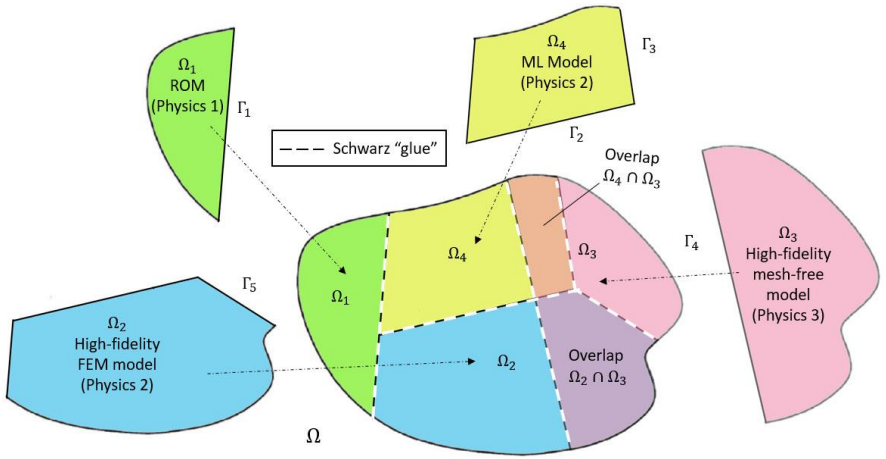

*Full-Order Model. #Reduced Order Model.

Numerical Results: 2D High Peclet Advection-Diffusion Problem

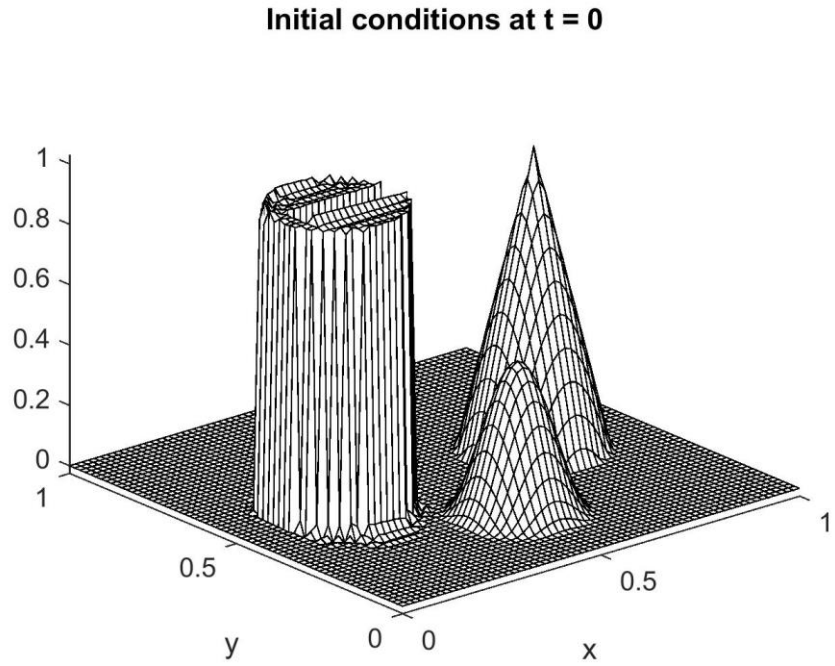

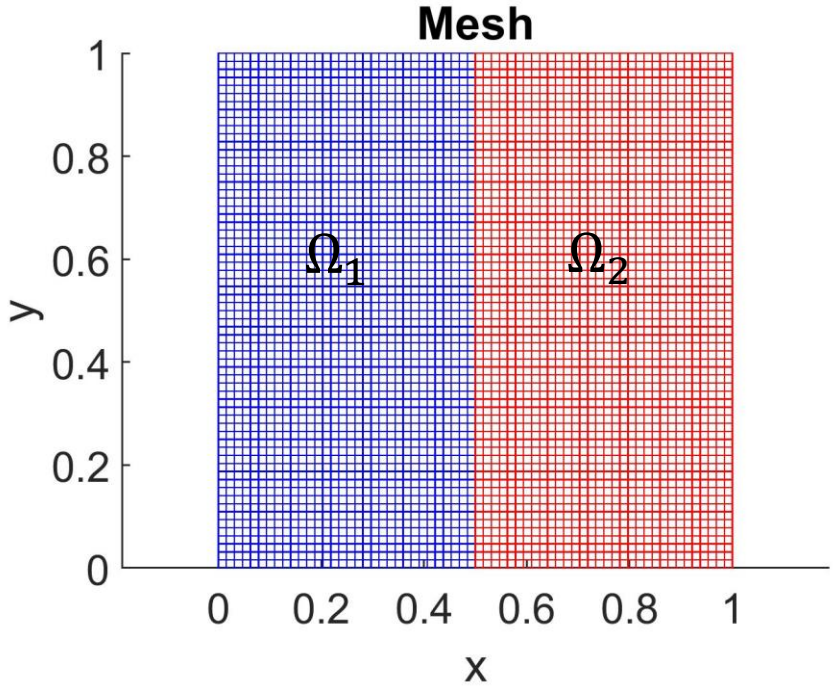

Figure top left: initial condition.
Figure top right: mesh and DD.

- Cone, cylinder and smooth hump **initial condition** (top left figure)
- **Rotating advection field** $(0.5 - y, x - 0.5)$ for one full rotation
- Snapshots from **monolithic FEM** on Ω with 4225 DOFs ($h = \frac{1}{64}$)
- **Two subdomains**, as shown in top right figure with 2145 DOFs/subdomain
- **High Peclet regime**: $\kappa_i = 10^{-5}$, for $k = 1,2$
- **Homogeneous** Dirichlet BCs
- **IMEX** version of **Crank-Nicholson** (treating LM explicitly), with snapshot time step $\Delta t_s = 6.734 \times 10^{-3}$

Numerical Results: 2D High Peclet Advection-Diffusion Problem

- **Reproductive POD/Galerkin ROM-ROM coupling** case test case
- **50 modes** capture 99.999% of the **snapshot energy** (figure right)
- For split basis ROM-ROM coupling, ~20 interior modes are needed and only **5 interface modes** are needed to capture 99% of their respective snapshot energies
- **Full LM (fLM) space** has dimension of 63 (# nodes on Γ) .
- **Reduced LM (rLM) space** has dimension:

$$N_{R,i\Gamma} = \min\left\{\frac{1}{4}N_{R,i0}, 63\right\}$$

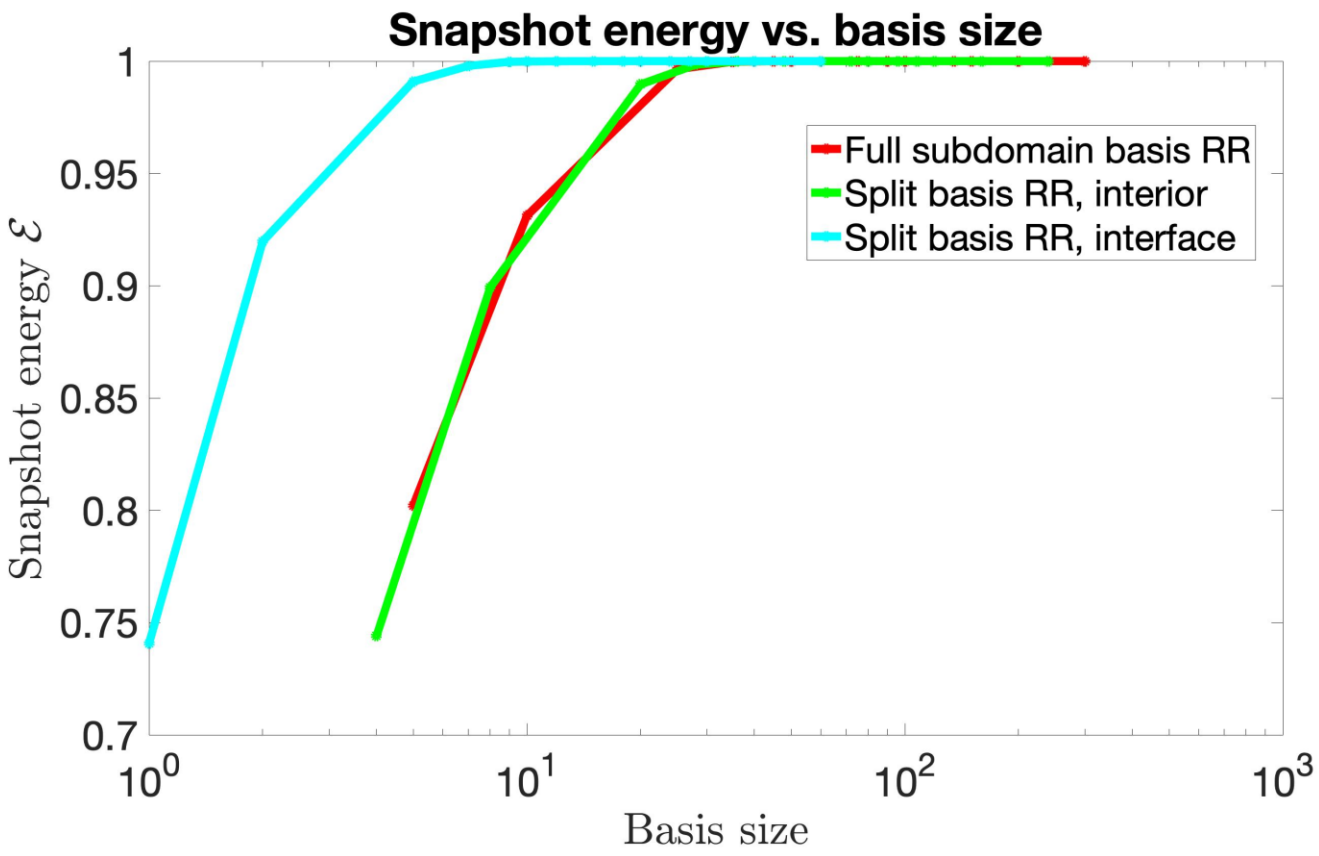

Figure above: snapshot energies as a function of the basis size for full subdomain basis and split basis approach. RR = ROM-ROM coupling.

Numerical Results: 2D High Peclet Advection-Diffusion Problem

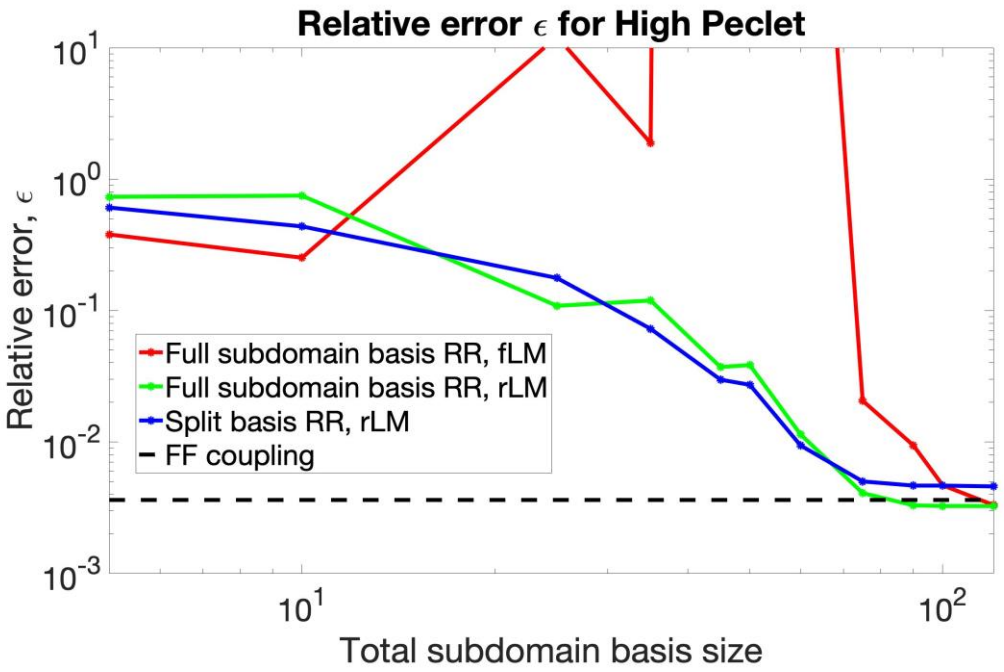

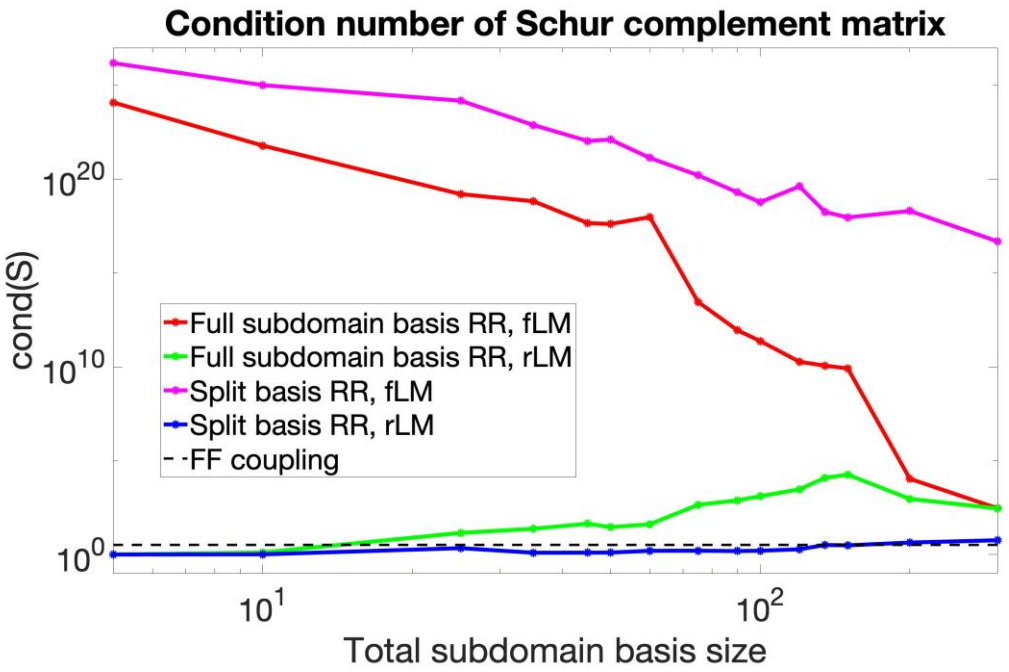

Figure above left: relative errors at final time 2π w.r.t. single-domain FOM solution.
Figure above right: Schur complement condition numbers for ROM-ROM (RR) and FOM-FOM (FF) couplings.

- **Instabilities** and **inaccuracies** observed for full subdomain ROM-ROM coupling with **full LM (fLM) space**
- Errors for **split basis ROM-ROM coupling** with **full** and **reduced LM (rLM) spaces identical** to machine precision
- **Full subdomain** ROM-ROM coupling with **rLM space** achieves **best accuracy**.
- Using **rLM space** improves **condition number**
- **Conditioning** of the Schur complement for **split basis ROM-ROM** formulation is essentially the **same** as for the **FOM-FOM coupling** (proven to be well-conditioned in [Peterson *et al*. 2019])

Numerical Results: 2D High Peclet Advection-Diffusion Problem

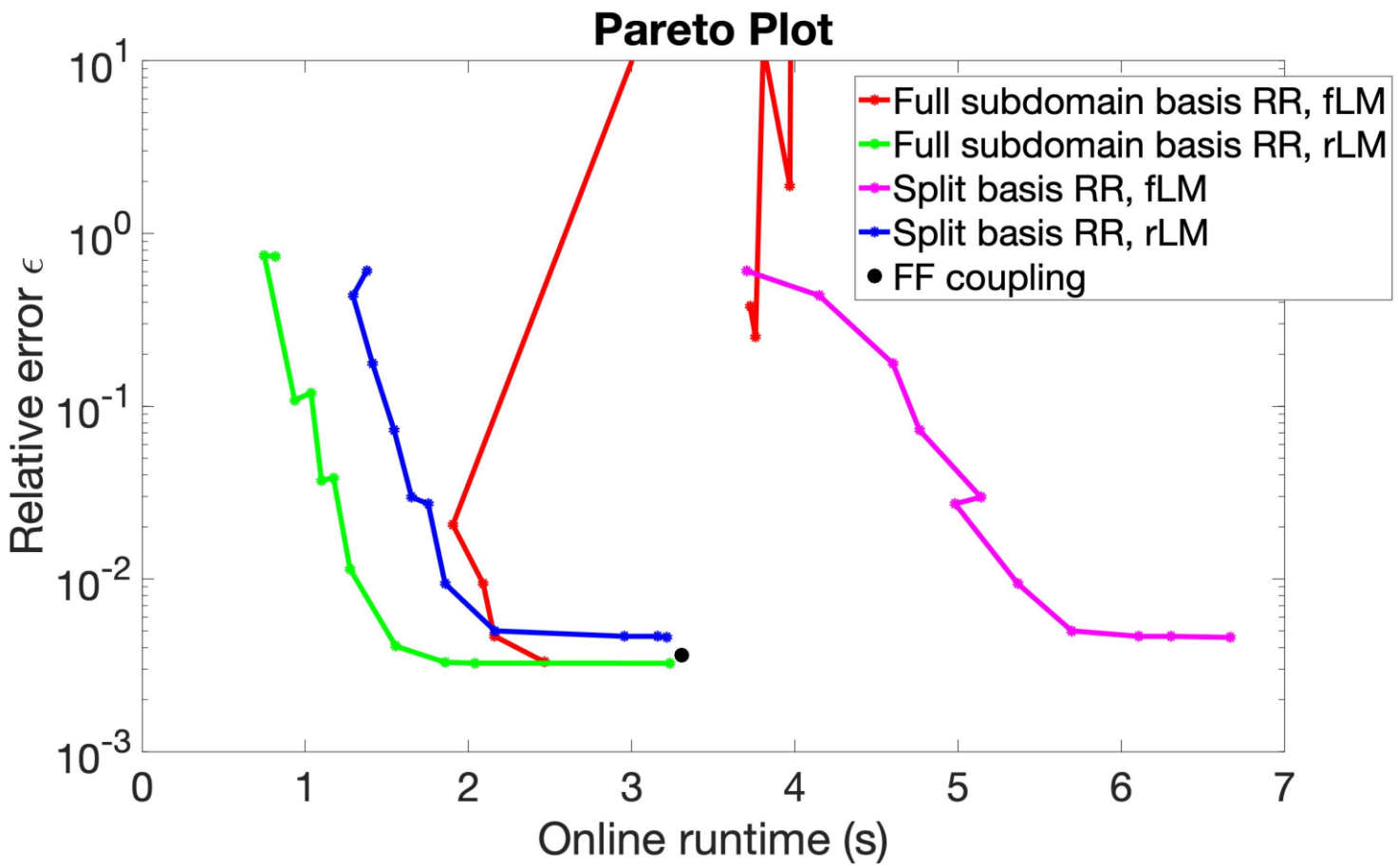

- Each coupling is capable of attaining an **error** on the **order of the relative error for the FOM-FOM coupling**
- **Reduced LM** variants achieve **optimal errors** in **less time**
- **Full subdomain basis ROM-ROM** with **reduced LM space** is the **coupling of choice** for this problem (but *not* provably stable!)

Figure above: Pareto plot for various couplings evaluated.

Numerical Results: 2D High-Peclet Advection-Diffusion Problem

ROM-ROM, full subdomain basis with fLM

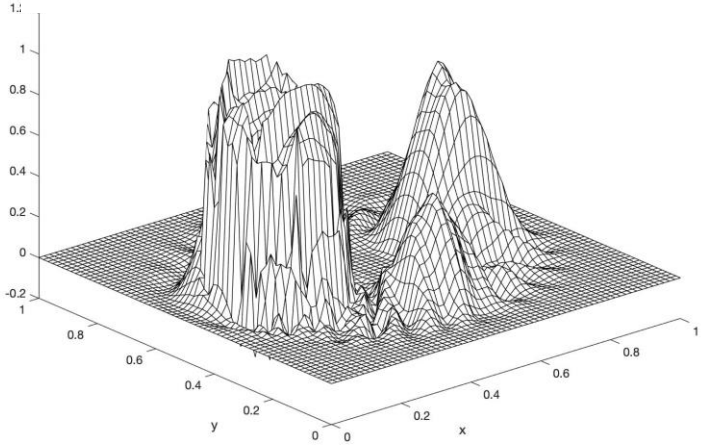

ROM-ROM, full subdomain basis with rLM

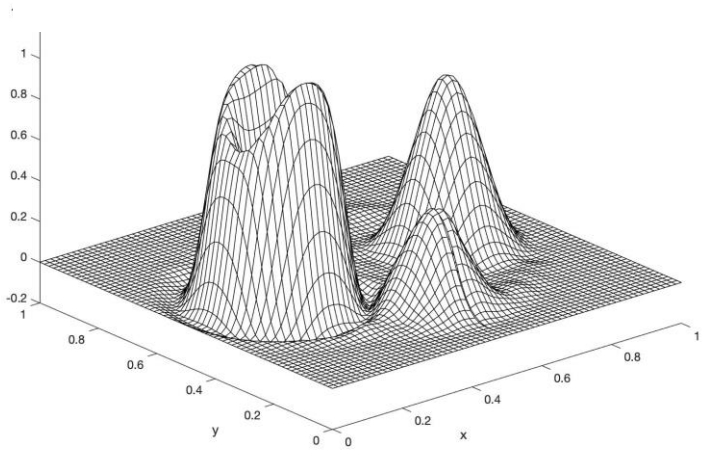

FOM-FOM

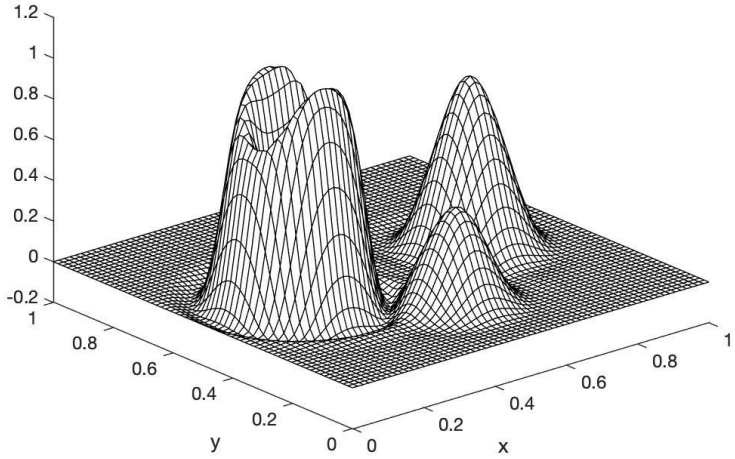

ROM-ROM, split basis with fLM

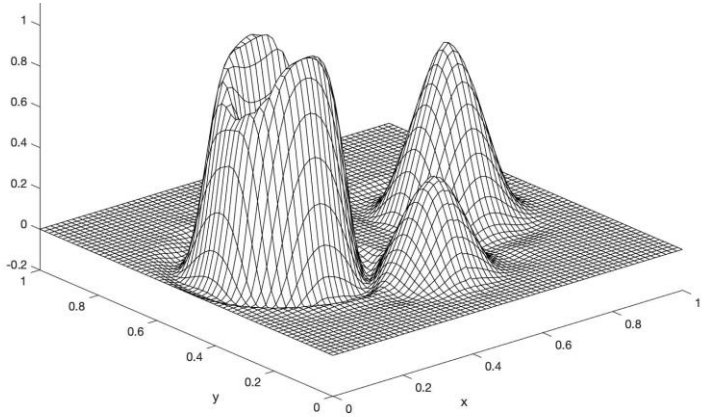

ROM-ROM, split basis with rLM

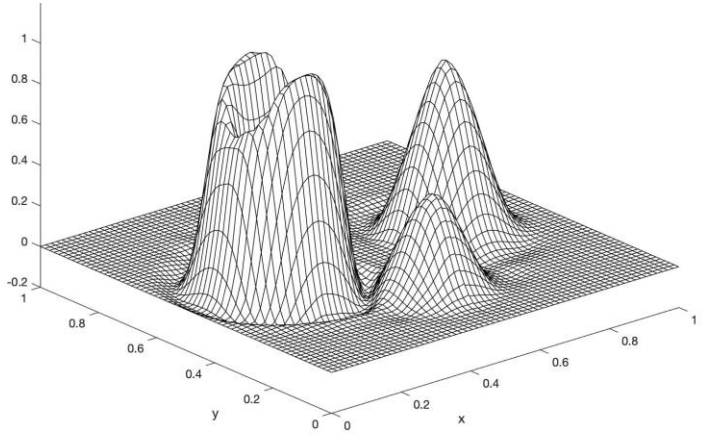

Figures left: solutions produced by various 50 mode **ROM-ROM couplings** compared at final time 2π compared to **FOM-FOM coupling** (*above*)

Numerical Results: 2D High-Peclet Advection-Diffusion Problem

ROM-ROM, full subdomain basis with fLM

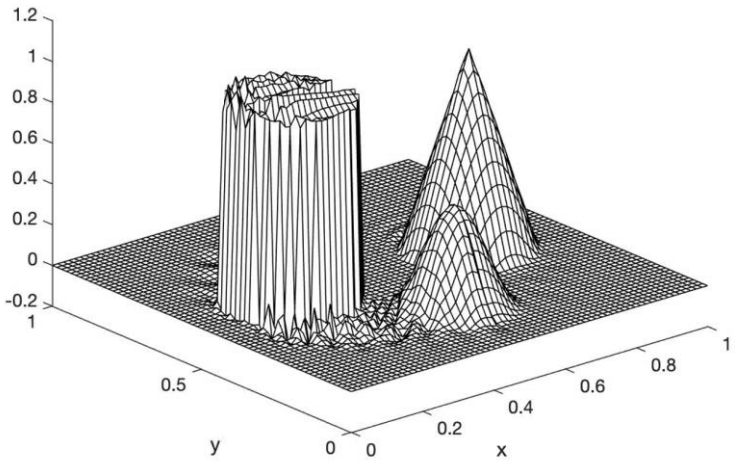

ROM-ROM, full subdomain basis with rLM

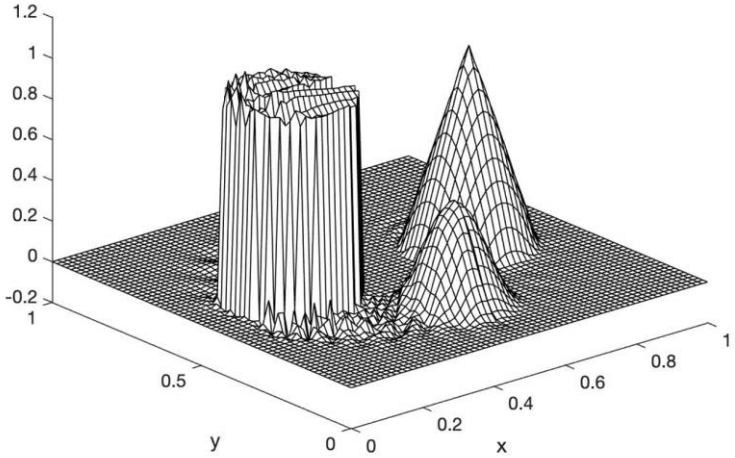

FOM-FOM

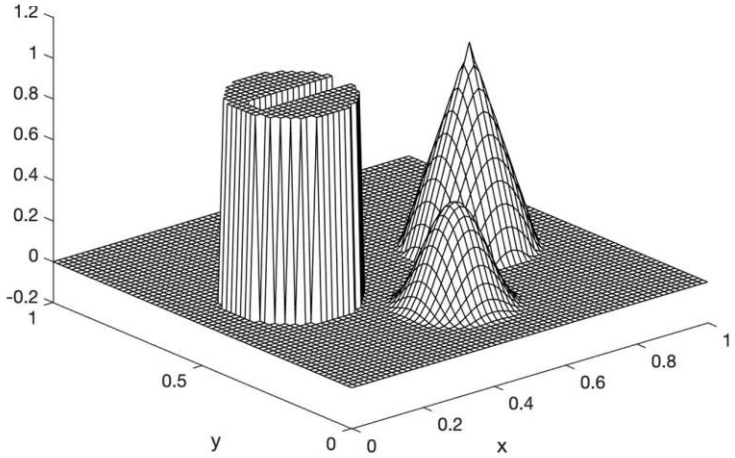

ROM-ROM, split basis with fLM

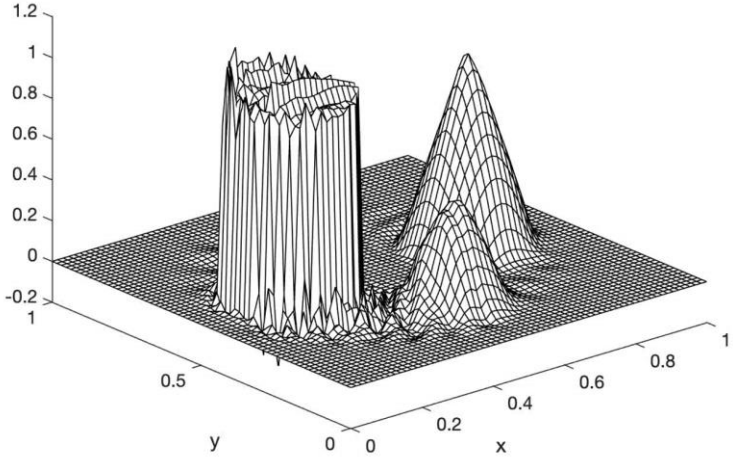

ROM-ROM, split basis with rLM

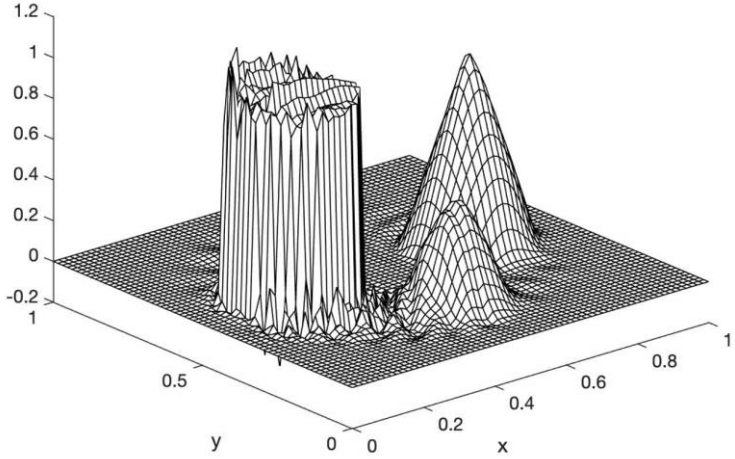

Movies left: solutions produced by various 50 mode **ROM-ROM couplings** compared to **FOM-FOM coupling** (*above*)

Numerical Results: 2D High-Peclet Advection-Diffusion Problem

ROM-ROM, full subdomain basis with fLM

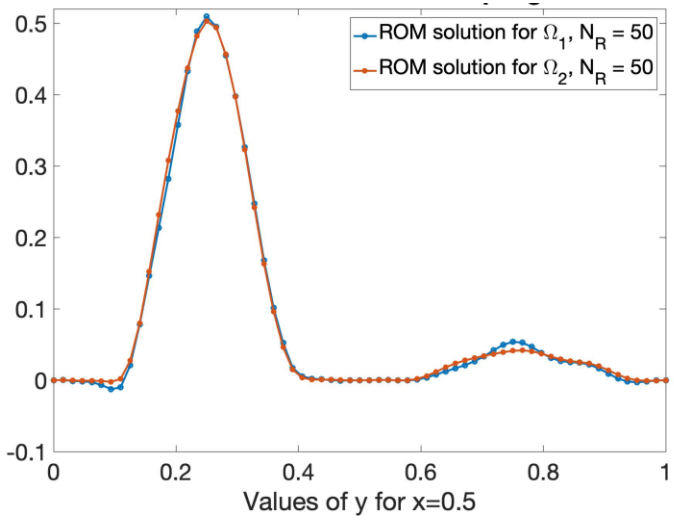

ROM-ROM, full subdomain basis with rLM

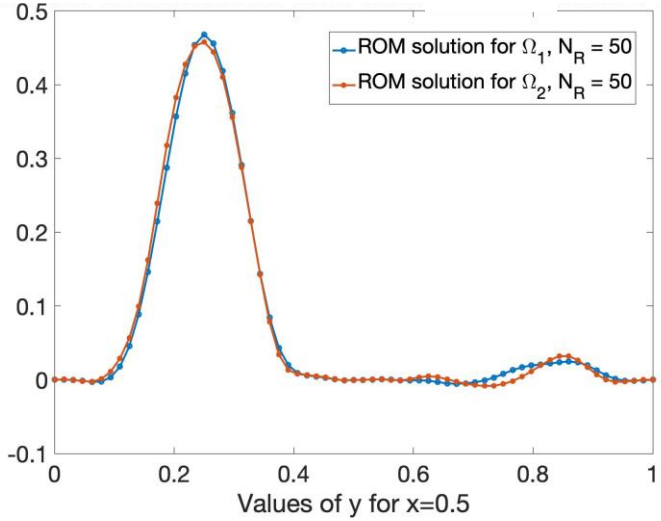

FOM-FOM

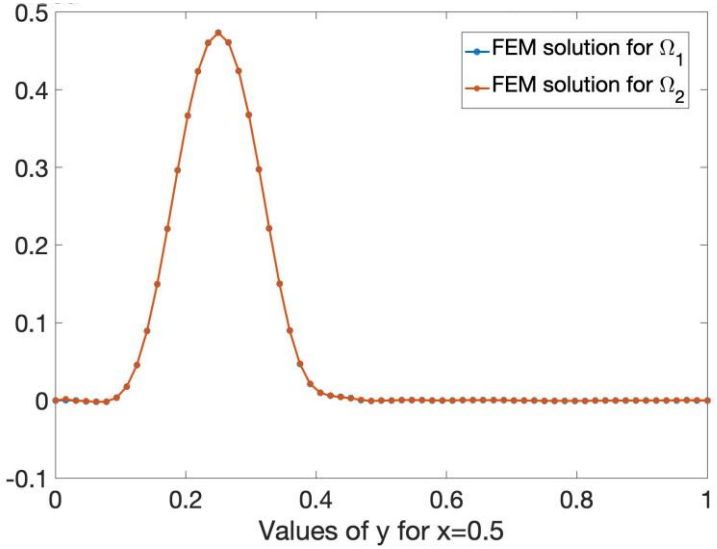

ROM-ROM, split basis with fLM

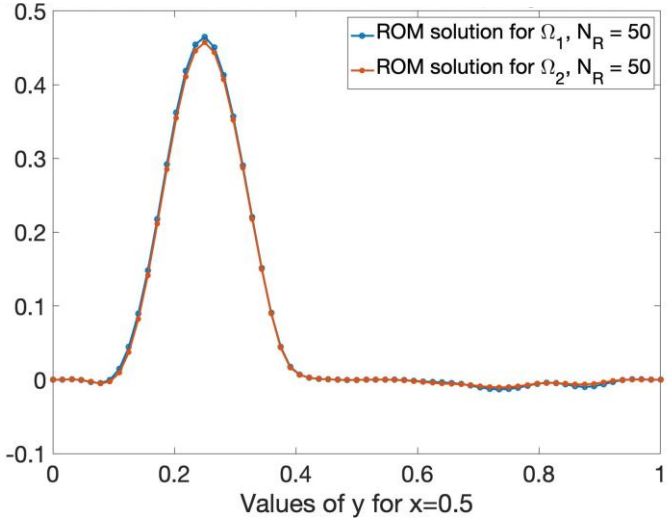

ROM-ROM, split basis with rLM

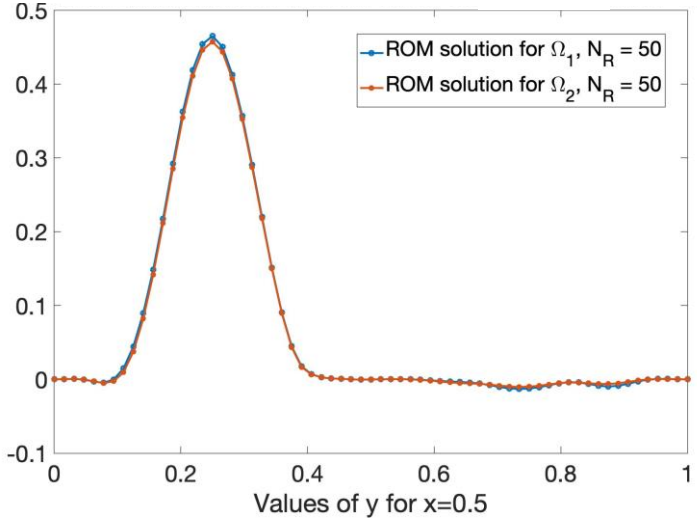

Figures left: solutions at final time 2π along interface Γ for various 50 mode **ROM-ROM couplings** compared to **FOM-FOM coupling** (*above*)

Numerical Results: 2D High-Peclet Advection-Diffusion Problem

ROM-ROM, full subdomain basis with fLM

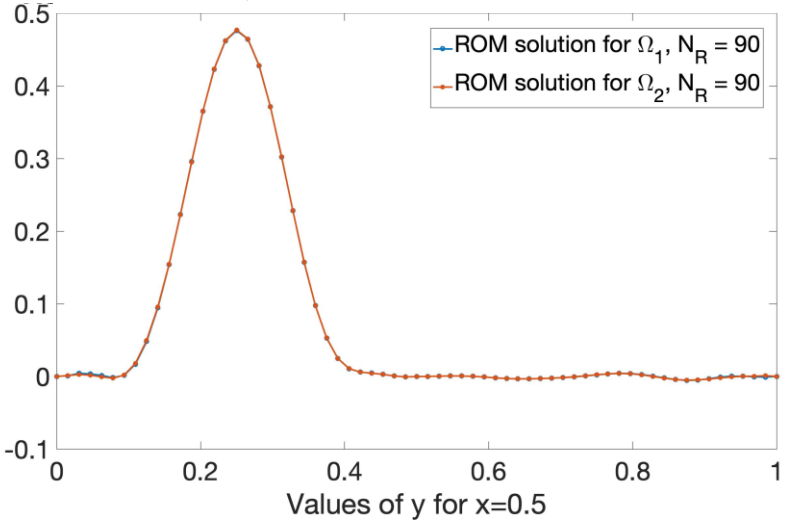

ROM-ROM, full subdomain basis with rLM

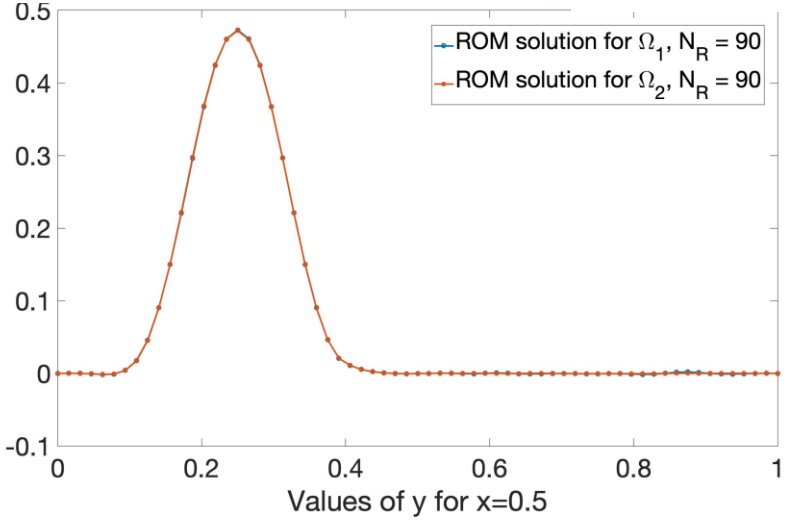

FOM-FOM

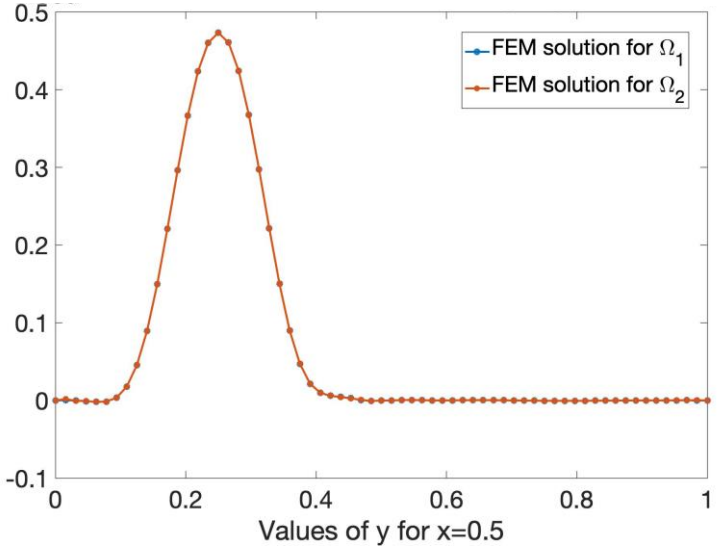

ROM-ROM, split basis with fLM

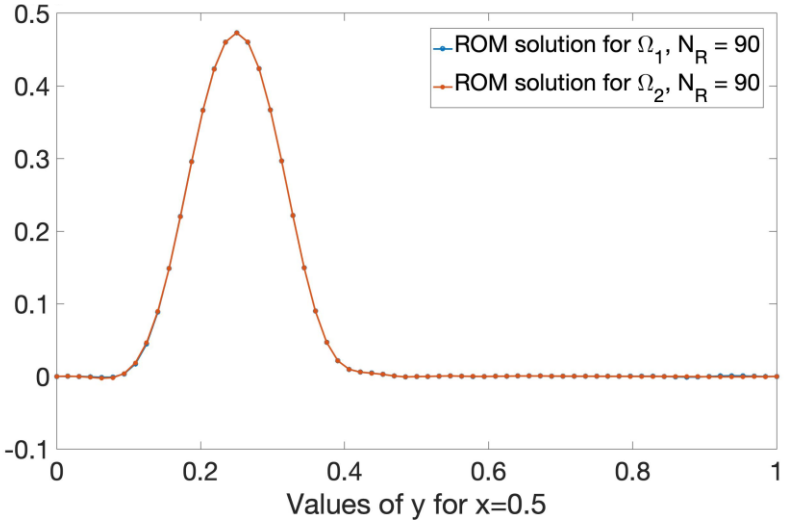

ROM-ROM, split basis with rLM

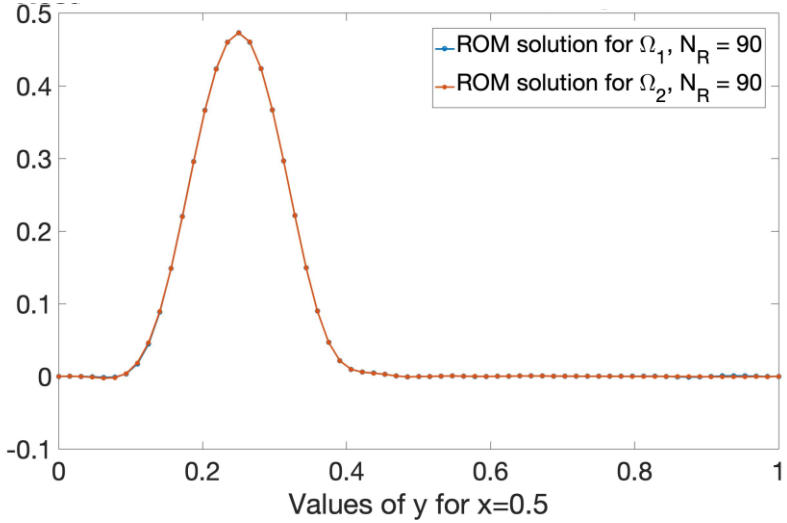

Figures left: solutions at final time 2π along interface Γ for various 90 mode **ROM-ROM couplings** compared to **FOM-FOM coupling** (*above*)

Outline

1. The Alternating Schwarz Method for FOM*-ROM# and ROM-ROM Coupling
   - Method Formulation
   - ROM Construction and Implementation
   - Numerical Example
2. A Lagrange Multiplier-based Partitioned Scheme for FOM-ROM and ROM-ROM Coupling
   - Method Formulation
   - ROM Construction and Implementation
   - Numerical Example
3. **Summary and Comparison of Methods**
4. Future Work

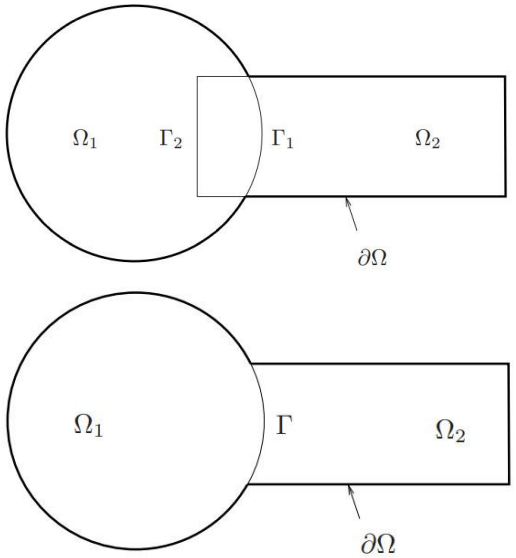

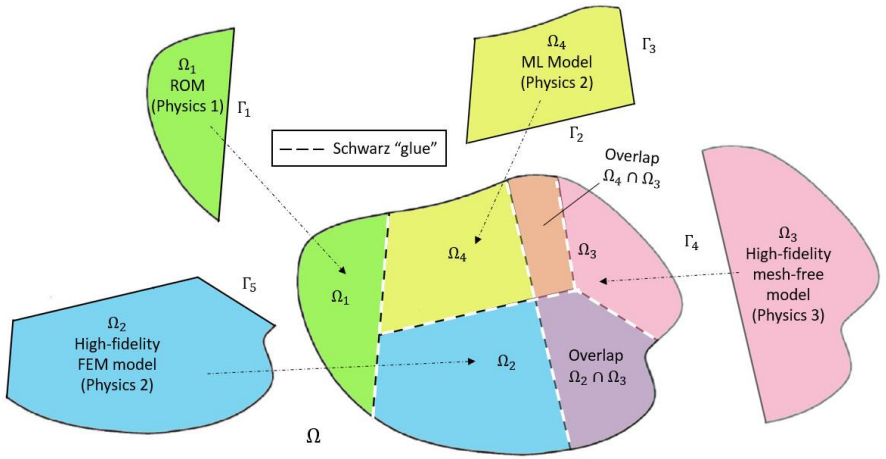

*Full-Order Model. #Reduced Order Model.

Summary

Opinion: *hybrid FOM-ROM models are the future!*

- **Two domain decomposition-based methods** for coupling projection-based ROMs with each other and with conventional full order models have been proposed
  - An **iterative** coupling formulation based on the **Schwarz alternating method** and an **overlapping** or **non-overlapping DD**
  - A **Lagrange multiplier-based** single-pass **(non-iterative)** partitioned **scheme** based on **non-overlapping DD**
- Numerical results show **promise** in using the proposed methods to create **heterogeneous coupled models** comprised of arbitrary combinations of **ROMs** and/or **FOMs**
  - Coupled models can be **computationally efficient** w.r.t analogous FOM-FOM couplings
  - Coupling introduces **no numerical artifacts** into the solution
- FOM-ROM and ROM-ROM have potential to **improve** the **predictive viability** of projection-based ROMs, by enabling the **spatial localization of ROMs** (via DD) and the **online integration of high-fidelity information** into these models (via FOM coupling)

Comparison of Methods

Alternating Schwarz-based Coupling Method

- Can do **FOM-FOM**, **FOM-ROM**, **ROM-ROM** coupling
- **Overlapping** or **non-overlapping** DD
- **Iterative** formulation (less intrusive but likely requires more CPU time)

- Can couple **different mesh resolutions** and **element types**
- Can use **different time-integrators** with **different time-steps** in different subdomains
- **No interface bases** required

- **Sequential subdomain solves** in multiplicative Schwarz variant
  - ➢ **Parallel** subdomain solves possible with **additive Schwarz** variant (not shown)

- **Extensible** in **straightforward** way to **PINN/DMD** data-driven model

Lagrange Multiplier-Based Partitioned Coupling Method

- Can do **FOM-FOM**, **FOM-ROM**, **ROM-ROM** coupling
- **Non-overlapping** DD
- **Monolithic** formulation requiring hybrid formulation (more intrusive but more efficient)

- Can couple **different mesh resolutions** and **element types**
- Can use **different explicit time-integrators** with **different time-steps** in different subdomains
- Provably convergent variant requires **interface bases**
- **Parallel subdomain solves** if explicit or IMEX time-integrator is employed

- **Extensions** to **PINN/DMD** data-driven models are **not obvious**

Outline

1. The Alternating Schwarz Method for FOM*-ROM# and ROM-ROM Coupling
   - Method Formulation
   - ROM Construction and Implementation
   - Numerical Example
2. A Lagrange Multiplier-based Partitioned Scheme for FOM-ROM and ROM-ROM Coupling
   - Method Formulation
   - ROM Construction and Implementation
   - Numerical Example
3. Summary and Comparison of Methods
4. **Future Work**

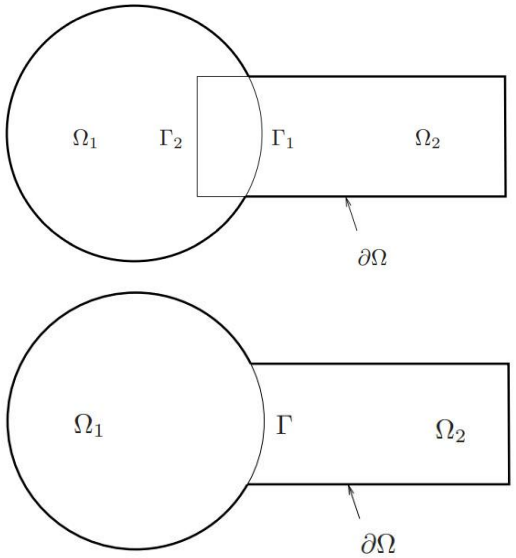

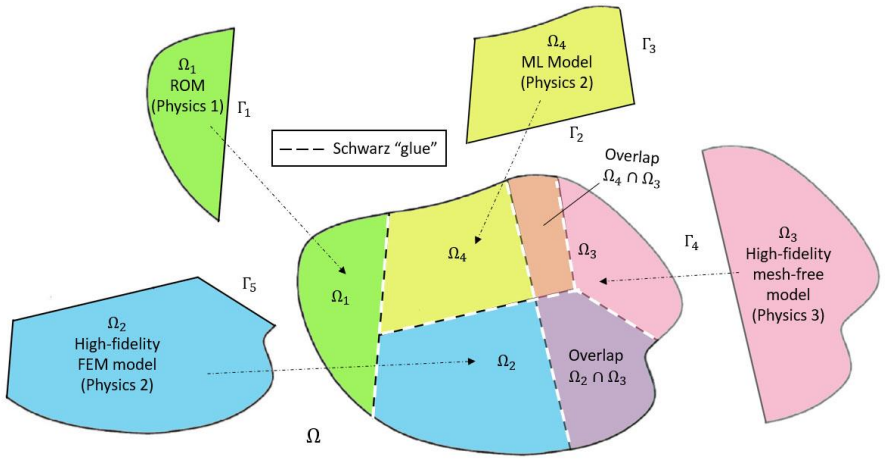

*Full-Order Model. #Reduced Order Model.

Ongoing & Future Work

***Journal articles** on both couplings are currently **in preparation**.*

Alternating Schwarz-based Coupling

- Extension/prototyping on **multi-D problems** (2D Burgers, 2D/3D compressible flow[1], 2D/3D solid mechanics[2])
- Implementation/testing of **additive Schwarz variant**, which admits more parallelism
- **Analysis** of method's convergence for ROM-FOM and ROM-ROM couplings
- **Learning** of **"optimal" transmission conditions** to ensure **structure preservation**
- Extension of coupling methods to coupling of **Physics Informed Neural Networks (PINNs)** (WIP)
- Exploration of **connections** between **iterative Schwarz** and **optimization-based coupling** [Iollo *et al.*, 2022]

Lagrange Multiplier-Based Partitioned Coupling

- **Predictive** regime tests
- Extension to **nonlinear** problems
- Alternate constructions for **reduced Lagrange multiplier space** (e.g., from snapshots of fluxes)

General

- **Numerical comparison** of alternating Schwarz and LM-based partitioned coupling methods
- Development of **smart domain decomposition approaches** based on error indicators, to determine optimal placement of ROM and FOM in a computational domain (including **on-the-fly ROM-FOM switching**)
- Extension of couplings to POD modes built from snapshots on **independently-simulated subdomains**
- Application to **other problems**, including **multi-physics problems** (e.g., FSI, Air-Sea coupling)

[1] https://github.com/ Pressio/pressio-demoapps
[2] https://github.com/lxmota/norma

Team & Acknowledgments

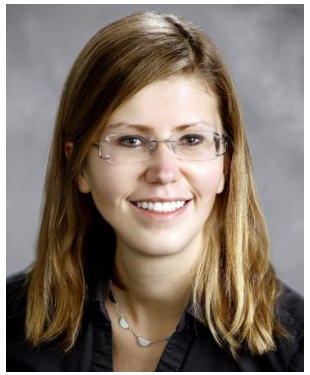

Irina Tezaur

Joshua Barnett

Alejandro Mota

Chris Wentland
New Postdoc

Sandia National Laboratories

LDRD
LABORATORY DIRECTED RESEARCH & DEVELOPMENT

Pavel Bochev

Amy De Castro

Paul Kuberry

U.S. DEPARTMENT OF ENERGY | Office of Science

$$\int \mathcal{M}^2 \mathrm{d}t$$

References

[1] A. Salinger, *et al*. "Albany: Using Agile Components to Develop a Flexible, Generic Multiphysics Analysis Code", *Int. J. Multiscale Comput. Engng*. 14(4) (2016) 415-438.

[2] H. Schwarz. “Über einen Grenzübergang durch alternierendes Verfahren”. In: Vierteljahrsschriftder Naturforschenden Gesellschaft in Zurich 15 (1870), pp. 272–286.

[3] S.L. Sobolev. “Schwarz’s Algorithm in Elasticity Theory”. In: Selected Works of S.L Sobolev. Volume I: equations of mathematical physics, computational mathematics and cubature formulats. Ed. By G.V. Demidenko and V.L. Vaskevich. New York: Springer, 2006.

[4] S. Mikhlin. “On the Schwarz algorithm”. In: Proceedings of the USSR Academy of Sciences 77 (1951), pp. 569–571.

[5] P.L. Lions. “On the Schwarz alternating method I.” In: 1988, First International Symposium on Domain Decomposition methods for Partial Differential Equations, SIAM, Philadelphia.

[6] SIERRA Solid Mechanics Team. Sierra/SM 4.48 User’s Guide. Tech. rep. SAND2018-2961. SNL Report, Oct. 2018.

[7] M. Gunzburger, J. Peterson, J. Shadid. “Reduced-order modeling of time-dependent PDEs with multiple parameters in the boundary data”. *CMAME* 196 (2007) 1030-1047.

[8] C. Hoang, Y. Choi, K. Carlberg. “Domain-decomposition least-squares Petrov–Galerkin (DD-LSPG) nonlinear model reduction”. *CMAME* 384 (2021) 113997.

[9] K. Smetana, T. Taddei. “Localized model reduction for nonlinear elliptic partial differential equations: localized training, partition of unity, and adaptive enrichment”, *ArXiV pre-print*, 2022.

[10] C. Farhat, T. Chapman, P. Avery. “Structure-preserving, stability & accuracy properties of the energy-conserving sampling and weighting method for the hyper reduction of nonlinear FE dynamic models”, *IJNME* 102 (2015) 1077-1110.

[11] M. Bergmann, A. Ferrero, A. Iollo, E. Lombardi, A. Scardigli, H. Telib. “A zonal Galerkin-free POD model for incompressible flows.” *JCP* 352 (2018) 301-325.

References (cont'd)

Email: ikalash@sandia.gov
URL: www.sandia.gov/~ikalash

[12] A. Iollo, G. Sambataro, T. Taddei. "A one-shot overlapping Schwarz method for component-based model reduction: application to nonlinear elasticity", *CMAME* 404 (2023) 115786.

[13] K. Peterson, P. Bochev, P. Kuberry, "Explicit synchronous partitioned algorithms for interface problems based on Lagrange multipliers", *Comput. Math. with Appl.*, 78 (2019), pp. 459–482.

[14] A. Mota, **I. Tezaur**, C. Alleman. "The Schwarz Alternating Method in Solid Mechanics", *Comput. Meth. Appl. Mech. Engng.* 319 (2017), 19-51.

[15] A. Mota, **I. Tezaur**, G. Phlipot. "The Schwarz Alternating Method for Dynamic Solid Mechanics", *Comput. Meth. Appl. Mech. Engng.* 121 (21) (2022) 5036-5071.

[16] J. Hoy, **I. Tezaur**, A. Mota. "The Schwarz alternating method for multiscale contact mechanics". in *Computer Science Research Institute Summer Proceedings 2021*, J.D. Smith and E. Galvan, eds., Technical Report SAND2021-0653R, Sandia National Labs, 360-378, 2021.

[17] J. Barnett, **I. Tezaur**, A. Mota. "The Schwarz alternating method for the seamless coupling of nonlinear reduced order models and full order models", in *Computer Science Research Institute Summer Proceedings 2022*, S.K. Seritan and J.D. Smith, eds., Technical Report SAND2022-10280R, Sandia National Laboratories, 2022, pp. 31-55.

[18] A. de Castro, P. Kuberry, **I. Tezaur**, P. Bochev. "A Novel Partitioned Approach for Reduced Order Model – Finite Element Model (ROM-FEM) and ROM-ROM Coupling", in *Proceedings of the ASCE Earth and Space 18th Biennial International Conference*, 475-489, 2023.

This talk

[19] A. de Castro, P. Kuberry, **I. Tezaur**, P. Bochev. "A synchronous partitioned scheme for coupled reduced order models based on separate reduced order bases for interface and interior variables", in *Computer Science Research Institute Summer Proceedings 2022*,. S. Seritan and J.D. Smith, eds., Technical Report SAND 2022-10280R, Sandia National Laboratories, 2022, pp. 78-92.

References (cont'd)

[20] J.M. Connors, K. Sockwell, A Multirate Discontinuous-Galerkin-in-Time Framework for Interface-Coupled Problems, *SIAM Journal on Numerical Analysis*, 5(60), 2373-2404, 2022.

[21] K. Sockwell, K. Peterson, P. Kuberry, P. Bochev, Interface Flux Recovery Framework for Constructing Partitioned Heterogeneous Time-Integration Methods, to appear.

Start of Backup Slides

Numerical Example: 1D Dynamic Wave Propagation Problem

- **Basis sizes** M_1 and M_2 vary from 60 to 300
  - Larger ROM used in Ω_1, since solution has **steeper gradient** here
- For couplings involving FOM and ROM/HROM, **FOM** is placed in $\boldsymbol{\Omega_1}$, since solution has steeper gradient here
- **Non-negative least-squares optimization problem** for ECSW weights solved using MATLAB's lsqnonneg function with early termination criterion (solution step-size tolerance = 10^{-4})
  - Ensures all HROMs have **consistent termination criterion** w.r.t. MATLAB implementation
  - However, **relative error tolerance** of selected reduced elements will differ
    - Switching to termination criterion based on relative error is work in progress and expected to improve HROM results
  - Convergence tolerance determines **size of sample mesh** $N_{e,i}$
  - **Boundary points** must be in sample mesh for application of Schwarz BC

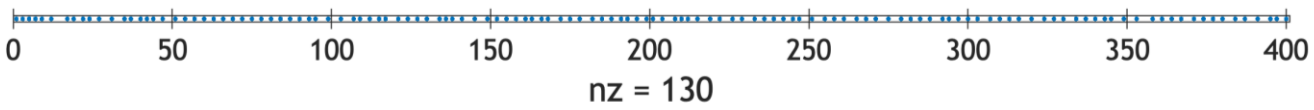

Figure left: sample sample mesh for 1D wave propagation problem

J. Barnett, I. Tezaur, A. Mota. "The Schwarz alternating method for the seamless coupling of nonlinear reduced order models and full order models", in Computer Science Research Institute Summer Proceedings 2022, S.K. Seritan and J.D. Smith, eds., Technical Report SAND2022-10280R, Sandia National Laboratories, 2022, pp. 31-55. (https://arxiv.org/abs/2210.12551)

Theoretical Foundation

Using the Schwarz alternating as a ***discretization method*** for PDEs is natural idea with a sound ***theoretical foundation***.

- **S.L. Sobolev (1936):** posed Schwarz method for ***linear elasticity*** in variational form and ***proved method's convergence*** by proposing a convergent sequence of energy functionals.
- **S.G. Mikhlin (1951):** ***proved convergence*** of Schwarz method for general linear elliptic PDEs.
- **P.-L. Lions (1988):** studied convergence of Schwarz for ***nonlinear monotone elliptic problems*** using max principle***.***
- **A. Mota, I. Tezaur, C. Alleman (2017):** proved ***convergence*** of the alternating Schwarz method for ***finite deformation quasi-static nonlinear PDEs*** (with energy functional $\boldsymbol{\Phi}[\boldsymbol{\varphi}]$) with a ***geometric convergence rate.***

$$\boldsymbol{\Phi}[\boldsymbol{\varphi}] = \int_B A(\boldsymbol{F},\boldsymbol{Z})\, dV - \int_B \boldsymbol{B}\cdot\boldsymbol{\varphi}\, dV$$
$$\nabla\cdot\boldsymbol{P} + \boldsymbol{B} = \boldsymbol{0}$$

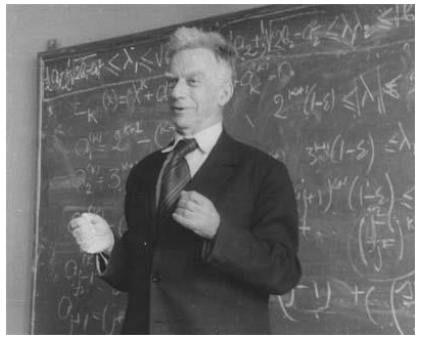

S.L. Sobolev (1908 – 1989)

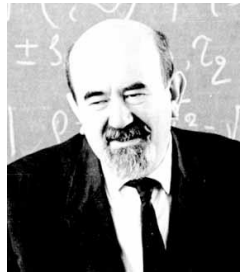

S.G. Mikhlin (1908 – 1990)

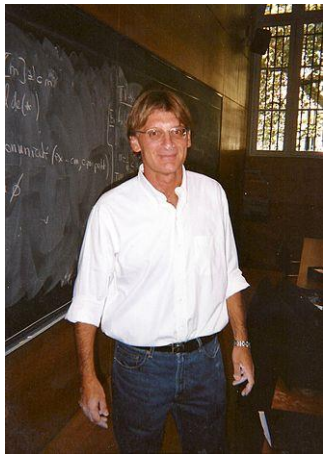

P.- L. Lions (1956-)

A. Mota, I. Tezaur, C. Alleman

Convergence Proof*

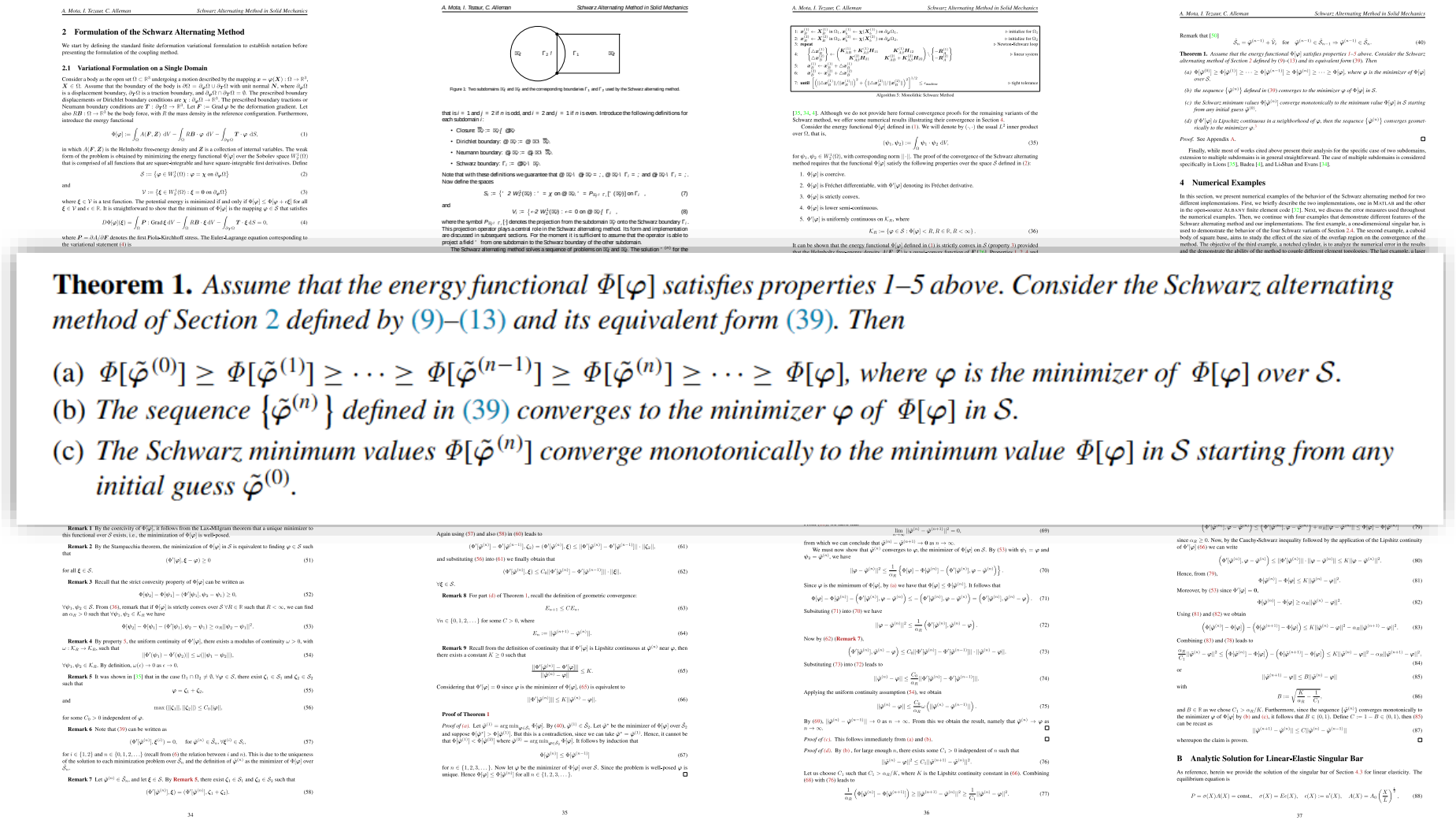

Theorem 1. *Assume that the energy functional $\Phi[\varphi]$ satisfies properties 1–5 above. Consider the Schwarz alternating method of Section 2 defined by (9)–(13) and its equivalent form (39). Then*

(a) $\Phi[\tilde{\varphi}^{(0)}] \geq \Phi[\tilde{\varphi}^{(1)}] \geq \cdots \geq \Phi[\tilde{\varphi}^{(n-1)}] \geq \Phi[\tilde{\varphi}^{(n)}] \geq \cdots \geq \Phi[\varphi]$, *where φ is the minimizer of $\Phi[\varphi]$ over $\mathcal{S}$.*

(b) *The sequence $\{\tilde{\varphi}^{(n)}\}$ defined in (39) converges to the minimizer φ of $\Phi[\varphi]$ in $\mathcal{S}$.*

(c) *The Schwarz minimum values $\Phi[\tilde{\varphi}^{(n)}]$ converge monotonically to the minimum value $\Phi[\varphi]$ in $\mathcal{S}$ starting from any initial guess $\tilde{\varphi}^{(0)}$.*

A. Mota, I. Tezaur, C. Alleman — Schwarz Alternating Method in Solid Mechanics

2 Formulation of the Schwarz Alternating Method

We start by defining the standard finite deformation variational formulation to establish notation before presenting the formulation of the coupling method.

2.1 Variational Formulation on a Single Domain

Consider a body as the open set $\Omega \subset \mathbb{E}^3$ undergoing a motion described by the mapping $\boldsymbol{x} = \boldsymbol{\varphi}(\boldsymbol{X}) : \Omega \to \mathbb{E}^3$, $\boldsymbol{X} \in \Omega$. Assume that the boundary of the body is $\partial\Omega = \partial_\varphi\Omega \cup \partial_T\Omega$ with unit normal $\boldsymbol{N}$, where $\partial_\varphi\Omega$ is a displacement boundary, $\partial_T\Omega$ is a traction boundary, and $\partial_\varphi\Omega \cap \partial_T\Omega = \emptyset$. The prescribed boundary displacements or Dirichlet boundary conditions are $\boldsymbol{\chi} : \partial_\varphi\Omega \to \mathbb{E}^3$. The prescribed boundary tractions or Neumann boundary conditions are $\boldsymbol{T} : \partial_T\Omega \to \mathbb{E}^3$. Let $\boldsymbol{F} := \mathrm{Grad}\,\boldsymbol{\varphi}$ be the deformation gradient. Let also $R\boldsymbol{B} : \Omega \to \mathbb{E}^3$ be the body force, with R the mass density in the reference configuration. Furthermore, introduce the energy functional

$$\Phi[\boldsymbol{\varphi}] := \int_\Omega A(\boldsymbol{F}, \boldsymbol{Z})\, \mathrm{d}V - \int_\Omega R\boldsymbol{B} \cdot \boldsymbol{\varphi}\, \mathrm{d}V - \int_{\partial_T\Omega} \boldsymbol{T} \cdot \boldsymbol{\varphi}\, \mathrm{d}S, \tag{1}$$

in which $A(\boldsymbol{F}, \boldsymbol{Z})$ is the Helmholtz free-energy density and $\boldsymbol{Z}$ is a collection of internal variables. The weak form of the problem is obtained by minimizing the energy functional $\Phi[\boldsymbol{\varphi}]$ over the Sobolev space $W_2^1(\Omega)$ that is comprised of all functions that are square-integrable first derivatives. Define

$$\mathcal{S} := \{\boldsymbol{\varphi} \in W_2^1(\Omega) : \boldsymbol{\varphi} = \boldsymbol{\chi} \text{ on } \partial_\varphi\Omega\} \tag{2}$$

and

$$\mathcal{V} := \{\boldsymbol{\xi} \in W_2^1(\Omega) : \boldsymbol{\xi} = \boldsymbol{0} \text{ on } \partial_\varphi\Omega\} \tag{3}$$

where $\boldsymbol{\xi} \in \mathcal{V}$ is a test function. The potential energy is minimized if and only if $\Phi[\boldsymbol{\varphi} + \epsilon\boldsymbol{\xi}]$ for all $\boldsymbol{\xi} \in \mathcal{V}$ and $\epsilon \in \mathbb{R}$. It is straightforward to show that the minimum of $\Phi[\boldsymbol{\varphi}]$ is the mapping $\boldsymbol{\varphi} \in \mathcal{S}$ that satisfies

$$D\Phi[\boldsymbol{\varphi}](\boldsymbol{\xi}) = \int_\Omega \boldsymbol{P} : \mathrm{Grad}\,\boldsymbol{\xi}\, \mathrm{d}V - \int_\Omega R\boldsymbol{B} \cdot \boldsymbol{\xi}\, \mathrm{d}V - \int_{\partial_T\Omega} \boldsymbol{T} \cdot \boldsymbol{\xi}\, \mathrm{d}S = 0, \tag{4}$$

where $\boldsymbol{P} = \partial A/\partial \boldsymbol{F}$ denotes the first Piola-Kirchhoff stress. The Euler-Lagrange equation corresponding to the variational statement (4) is

A. Mota, I. Tezaur, C. Alleman — Schwarz Alternating Method in Solid Mechanics

Figure 1: Two subdomains Ω_I and Ω_{II} and the corresponding boundaries Γ_I and Γ_{II} used by the Schwarz alternating method.

that is $i = 1$ and $j = 2$ if n is odd, and $i = 2$ and $j = 1$ if n is even. Introduce the following definitions for each subdomain i:

- Closure: $\overline{\Omega}_i := \Omega_i \cup \partial\Omega_i$.
- Dirichlet boundary: $\partial\Omega_i := \partial\Omega_i \cap \partial\Omega$.
- Neumann boundary: $\partial\Omega_i := \partial\Omega_i \cap \partial\Omega$.
- Schwarz boundary: $\Gamma_i := \partial\Omega_i \setminus \partial\Omega$.

Note that with these definitions we guarantee that $\partial\Omega_I \cup \partial\Omega_I = \partial\Omega_{II} \cup \partial\Omega_{II} = \partial\Omega$, $\partial\Omega_I \setminus \Gamma_I = \partial\Omega_{II} \setminus \Gamma_{II} = \partial\Omega$, and $\partial\Omega_I \setminus \Gamma_I = \partial\Omega_{II} \setminus \Gamma_{II}$. Now define the spaces

$$\mathcal{S}_i := \{\boldsymbol{\varphi}^i \in W_2^1(\Omega_i) : \boldsymbol{\varphi}^i = \boldsymbol{\chi} \text{ on } \partial\Omega_i,\ \boldsymbol{\varphi}^i = P_{\Omega_j \to \Gamma_i}[\boldsymbol{\varphi}^j] \text{ on } \Gamma_i\} \tag{7}$$

and

$$\mathcal{V}_i := \{\boldsymbol{\xi}^i \in W_2^1(\Omega_i) : \boldsymbol{\xi}^i = \boldsymbol{0} \text{ on } \partial\Omega_i,\ \boldsymbol{\xi}^i = P_{\Omega_j \to \Gamma_i}[\boldsymbol{\xi}^j] \text{ on } \Gamma_i\} \tag{8}$$

where the symbol $P_{\Omega_j \to \Gamma_i}[\cdot]$ denotes the projection from the subdomain Ω_j onto the Schwarz boundary Γ_i. This projection operator plays a central role in the Schwarz alternating method. Its form and implementation are discussed in subsequent sections. For the moment it is sufficient to assume that the operator is able to project a field $\boldsymbol{\varphi}^j$ from one subdomain to the Schwarz boundary of the other subdomain.

The Schwarz alternating method solves a sequence of problems on Ω_I and Ω_{II}. The solution $\boldsymbol{\varphi}^{(n)}$ for the

A. Mota, I. Tezaur, C. Alleman — Schwarz Alternating Method in Solid Mechanics

Algorithm 5: Monolithic Schwarz Method

[35, 34, 4]. Although we do not provide here formal convergence proofs for the remaining variants of the Schwarz method, we offer some numerical results illustrating their convergence in Section 4.

Consider the energy functional $\Phi[\boldsymbol{\varphi}]$ defined in (1). We will denote by $\langle \cdot, \cdot \rangle$ the usual L^2 inner product over Ω, that is,

$$\langle \boldsymbol{\psi}_1, \boldsymbol{\psi}_2 \rangle := \int_\Omega \boldsymbol{\psi}_1 \cdot \boldsymbol{\psi}_2\, \mathrm{d}V, \tag{35}$$

for $\boldsymbol{\psi}_1, \boldsymbol{\psi}_2 \in W_2^1(\Omega)$, with corresponding norm $\|\cdot\|$. The proof of the convergence of the Schwarz alternating method requires that the functional $\Phi[\boldsymbol{\varphi}]$ satisfy the following properties over the space $\mathcal{S}$ defined in (2):

1. $\Phi[\boldsymbol{\varphi}]$ is coercive.
2. $\Phi[\boldsymbol{\varphi}]$ is Fréchet differentiable, with $\Phi'[\boldsymbol{\varphi}]$ denoting its Fréchet derivative.
3. $\Phi[\boldsymbol{\varphi}]$ is strictly convex.
4. $\Phi[\boldsymbol{\varphi}]$ is lower semi-continuous.
5. $\Phi'[\boldsymbol{\varphi}]$ is uniformly continuous on K_R, where

$$K_R := \{\boldsymbol{\varphi} \in \mathcal{S} : \Phi[\boldsymbol{\varphi}] < R, R \in \mathbb{R}, R < \infty\}. \tag{36}$$

It can be shown that the energy functional $\Phi[\boldsymbol{\varphi}]$ defined in (1) is strictly convex in $\mathcal{S}$ (property 3) provided that the Helmholtz free-energy density $A(\boldsymbol{F}, \boldsymbol{Z})$ is a convex function of $\boldsymbol{F}$ [10]. Properties 1, 4, 5 and

A. Mota, I. Tezaur, C. Alleman — Schwarz Alternating Method in Solid Mechanics

Remark that [50]

$$\tilde{\mathcal{S}}_n = \tilde{\varphi}^{(n-1)} + \tilde{\mathcal{V}}_i \quad \text{for} \quad \tilde{\varphi}^{(n-1)} \in \tilde{\mathcal{S}}_{n-1} \Rightarrow \tilde{\varphi}^{(n-1)} \in \tilde{\mathcal{S}}_n. \tag{40}$$

Theorem 1. *Assume that the energy functional $\Phi[\boldsymbol{\varphi}]$ satisfies properties 1–5 above. Consider the Schwarz alternating method of Section 2 defined by (9)–(13) and its equivalent form (39). Then*

(a) $\Phi[\tilde{\varphi}^{(0)}] \geq \Phi[\tilde{\varphi}^{(1)}] \geq \cdots \geq \Phi[\tilde{\varphi}^{(n-1)}] \geq \cdots \geq \Phi[\varphi]$, where φ is the minimizer of $\Phi[\varphi]$ over $\mathcal{S}$.

(b) the sequence $\{\tilde{\varphi}^{(n)}\}$ defined in (39) converges to the minimizer φ of $\Phi[\varphi]$ in $\mathcal{S}$.

(c) the Schwarz minimum values $\Phi[\tilde{\varphi}^{(n)}]$ converge monotonically to the minimum value $\Phi[\varphi]$ in $\mathcal{S}$ starting from any initial guess $\tilde{\varphi}^{(0)}$.

(d) if $\Phi'[\varphi]$ is Lipschitz continuous in a neighborhood of φ, then the sequence $\{\tilde{\varphi}^{(n)}\}$ converges geometrically to the minimizer φ.

Proof. See Appendix A. □

Finally, while most of works cited above present their analysis for the specific case of two subdomains, extension to multiple subdomains is in general straightforward. The case of multiple subdomains is considered specifically in Lions [35], Badea [4], and Li-Shan and Evans [36].

4 Numerical Examples

In this section, we present numerical examples of the behavior of the Schwarz alternating method for two different implementations. First, we briefly describe the two implementations, one in MATLAB and the other in the open-source ALBANY finite element code [12]. Next, we discuss the error measures used throughout the numerical examples. Then, we continue with four examples that demonstrate different features of the Schwarz alternating method and our implementations. The first example, a one-dimensional singular bar, is used to demonstrate the behavior of the four Schwarz variants of Section 2.4. The second example, a cuboid body of square base, aims to study the effect of the size of the overlap region on the convergence of the method. The objective of the third example, a notched cylinder, is to analyze the numerical error in the results and to demonstrate the ability of the method to couple different element topologies. The last example, a laser

Remark 1 By the coercivity of $\Phi[\boldsymbol{\varphi}]$, it follows from the Lax-Milgram theorem that a unique minimizer to this functional over $\mathcal{S}$ exists, i.e., the minimization of $\Phi[\boldsymbol{\varphi}]$ is well-posed.

Remark 2 By the Stampacchia theorem, the minimization of $\Phi[\boldsymbol{\varphi}]$ in $\mathcal{S}$ is equivalent to finding $\boldsymbol{\varphi} \in \mathcal{S}$ such that

$$\langle \Phi'[\boldsymbol{\varphi}], \boldsymbol{\xi} - \boldsymbol{\varphi} \rangle \geq 0 \tag{51}$$

for all $\boldsymbol{\xi} \in \mathcal{S}$.

Remark 3 Recall that the strict convexity property of $\Phi[\boldsymbol{\varphi}]$ can be written as

$$\Phi[\boldsymbol{\psi}_2] - \Phi[\boldsymbol{\psi}_1] - \langle \Phi'[\boldsymbol{\psi}_1], \boldsymbol{\psi}_2 - \boldsymbol{\psi}_1 \rangle \geq 0, \tag{52}$$

$\forall \boldsymbol{\psi}_1, \boldsymbol{\psi}_2 \in \mathcal{S}$. From (36), remark that if $\Phi[\boldsymbol{\varphi}]$ is strictly convex over $\mathcal{S} \cap R \in \mathbb{R}$ such that $R < \infty$, we can find an $\alpha_R > 0$ such that $\forall \boldsymbol{\psi}_1, \boldsymbol{\psi}_2 \in K_R$ we have

$$\Phi[\boldsymbol{\psi}_2] - \Phi[\boldsymbol{\psi}_1] - \langle \Phi'[\boldsymbol{\psi}_1], \boldsymbol{\psi}_2 - \boldsymbol{\psi}_1 \rangle \geq \alpha_R \|\boldsymbol{\psi}_2 - \boldsymbol{\psi}_1\|^2. \tag{53}$$

Remark 4 By property 5, the uniform continuity of $\Phi'[\boldsymbol{\varphi}]$, there exists a modulus of continuity $\omega > 0$, with $\omega : K_R \to K_R$, such that

$$\|\Phi'(\boldsymbol{\psi}_1) - \Phi'(\boldsymbol{\psi}_2)\| \leq \omega(\|\boldsymbol{\psi}_1 - \boldsymbol{\psi}_2\|), \tag{54}$$

$\forall \boldsymbol{\psi}_1, \boldsymbol{\psi}_2 \in K_R$. By definition, $\omega(\epsilon) \to 0$ as $\epsilon \to 0$.

Remark 5 It was shown in [35] that in the case $\Omega_I \cap \Omega_{II} \neq \emptyset$, $\forall \boldsymbol{\varphi} \in \mathcal{S}$, there exist $\boldsymbol{\zeta}_1 \in \mathcal{S}_1$ and $\boldsymbol{\zeta}_2 \in \mathcal{S}_2$ such that

$$\boldsymbol{\varphi} = \boldsymbol{\zeta}_1 + \boldsymbol{\zeta}_2, \tag{55}$$

and

$$\max\left(\|\boldsymbol{\zeta}_1\|, \|\boldsymbol{\zeta}_2\|\right) \leq C_0 \|\boldsymbol{\varphi}\|, \tag{56}$$

for some $C_0 > 0$ independent of $\boldsymbol{\varphi}$.

Remark 6 Note that (39) can be written as

$$\langle \Phi'[\tilde{\boldsymbol{\varphi}}^{(n)}], \boldsymbol{\xi}^{(i)} \rangle = 0, \quad \text{for } \tilde{\boldsymbol{\varphi}}^{(n)} \in \tilde{\mathcal{S}}_n, \forall \boldsymbol{\xi}^{(i)} \in \mathcal{S}_i, \tag{57}$$

for $i \in \{1, 2\}$ and $n \in \{0, 1, 2, \ldots\}$ (recall from (6) the relation between i and n). This is due to the uniqueness of the solution to each minimization problem over $\tilde{\mathcal{S}}_n$ and the definition of $\tilde{\boldsymbol{\varphi}}^{(n)}$ as the minimizer of $\Phi[\tilde{\boldsymbol{\varphi}}]$ over $\tilde{\mathcal{S}}_n$.

Remark 7 Let $\tilde{\boldsymbol{\varphi}}^{(n)} \in \tilde{\mathcal{S}}_n$, and let $\boldsymbol{\xi} \in \mathcal{S}$. By Remark 5, there exist $\boldsymbol{\zeta}_1 \in \mathcal{S}_1$ and $\boldsymbol{\zeta}_2 \in \mathcal{S}_2$ such that

$$\langle \Phi'[\tilde{\boldsymbol{\varphi}}^{(n)}], \boldsymbol{\xi} \rangle = \langle \Phi'[\tilde{\boldsymbol{\varphi}}^{(n)}], \boldsymbol{\zeta}_1 + \boldsymbol{\zeta}_2 \rangle. \tag{58}$$

Again using (57) and also (58) in (60) leads to

$$\langle \Phi'[\tilde{\boldsymbol{\varphi}}^{(n)}] - \Phi'[\tilde{\boldsymbol{\varphi}}^{(n-1)}], \boldsymbol{\zeta}_2 \rangle = \langle \Phi'[\tilde{\boldsymbol{\varphi}}^{(n)}], \boldsymbol{\xi} \rangle \leq \|\Phi'[\tilde{\boldsymbol{\varphi}}^{(n)}] - \Phi'[\tilde{\boldsymbol{\varphi}}^{(n-1)}]\| \cdot \|\boldsymbol{\zeta}_2\|, \tag{61}$$

and substituting (56) into (61) we finally obtain that

$$\langle \Phi'[\tilde{\boldsymbol{\varphi}}^{(n)}], \boldsymbol{\xi} \rangle \leq C_0 \|\Phi'[\tilde{\boldsymbol{\varphi}}^{(n)}] - \Phi'[\tilde{\boldsymbol{\varphi}}^{(n-1)}]\| \cdot \|\boldsymbol{\xi}\|, \tag{62}$$

$\forall \boldsymbol{\xi} \in \mathcal{S}$.

Remark 8 For part (d) of Theorem 1, recall the definition of geometric convergence:

$$E_{n+1} \leq C E_n, \tag{63}$$

$\forall n \in \{0, 1, 2, \ldots\}$ for some $C > 0$, where

$$E_n := \|\tilde{\boldsymbol{\varphi}}^{(n+1)} - \tilde{\boldsymbol{\varphi}}^{(n)}\|. \tag{64}$$

Remark 9 Recall from the definition of continuity that if $\Phi'[\tilde{\boldsymbol{\varphi}}]$ is Lipshitz continuous at $\tilde{\boldsymbol{\varphi}}^{(n)}$ near $\boldsymbol{\varphi}$, then there exists a constant $K \geq 0$ such that

$$\frac{\|\Phi'[\tilde{\boldsymbol{\varphi}}^{(n)}] - \Phi'[\boldsymbol{\varphi}]\|}{\|\tilde{\boldsymbol{\varphi}}^{(n)} - \boldsymbol{\varphi}\|} \leq K. \tag{65}$$

Considering that $\Phi'[\boldsymbol{\varphi}] = \boldsymbol{0}$ since $\boldsymbol{\varphi}$ is the minimizer of $\Phi[\boldsymbol{\varphi}]$, (65) is equivalent to

$$\|\Phi'[\tilde{\boldsymbol{\varphi}}^{(n)}]\| \leq K \|\tilde{\boldsymbol{\varphi}}^{(n)} - \boldsymbol{\varphi}\|. \tag{66}$$

Proof of Theorem 1

Proof of (a). Let $\tilde{\boldsymbol{\varphi}}^{(1)} = \arg\min_{\tilde{\boldsymbol{\varphi}} \in \tilde{\mathcal{S}}_1} \Phi[\tilde{\boldsymbol{\varphi}}]$. By (40), $\tilde{\boldsymbol{\varphi}}^{(1)} \in \tilde{\mathcal{S}}_2$. Let $\tilde{\boldsymbol{\varphi}}^*$ be the minimizer of $\Phi[\tilde{\boldsymbol{\varphi}}]$ over $\tilde{\mathcal{S}}_2$ and suppose $\Phi[\tilde{\boldsymbol{\varphi}}^*] > \Phi[\tilde{\boldsymbol{\varphi}}^{(1)}]$. But this is a contradiction, since we can take $\tilde{\boldsymbol{\varphi}}^* = \tilde{\boldsymbol{\varphi}}^{(1)}$. Hence, it cannot be that $\Phi[\tilde{\boldsymbol{\varphi}}^{(1)}] < \Phi[\tilde{\boldsymbol{\varphi}}^{(2)}]$ where $\tilde{\boldsymbol{\varphi}}^{(2)} = \arg\min_{\tilde{\boldsymbol{\varphi}} \in \tilde{\mathcal{S}}_2} \Phi[\tilde{\boldsymbol{\varphi}}]$. It follows by induction that

$$\Phi[\tilde{\boldsymbol{\varphi}}^{(n)}] \leq \Phi[\tilde{\boldsymbol{\varphi}}^{(n-1)}] \tag{67}$$

for $n \in \{1, 2, 3, \ldots\}$. Now let $\boldsymbol{\varphi}$ be the minimizer of $\Phi[\boldsymbol{\varphi}]$ over $\mathcal{S}$. Since the problem is well-posed $\boldsymbol{\varphi}$ is unique. Hence $\Phi[\boldsymbol{\varphi}] \leq \Phi[\tilde{\boldsymbol{\varphi}}^{(n)}]$ for all $n \in \{1, 2, 3, \ldots\}$. □

$$\lim_{n \to \infty} \|\tilde{\boldsymbol{\varphi}}^{(n)} - \tilde{\boldsymbol{\varphi}}^{(n+1)}\|^2 = 0, \tag{69}$$

from which we can conclude that $\tilde{\boldsymbol{\varphi}}^{(n)} - \tilde{\boldsymbol{\varphi}}^{(n+1)} \to \boldsymbol{0}$ as $n \to \infty$.

We must now show that $\tilde{\boldsymbol{\varphi}}^{(n)}$ converges to $\boldsymbol{\varphi}$, the minimizer of $\Phi[\boldsymbol{\varphi}]$ on $\mathcal{S}$. By (53) with $\boldsymbol{\psi}_1 = \boldsymbol{\varphi}$ and $\boldsymbol{\psi}_2 = \tilde{\boldsymbol{\varphi}}^{(n)}$, we have

$$\|\boldsymbol{\varphi} - \tilde{\boldsymbol{\varphi}}^{(n)}\|^2 \leq \frac{1}{\alpha_R} \left\{ \Phi[\boldsymbol{\varphi}] - \Phi[\tilde{\boldsymbol{\varphi}}^{(n)}] - \left\langle \Phi'[\tilde{\boldsymbol{\varphi}}^{(n)}], \boldsymbol{\varphi} - \tilde{\boldsymbol{\varphi}}^{(n)} \right\rangle \right\}. \tag{70}$$

Since $\boldsymbol{\varphi}$ is the minimum of $\Phi[\boldsymbol{\varphi}]$, by (a) we have that $\Phi[\boldsymbol{\varphi}] \leq \Phi[\tilde{\boldsymbol{\varphi}}^{(n)}]$. It follows that

$$\Phi[\boldsymbol{\varphi}] - \Phi[\tilde{\boldsymbol{\varphi}}^{(n)}] - \left\langle \Phi'[\tilde{\boldsymbol{\varphi}}^{(n)}], \boldsymbol{\varphi} - \tilde{\boldsymbol{\varphi}}^{(n)} \right\rangle \leq - \left\langle \Phi'[\tilde{\boldsymbol{\varphi}}^{(n)}], \boldsymbol{\varphi} - \tilde{\boldsymbol{\varphi}}^{(n)} \right\rangle = \left\langle \Phi'[\tilde{\boldsymbol{\varphi}}^{(n)}], \tilde{\boldsymbol{\varphi}}^{(n)} - \boldsymbol{\varphi} \right\rangle. \tag{71}$$

Subsituting (71) into (70) we have

$$\|\boldsymbol{\varphi} - \tilde{\boldsymbol{\varphi}}^{(n)}\|^2 \leq \frac{1}{\alpha_R} \left\langle \Phi'[\tilde{\boldsymbol{\varphi}}^{(n)}], \tilde{\boldsymbol{\varphi}}^{(n)} - \boldsymbol{\varphi} \right\rangle. \tag{72}$$

Now by (62) (Remark 7),

$$\left\langle \Phi'[\tilde{\boldsymbol{\varphi}}^{(n)}], \tilde{\boldsymbol{\varphi}}^{(n)} - \boldsymbol{\varphi} \right\rangle \leq C_0 \|\Phi'[\tilde{\boldsymbol{\varphi}}^{(n)}] - \Phi'[\tilde{\boldsymbol{\varphi}}^{(n-1)}]\| \cdot \|\tilde{\boldsymbol{\varphi}}^{(n)} - \boldsymbol{\varphi}\|. \tag{73}$$

Substituting (73) into (72) leads to

$$\|\tilde{\boldsymbol{\varphi}}^{(n)} - \boldsymbol{\varphi}\| \leq \frac{C_0}{\alpha_R} \|\Phi'[\tilde{\boldsymbol{\varphi}}^{(n)}] - \Phi'[\tilde{\boldsymbol{\varphi}}^{(n-1)}]\|. \tag{74}$$

Applying the uniform continuity assumption (54), we obtain

$$\|\tilde{\boldsymbol{\varphi}}^{(n)} - \boldsymbol{\varphi}\| \leq \frac{C_0}{\alpha_R} \omega\left(\|\tilde{\boldsymbol{\varphi}}^{(n)} - \tilde{\boldsymbol{\varphi}}^{(n-1)}\|\right). \tag{75}$$

By (69), $\|\tilde{\boldsymbol{\varphi}}^{(n)} - \tilde{\boldsymbol{\varphi}}^{(n-1)}\| \to 0$ as $n \to \infty$. From this we obtain the result, namely that $\tilde{\boldsymbol{\varphi}}^{(n)} \to \boldsymbol{\varphi}$ as $n \to \infty$. □

Proof of (c). This follows immediately from (a) and (b). □

Proof of (d). By (b), for large enough n, there exists some $C_1 > 0$ independent of n such that

$$\|\tilde{\boldsymbol{\varphi}}^{(n)} - \boldsymbol{\varphi}\|^2 \leq C_1 \|\tilde{\boldsymbol{\varphi}}^{(n+1)} - \tilde{\boldsymbol{\varphi}}^{(n)}\|^2. \tag{76}$$

Let us choose C_1 such that $C_1 > \alpha_R/K$, where K is the Lipshitz continuity constant in (66). Combining (68) with (76) leads to

$$\frac{1}{\alpha_R} \left(\Phi[\tilde{\boldsymbol{\varphi}}^{(n)}] - \Phi[\tilde{\boldsymbol{\varphi}}^{(n+1)}] \right) \geq \|\tilde{\boldsymbol{\varphi}}^{(n+1)} - \tilde{\boldsymbol{\varphi}}^{(n)}\|^2 \geq \frac{1}{C_1} \|\tilde{\boldsymbol{\varphi}}^{(n)} - \boldsymbol{\varphi}\|^2. \tag{77}$$

$$\left\langle \Phi'[\tilde{\boldsymbol{\varphi}}^{(n)}], \tilde{\boldsymbol{\varphi}}^{(n)} - \boldsymbol{\varphi} \right\rangle \leq \left\langle \Phi'[\tilde{\boldsymbol{\varphi}}^{(n)}], \tilde{\boldsymbol{\varphi}}^{(n)} - \tilde{\boldsymbol{\varphi}}^{(n-1)} \right\rangle + \alpha_R \|\tilde{\boldsymbol{\varphi}}^{(n)} - \tilde{\boldsymbol{\varphi}}^{(n-1)}\| \leq \Phi[\tilde{\boldsymbol{\varphi}}] - \Phi[\tilde{\boldsymbol{\varphi}}^{(n)}] \tag{78}$$

since $\alpha_R \geq 0$. Now, by the Cauchy-Schwarz inequality followed by the application of the Lipshitz continuity of $\Phi'[\boldsymbol{\varphi}]$ (66) we can write

$$\left\langle \Phi'[\tilde{\boldsymbol{\varphi}}^{(n)}], \boldsymbol{\varphi} - \tilde{\boldsymbol{\varphi}}^{(n)} \right\rangle \leq \|\Phi'[\tilde{\boldsymbol{\varphi}}^{(n)}]\| \cdot \|\boldsymbol{\varphi} - \tilde{\boldsymbol{\varphi}}^{(n)}\| \leq K \|\boldsymbol{\varphi} - \tilde{\boldsymbol{\varphi}}^{(n)}\|^2. \tag{80}$$

Hence, from (79),

$$\Phi[\tilde{\boldsymbol{\varphi}}^{(n)}] - \Phi[\boldsymbol{\varphi}] \leq K \|\tilde{\boldsymbol{\varphi}}^{(n)} - \boldsymbol{\varphi}\|^2. \tag{81}$$

Moreover, by (53) since $\Phi'[\boldsymbol{\varphi}] = \boldsymbol{0}$,

$$\Phi[\tilde{\boldsymbol{\varphi}}^{(n)}] - \Phi[\boldsymbol{\varphi}] \geq \alpha_R \|\tilde{\boldsymbol{\varphi}}^{(n)} - \boldsymbol{\varphi}\|^2. \tag{82}$$

Using (81) and (82) we obtain

$$\left(\Phi[\tilde{\boldsymbol{\varphi}}^{(n)}] - \Phi[\boldsymbol{\varphi}] \right) - \left(\Phi[\tilde{\boldsymbol{\varphi}}^{(n+1)}] - \Phi[\boldsymbol{\varphi}] \right) \leq K \|\tilde{\boldsymbol{\varphi}}^{(n)} - \boldsymbol{\varphi}\|^2 - \alpha_R \|\tilde{\boldsymbol{\varphi}}^{(n+1)} - \boldsymbol{\varphi}\|^2. \tag{83}$$

Combining (83) and (78) leads to

$$\frac{\alpha_R}{C_1} \|\tilde{\boldsymbol{\varphi}}^{(n)} - \boldsymbol{\varphi}\|^2 \leq \left(\Phi[\tilde{\boldsymbol{\varphi}}^{(n)}] - \Phi[\boldsymbol{\varphi}] \right) - \left(\Phi[\tilde{\boldsymbol{\varphi}}^{(n+1)}] - \Phi[\boldsymbol{\varphi}] \right) \leq K \|\tilde{\boldsymbol{\varphi}}^{(n)} - \boldsymbol{\varphi}\|^2 - \alpha_R \|\tilde{\boldsymbol{\varphi}}^{(n+1)} - \boldsymbol{\varphi}\|^2, \tag{84}$$

or

$$\|\tilde{\boldsymbol{\varphi}}^{(n+1)} - \boldsymbol{\varphi}\| \leq B \|\tilde{\boldsymbol{\varphi}}^{(n)} - \boldsymbol{\varphi}\| \tag{85}$$

with

$$B := \sqrt{\frac{K}{\alpha_R} - \frac{1}{C_1}} \tag{86}$$

and $B \in \mathbb{R}$ as we chose $C_1 > \alpha_R/K$. Furthermore, since the sequence $\{\tilde{\boldsymbol{\varphi}}^{(n)}\}$ converges monotonically to the minimizer $\boldsymbol{\varphi}$ of $\Phi[\boldsymbol{\varphi}]$ by (b) and (c), it follows that $B \in [0, 1)$. Define $C := 1 - B \in (0, 1)$, then (85) can be recast as

$$\|\tilde{\boldsymbol{\varphi}}^{(n+1)} - \tilde{\boldsymbol{\varphi}}^{(n)}\| \leq C \|\tilde{\boldsymbol{\varphi}}^{(n)} - \tilde{\boldsymbol{\varphi}}^{(n-1)}\| \tag{87}$$

whereupon the claim is proven. □

B Analytic Solution for Linear-Elastic Singular Bar

As reference, herein we provide the solution of the singular bar of Section 4.3 for linear elasticity. The equilibrium equation is

$$P = \sigma(X) A(X) = \text{const.}, \quad \sigma(X) = E\epsilon(X), \quad \epsilon(X) := u'(X), \quad A(X) = A_0 \left(\frac{X}{L} \right)^{\frac{1}{2}}. \tag{88}$$

*A. Mota, **I. Tezaur**, C. Alleman. "The Schwarz Alternating Method in Solid Mechanics", *CMAME* 319 (2017), 19-51.

Schwarz Alternating Method for Dynamic Multiscale Coupling: Theory

- Like for quasistatics, dynamic alternating Schwarz method converges provided each single-domain problem is ***well-posed*** and ***overlap region*** is ***non-empty,*** under some ***conditions*** on Δt.
- ***Well-posedness*** for the dynamic problem requires that action functional $S[\boldsymbol{\varphi}] \coloneqq \int_I \int_\Omega L(\boldsymbol{\varphi}, \dot{\boldsymbol{\varphi}}) dV dt$ be ***strictly convex*** or ***strictly concave***, where $L(\boldsymbol{\varphi}, \dot{\boldsymbol{\varphi}}) \coloneqq T(\dot{\boldsymbol{\varphi}}) + V(\boldsymbol{\varphi})$ is the Lagrangian.
  - ➢ This is studied by looking at its second variation $\delta^2 S[\boldsymbol{\varphi}_h]$
- We can show assuming a ***Newmark*** time-integration scheme that for the ***fully-discrete*** problem:

$$\delta^2 S[\boldsymbol{\varphi}_h] = \boldsymbol{x}^T \left[\frac{\gamma^2}{(\beta \Delta t)^2} \boldsymbol{M} - \boldsymbol{K} \right] \boldsymbol{x}$$

  - ➢ $\delta^2 S[\boldsymbol{\varphi}_h]$ can always be made positive by choosing a ***sufficiently small*** Δt
  - ➢ Numerical experiments reveal that Δt requirements for ***stability/accuracy*** typically lead to automatic satisfaction of this bound.

Numerical Example: Linear Elastic Wave Propagation Problem

- Linear elastic ***clamped beam*** with Gaussian initial condition.
- Simple problem with analytical exact solution but very ***stringent test*** for discretization/coupling methods.
- ***Couplings tested:*** FOM-FOM, FOM-ROM, ROM-ROM, implicit-explicit, implicit-implicit, explicit-explicit.
- ROMs are ***reproductive*** and based on the ***POD/Galerkin*** method.
  - ➢ 50 POD modes capture ~100% snapshot energy

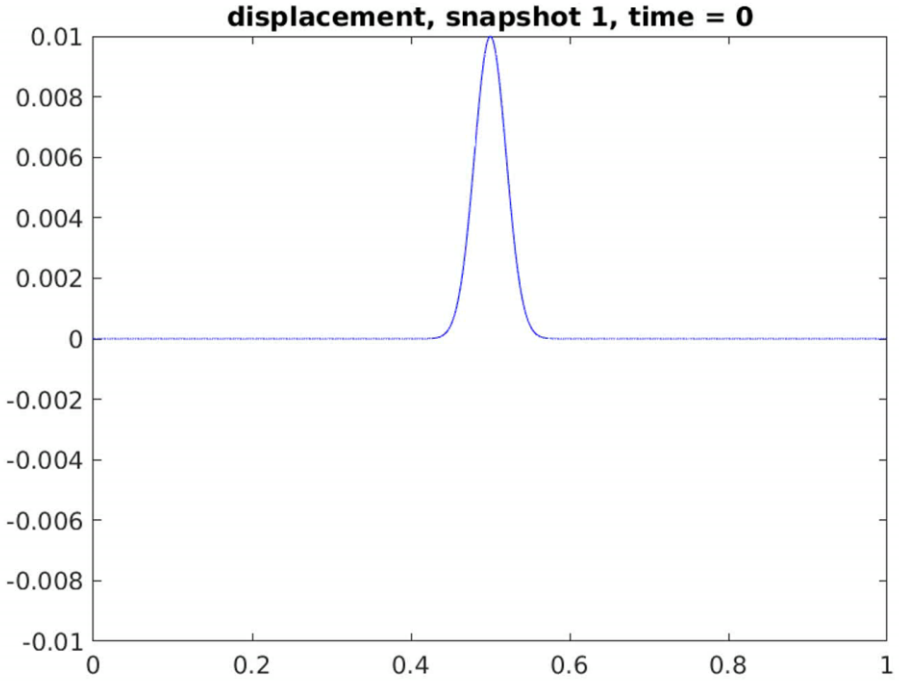

Above: 3D rendering of clamped beam with Gaussian initial condition.
Right: Initial condition (blue) and final solution (red). Wave profile is negative of initial profile at time T = 1.0e-3.

Linear Elastic Wave Propagation Problem: FOM-ROM and ROM-ROM Couplings

Coupling delivers accurate solution if each subdomain model is reasonably accurate, can couple different discretizations with different Δx, Δt and basis sizes.

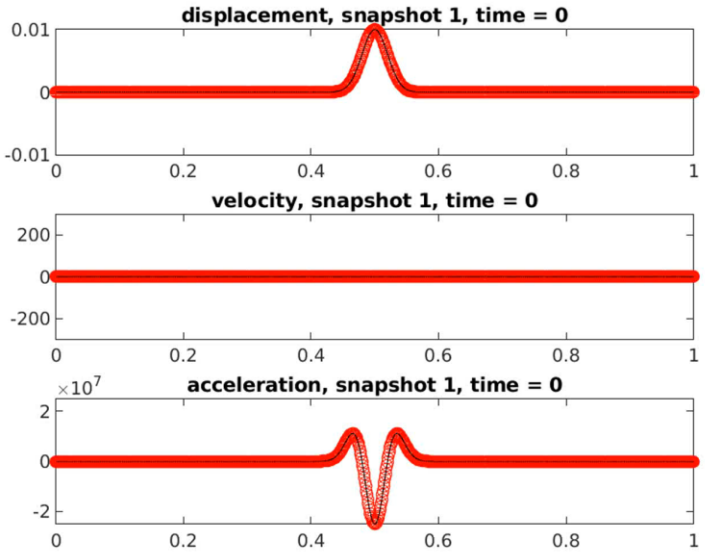

Single Domain FOM

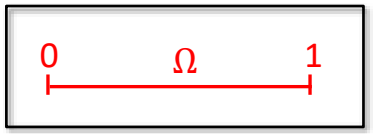

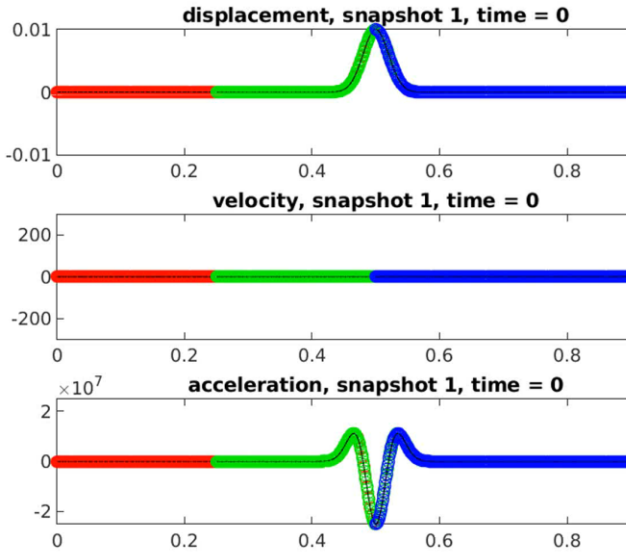

3 overlapping subdomain ROM[1]-FOM[2]-ROM[3]

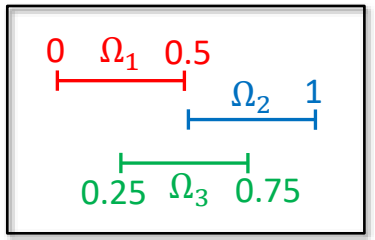

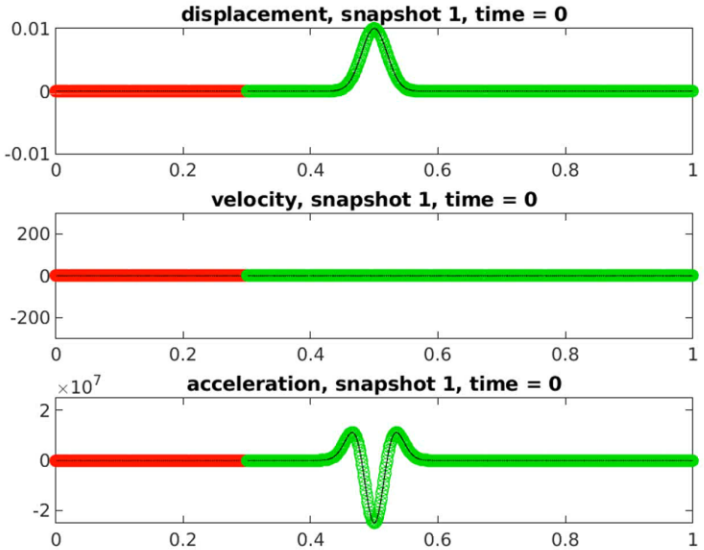

2 non-overlapping subdomain FOM[4]-ROM[5] ($\theta = 1$)

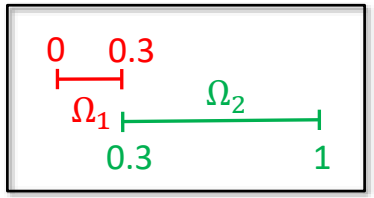

[1]Implicit 40 mode POD ROM, Δt=1e-6, Δx=1.25e-3
[2]Implicit FOM, Δt =1e-6, Δx =8.33e-4
[3]Explicit 50 mode POD ROM, Δt =1e-7, Δx =1e-3

[5]Implicit FOM, Δt =2.25e-7, Δx =1e-6
[4]Explicit 50 mode POD ROM, Δt =2.25e-7, Δx =1e-6

Linear Elastic Wave Propagation Problem: FOM-ROM and ROM-ROM Couplings

Coupled models are reasonably accurate w.r.t. FOM-FOM coupled analogs and convergence with respect to basis refinement for FOM-ROM and ROM-ROM coupling is observed.

	disp MSE[6]	velo MSE	acce MSE
Overlapping ROM[1]-FOM[2]-ROM[3]	1.05e-4	1.40e-3	2.32e-2
Non-overlapping FOM[4]-ROM[5]	2.78e-5	2.20e-4	3.30e-3

[1]Implicit 40 mode POD ROM, Δt =1e-6, Δx =1.25e-3
[2]Implicit FOM, Δt =1e-6, Δx =8.33e-4
[3]Explicit 50 mode POD ROM, Δt =1e-7, Δx =1e-3
[4]Implicit FOM, Δt =2.25e-7, Δx =1e-6
[5]Explicit 50 mode POD ROM, Δt =2.25e-7, Δx =1e-6

[6]MSE= mean squared error $= \sqrt{\sum_{n=1}^{N_t} \left\| \widetilde{\boldsymbol{u}}^n(\boldsymbol{\mu}) - \boldsymbol{u}^n(\boldsymbol{\mu}) \right\|_2^2} \Big/ \sqrt{\sum_{n=1}^{N_t} \left\| \boldsymbol{u}^n(\boldsymbol{\mu}) \right\|_2^2}.$

Linear Elastic Wave Propagation Problem: ROM-ROM Couplings

ROM-ROM coupling gives errors < O(1e-6) & speedups over FOM-FOM coupling for basis sizes > 40.

MSE in displacement for 2 subdomain ROM-ROM coupling

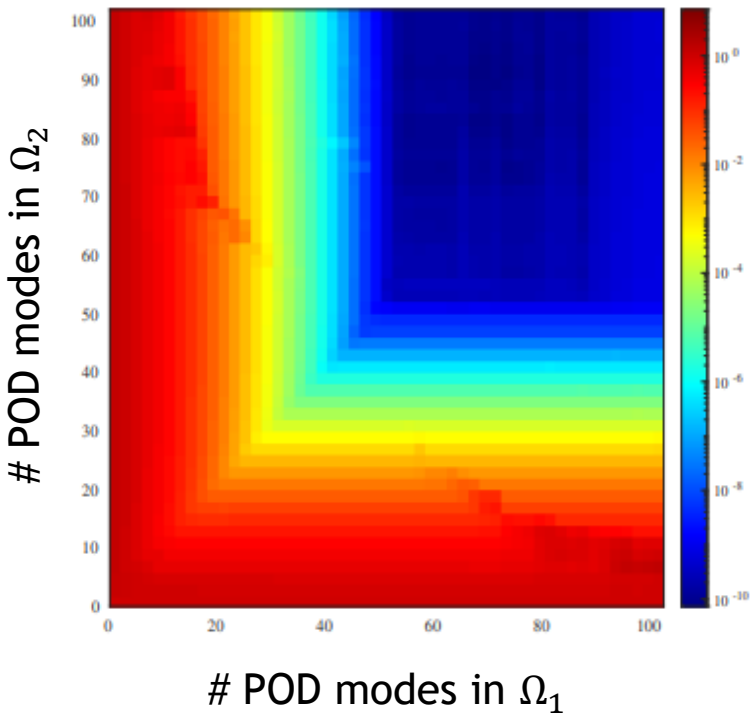

CPU times for 2 subdomain ROM-ROM coupling normalized by FOM-FOM CPU time

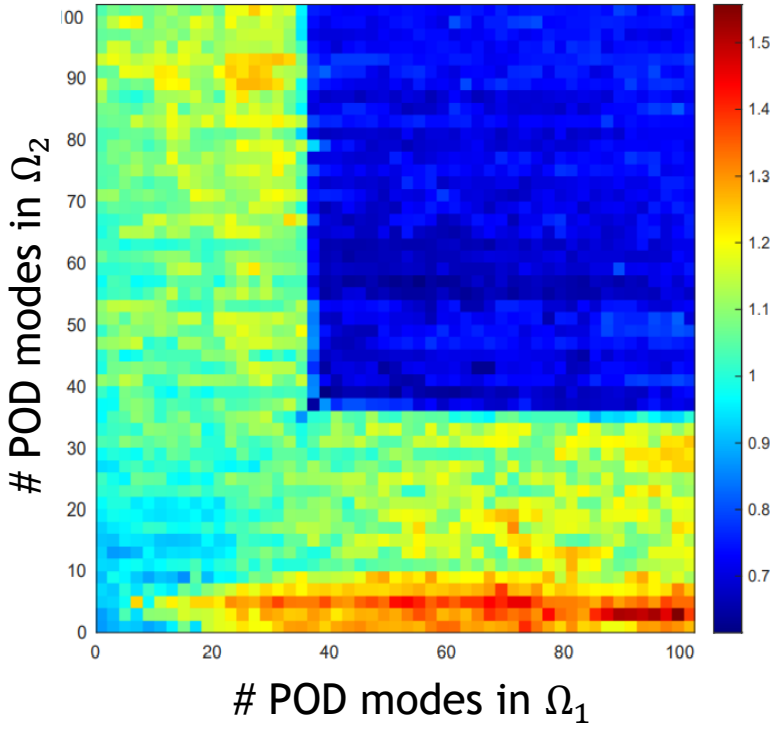

Average # Schwarz iterations for 2 subdomain ROM-ROM coupling

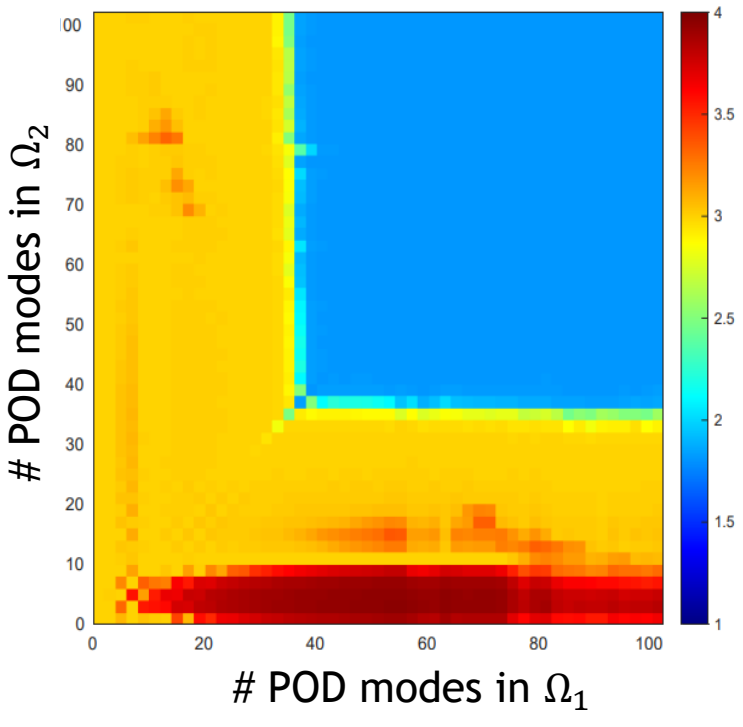

- **Smaller ROMs** are **not** the **fastest**: less accurate & require more Schwarz iterations to converge.
- All couplings converge in $\leq$ **4 Schwarz iterations** on average (FOM-FOM coupling requires average of 2.4 Schwarz iterations).

Overlapping implicit-implicit coupling with $\Omega_1 = [0, 0.75]$, $\Omega_2 = [0.25, 1]$

Linear Elastic Wave Propagation Problem: FOM-ROM Couplings

FOM-ROM coupling shows convergence with basis refinement. FOM-ROM couplings are 10-15% slower than comparable FOM-FOM coupling due to increased # Schwarz iterations.

MSE for 2 subdomain FOM-ROM coupling

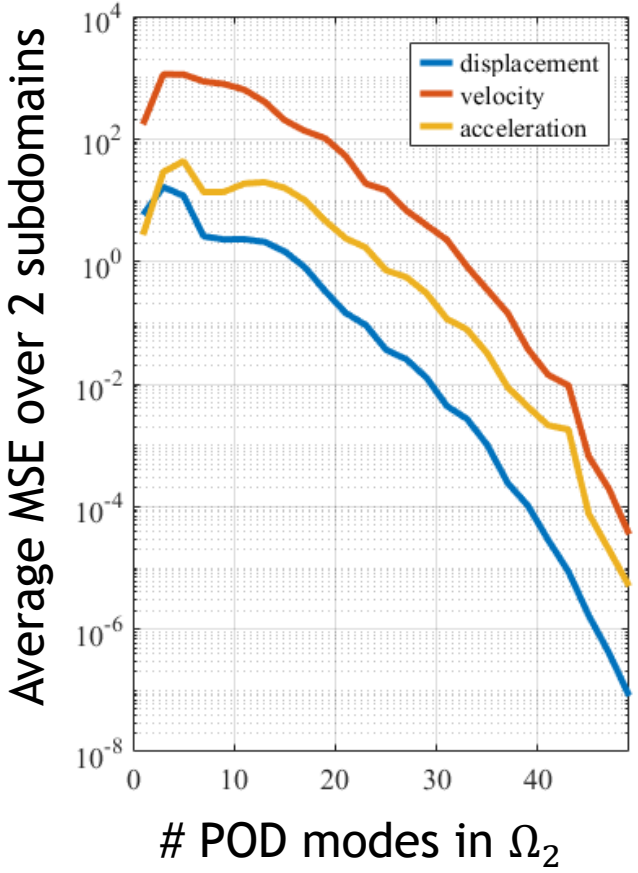

CPU times for 2 subdomain FOM-ROM coupling normalized by FOM-FOM CPU time

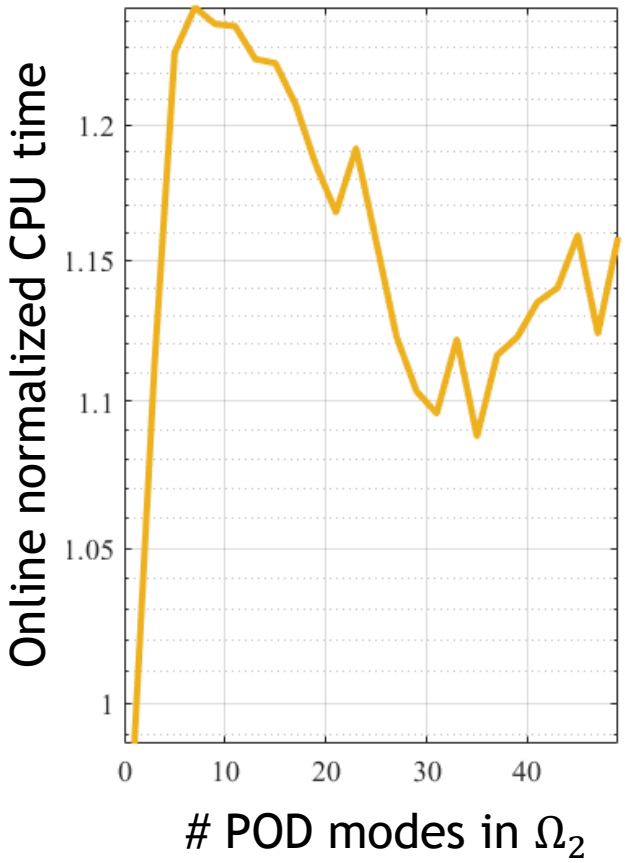

Average # Schwarz iterations for 2 subdomain couplings

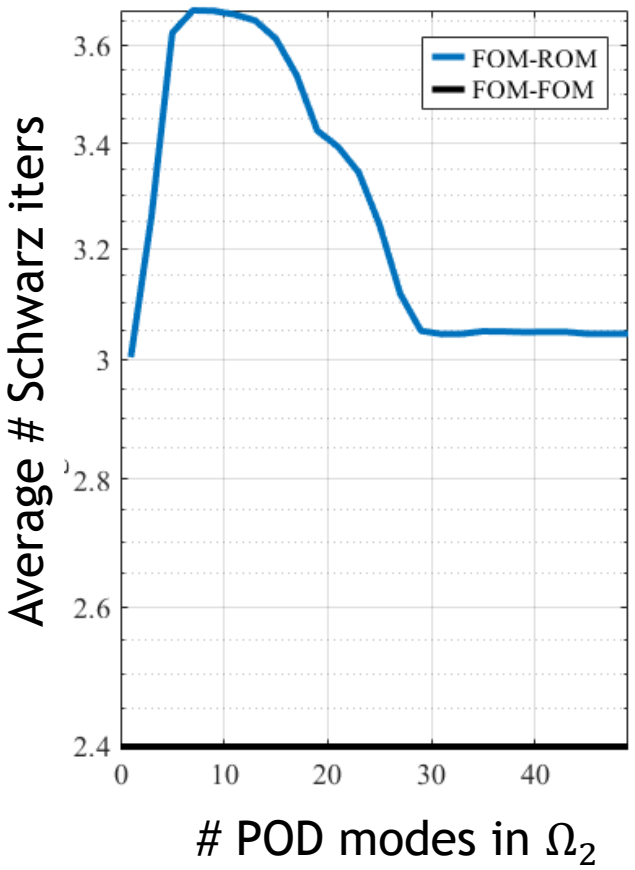

WIP: *understanding & improving FOM-ROM coupling performance.*

Overlapping implicit-implicit coupling with $\Omega_1 = [0, 0.75]$, $\Omega_2 = [0.25, 1]$

Linear Elastic Wave Propagation Problem: FOM-ROM and ROM-ROM Couplings

Inaccurate model + accurate model ≠ accurate model.

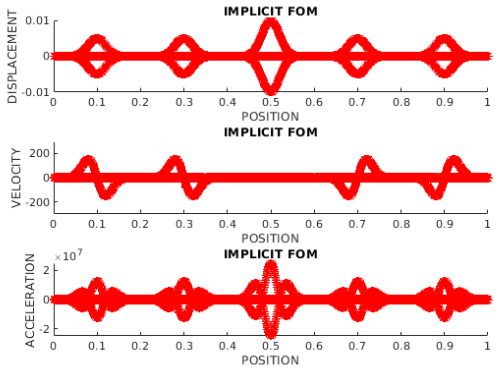

Single Domain, FOM (truth)

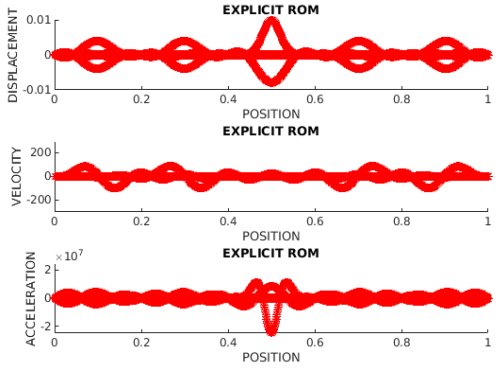

Single Domain, 10 mode POD

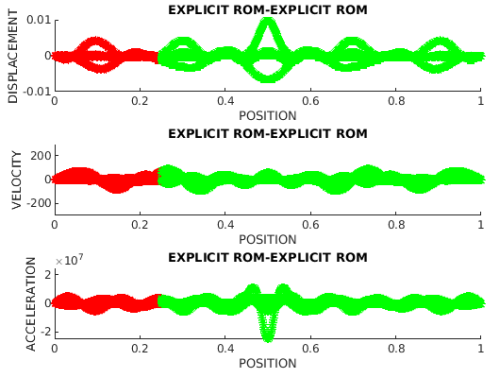

10 mode POD – 10 mode POD

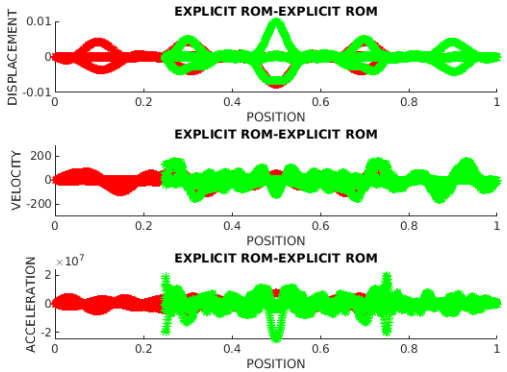

10 mode POD – 50 mode POD

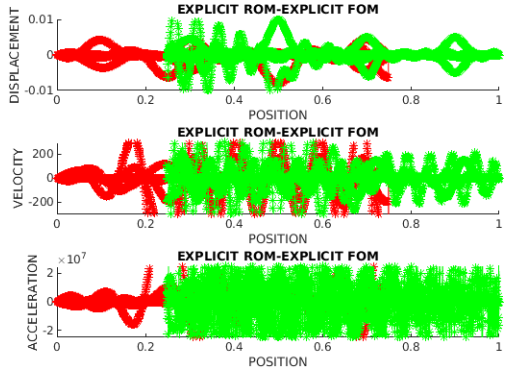

10 mode POD – FOM

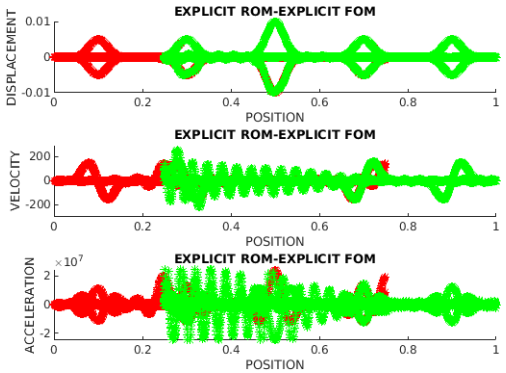

20 mode POD - FOM

Figures above: $\Omega_1 = [0, 0.75]$, $\Omega_2 = [0.25, 1]$

Observation suggests need for **"smart" domain decomposition.**

Accuracy can be improved by "gluing" several smaller, spatially-local models

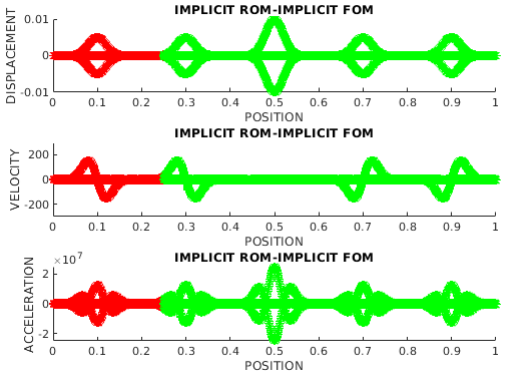

Figure above: $\Omega_1 = [0, 0.3]$, $\Omega_2 = [0.25, 1]$, 20 mode POD - FOM

Figure below: $\Omega_1 = [0, 0.26]$, $\Omega_2 = [0.25, 0.75]$, $\Omega_3 = [0.74, 1]$, 15 mode POD - 30 mode POD - 15 mode POD

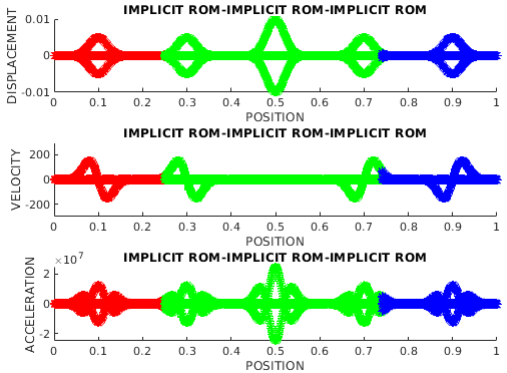

2D Burgers FOM: New Python Code

$$\frac{\partial u}{\partial t} + \frac{1}{2}\left(\frac{\partial u^2}{\partial x} + \frac{\partial uv}{\partial y}\right) = 0.02\exp(\mu_2 x)$$

$$\frac{\partial v}{\partial t} + \frac{1}{2}\left(\frac{\partial vu}{\partial x} + \frac{\partial v^2}{\partial y}\right) = 0$$

$$u(x=0, y, t; \boldsymbol{\mu}) = \mu_1$$

$$u(x, y, t=0) = v(x, y, t=0) = 1$$

$$x, y \in [0, 100], t \in [0, T_f]$$

- Spatial discretization given by a **Godunov-type scheme** with N = 250 elements in each dimension
- Temporal discretization given by the **trapezoidal method** with fixed Δt = 0.05 where T_f = 25.0 for a total of 500 time steps

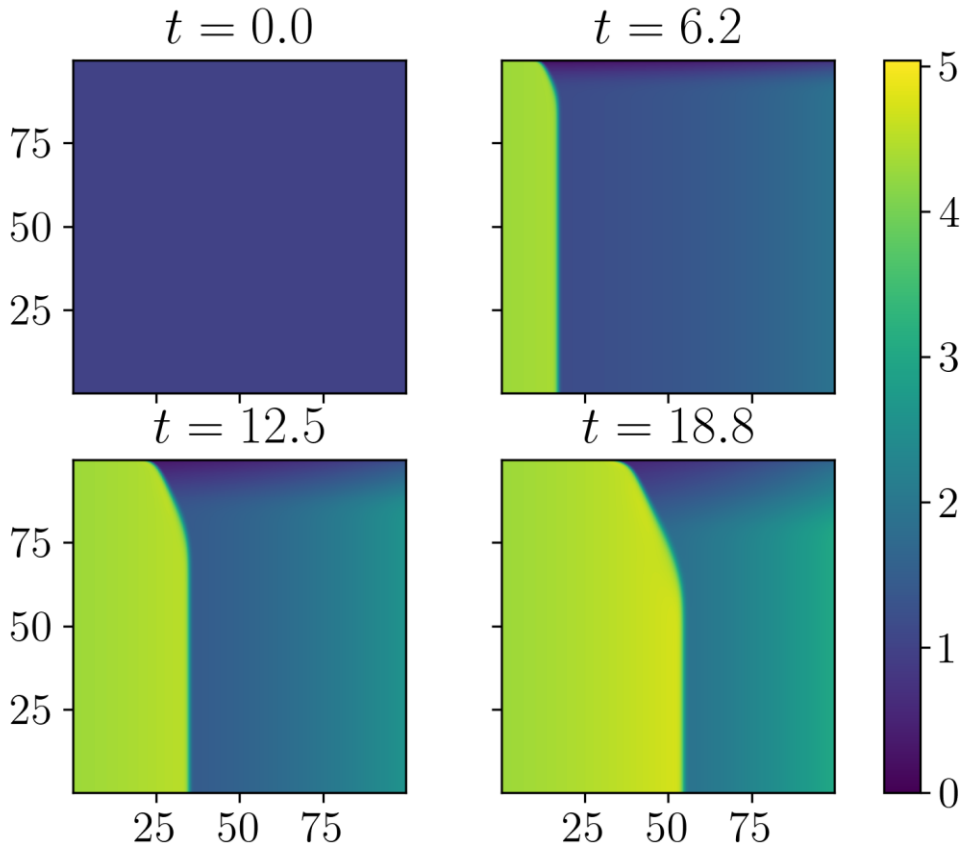

Figure above: solution of u component at various times

2D Burgers: Verifying Implicit Implementation

- The plot to the right shows the solution of the u component at various times along **mid-axis slices of the 2D domain**
- FOM and ROM solutions are the **same**

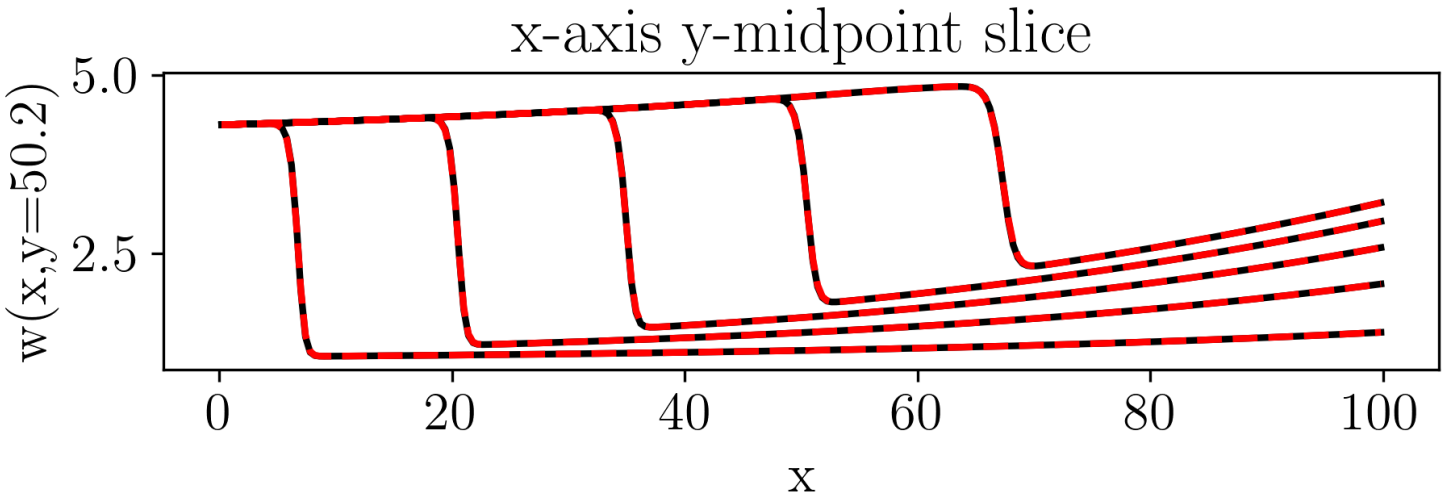

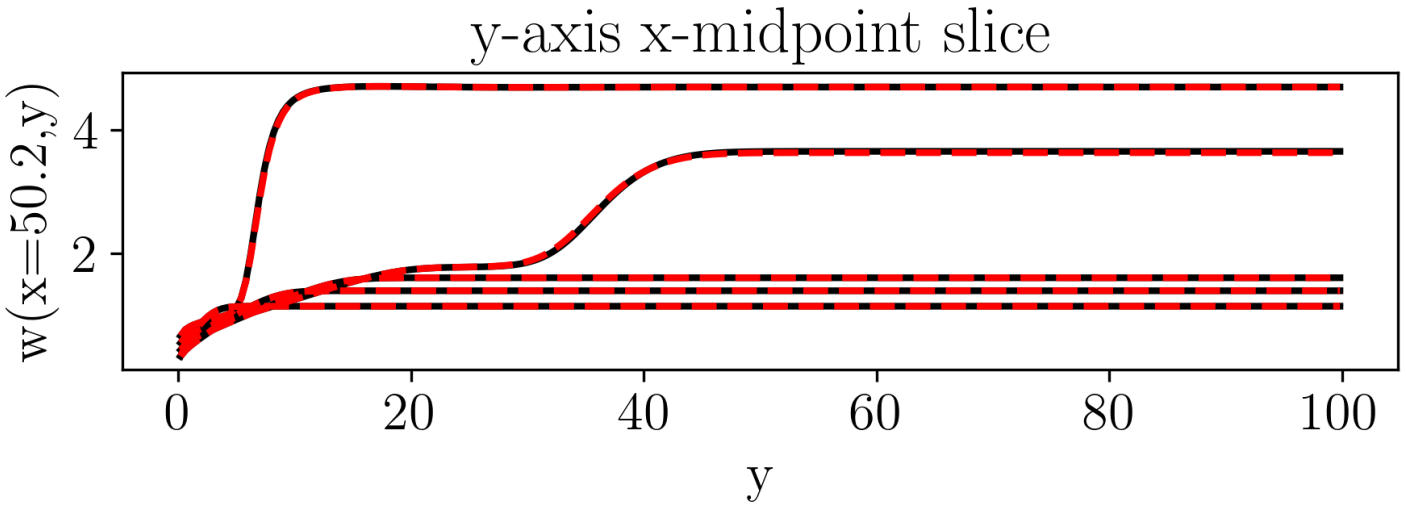

2D Burgers: LSPG PROM

- **Predictive case** where **μ** = [4.7, 0.026]
- Train bases using **9 total runs** of the FOM with all combinations of μ_1 = [(4.25),(4.875),(5.5)] with μ_2 = [(0.015),(0.0225),(0.03)]
- Using 113 POD modes
- Relative error of 0.61%
- 321 s wall clock time

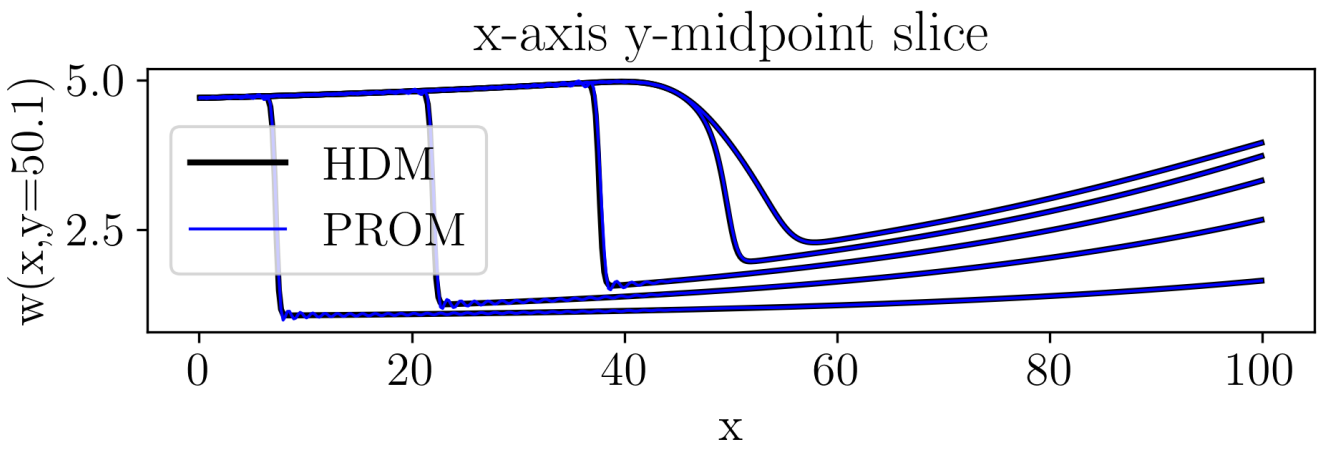

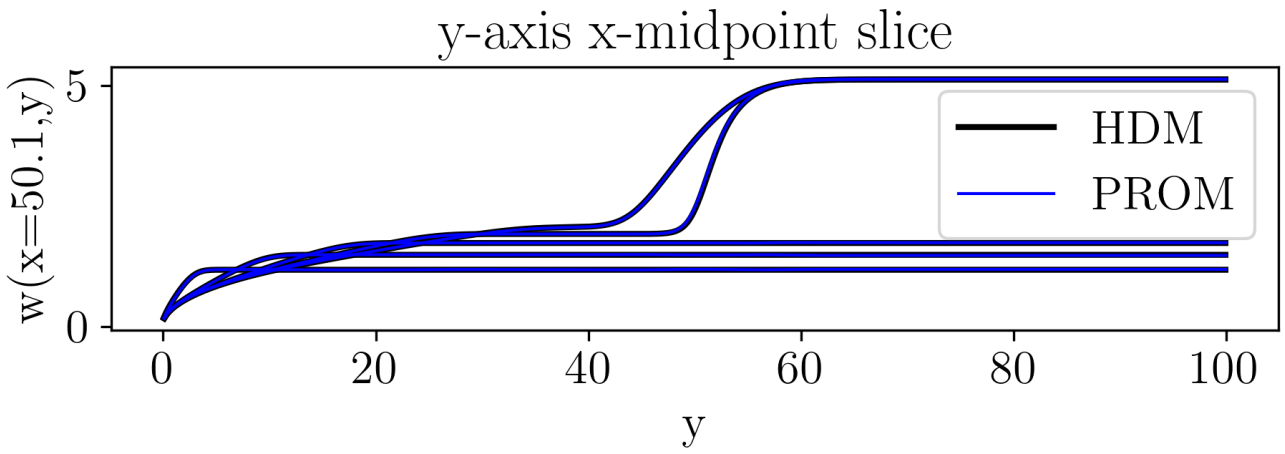

Energy-Conserving Sampling and Weighting (ECSW)

- **Project-then-approximate** paradigm (as opposed to approximate-then-project)

$$r_k(q_k, t) = W^T r(\tilde{u}, t)$$
$$= \sum_{e \in \mathcal{E}} W^T L_e^T r_e(L_{e^+}\tilde{u}, t)$$

- $L_e \in \{0,1\}^{d_e \times N}$ where d_e is the **number of degrees of freedom** associated with each mesh element (this is in the context of meshes used in first-order hyperbolic problems where there are N_e mesh elements)
- $L_{e^+} \in \{0,1\}^{d_e \times N}$ selects degrees of freedom necessary for **flux reconstruction**
- Equality can be **relaxed**

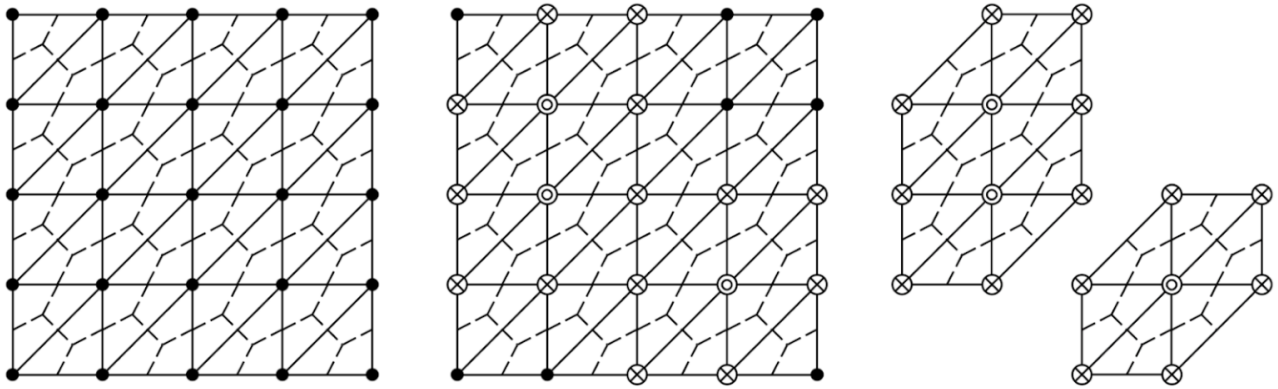

Augmented reduced mesh: ⊚ represents a selected node attached to a selected element; and ⊗ represents an added node to enable the full representation of the computational stencil at the selected node/element

ECSW: Generating the Reduced Mesh and Weights

- Using a subset of the same snapshots $u_i, i \in 1, \dots, n_h$ used to generate the **state basis** V, we can train the reduced mesh
- Snapshots are first **projected** onto their associated basis and then **reconstructed**

$$c_{se} = W^T L_e^T r_e \left(L_{e^+} \left(u_{ref} + V\, V^T \left(u_s - u_{ref} \right) \right), t \right) \in \mathbb{R}^n$$
$$d_s = r_k(\tilde{u}, t) \in \mathbb{R}^n, \qquad s = 1, \dots, n_h$$

- We can then form the **system**

$$\boldsymbol{C} = \begin{pmatrix} c_{11} & \cdots & c_{1N_e} \\ \vdots & \ddots & \vdots \\ c_{n_h 1} & \cdots & c_{n_h N_e} \end{pmatrix}, \qquad \boldsymbol{d} = \begin{pmatrix} d_1 \\ \vdots \\ d_{n_h} \end{pmatrix}$$

- Where $\boldsymbol{C}\boldsymbol{\xi} = \boldsymbol{d}, \boldsymbol{\xi} \in \mathbb{R}^{N_e}$, $\boldsymbol{\xi} = \mathbf{1}$ must be the solution
- Further relax the equality to yield **non-negative least-squares problem:**

$$\boldsymbol{\xi} = \arg\min_{\boldsymbol{x} \in \mathbb{R}^n} ||\boldsymbol{C}\boldsymbol{x} - \boldsymbol{d}||_2 \text{ subject to } \boldsymbol{x} \geq \mathbf{0}$$

- Solve the above optimization problem using a **non-negative least squares solver** with an **early termination condition** to **promote sparsity** of the vector $\boldsymbol{\xi}$

Numerical Example: 1D Dynamic Wave Propagation Problem

- Alternating **Dirichlet-Neumann** Schwarz BCs with **no relaxation** ($\theta = 1$) on Schwarz boundary Γ

$$\begin{cases} \text{Div}\, \boldsymbol{P}_1^{(n+1)} + \rho \boldsymbol{B}(t_i) = \boldsymbol{0}\ , \text{ in } \Omega_1 \\ \boldsymbol{\varphi}_1^{(n+1)} = \boldsymbol{\chi}, & \text{on } \partial\Omega_1 \backslash \Gamma \\ \boldsymbol{\varphi}_1^{(n+1)} = \boldsymbol{\lambda}_{n+1} & \text{on } \Gamma \end{cases}$$

$$\begin{cases} \text{Div}\, \boldsymbol{P}_2^{(n+1)} + \rho \boldsymbol{B}(t_i) = \boldsymbol{0}\ , \text{ in } \Omega_2 \\ \boldsymbol{\varphi}_2^{(n+1)} = \boldsymbol{\chi}, & \text{on } \partial\Omega_2 \backslash \Gamma \\ \boldsymbol{P}_2^{(n+1)} \boldsymbol{n} = \boldsymbol{P}_1^{(n+1)} \boldsymbol{n}, & \text{on } \Gamma \end{cases}$$

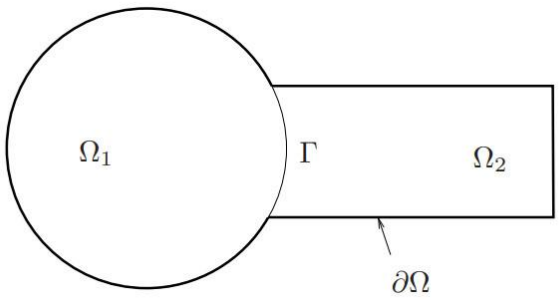

$$\boldsymbol{\lambda}_{n+1} = \theta \boldsymbol{\varphi}_2^{(n)} + (1-\theta)\boldsymbol{\lambda}_n, \text{on } \Gamma, \text{for } n \geq 1$$

θ	Min # Schwarz Iters	Max # Schwarz Iters	Total # Schwarz Iters
1.10	3	9	59,258
1.00	1	4	24,630
0.99	1	5	35,384
0.95	3	6	45,302
0.90	3	8	56,114

  - A **parameter sweep study** revealed $\theta = 0$ gave best performance (min # Schwarz iterations)

- All couplings were **implicit-implicit** with $\Delta t_1 = \Delta t_2 = \Delta T = 10^{-7}$ and $\Delta x_1 = \Delta x_2 = 10^{-3}$
  - Time-step and spatial resolution chosen to be small enough to resolve the propagating wave

- All reproductive cases run on the **same RHEL8 machine** and all predictive cases run on the **same RHEL7 machine**, in MATLAB

- Model **accuracy** evaluated w.r.t. analogous FOM-FOM coupling using **mean square error (MSE)**:

$$\varepsilon_{MSE}(\widetilde{\boldsymbol{u}}_i) := \frac{\sqrt{\sum_{n=1}^{S} ||\widetilde{\boldsymbol{u}}_i^n - \boldsymbol{u}_i^n||_2^2}}{\sqrt{\sum_{n=1}^{S} ||\boldsymbol{u}_i^n||_2^2}}$$

Overlapping Coupling, Nonlinear Henky MM, 2 Subdomains

- $\Omega = [0, 0.7] \cup [0.3, 1]$, implicit-implicit FOM-FOM coupling, dt = 1e-7, dx=1e-3.

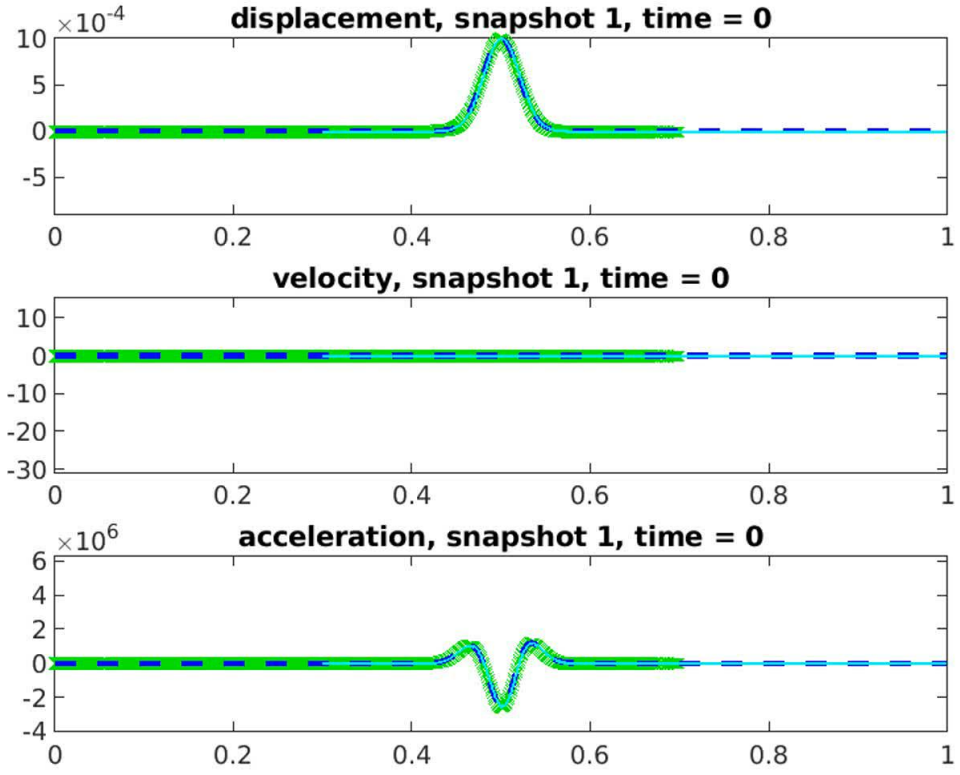

Multiplicative Schwarz

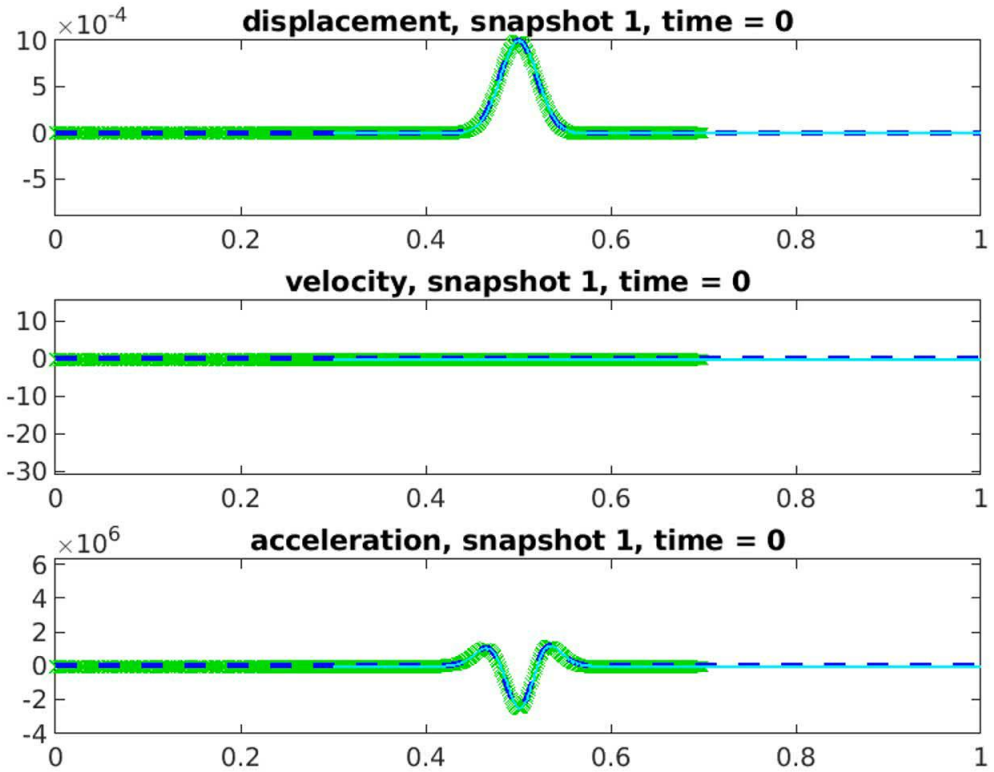

Additive Schwarz

Overlapping Coupling, Nonlinear Henky MM, 2 Subdomains

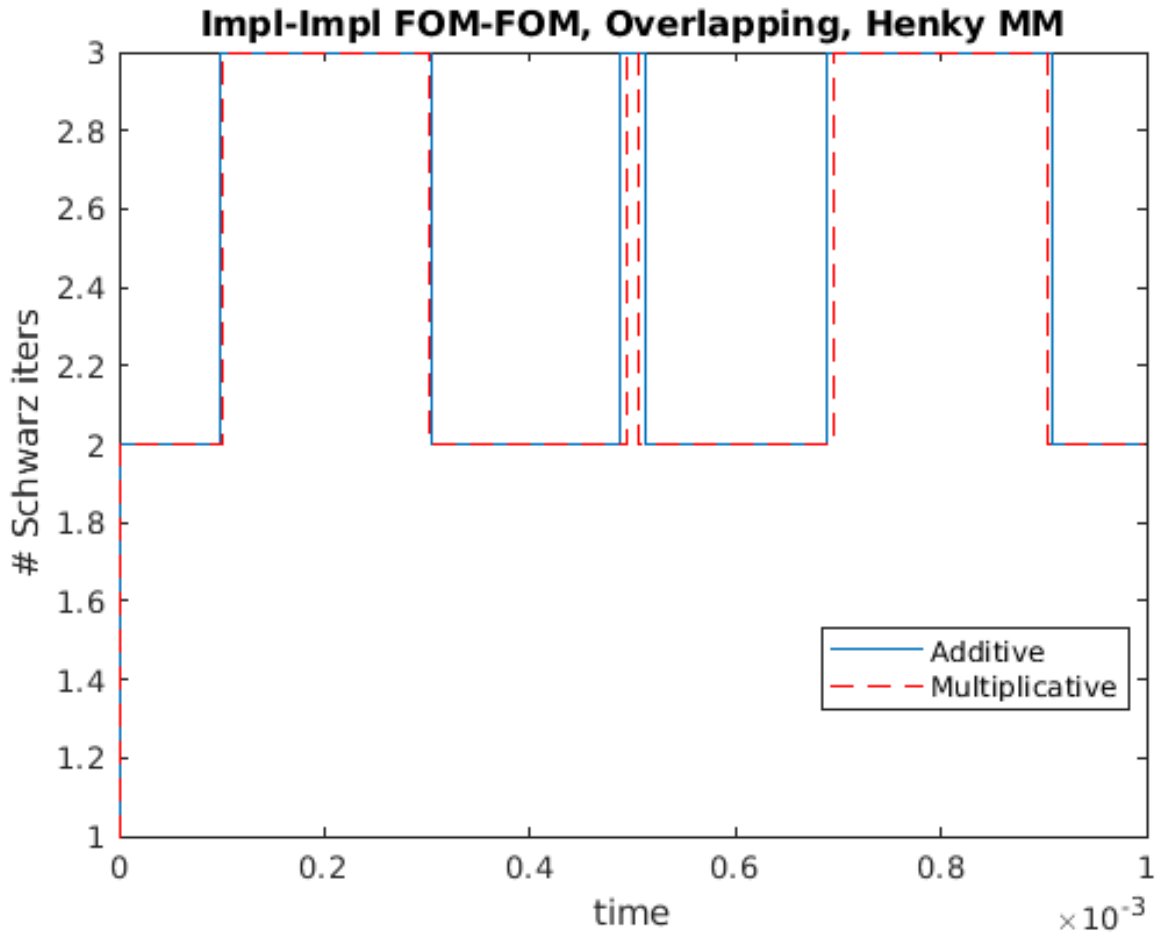

- $\Omega = [0, 0.7] \cup [0.3, 1]$, implicit-implicit FOM-FOM coupling, dt = 1e-7, dx=1e-3.
- Additive Schwarz requires slightly more Schwarz iterations but is actually faster.
- Solutions agree effectively to machine precision in mean square (MS) sense.

	Additive	Multiplicative
Total # Schwarz iters	24495	24211
CPU time	2.03e3s	2.16e3
MS difference in disp	6.34e-13/6.12e-13	
MS difference in velo	1.35e-11/1.86e-11	
MS difference in acce	5.92e-10/1.07e-9	

Overlapping Coupling, Nonlinear Henky MM, 3 Subdomains

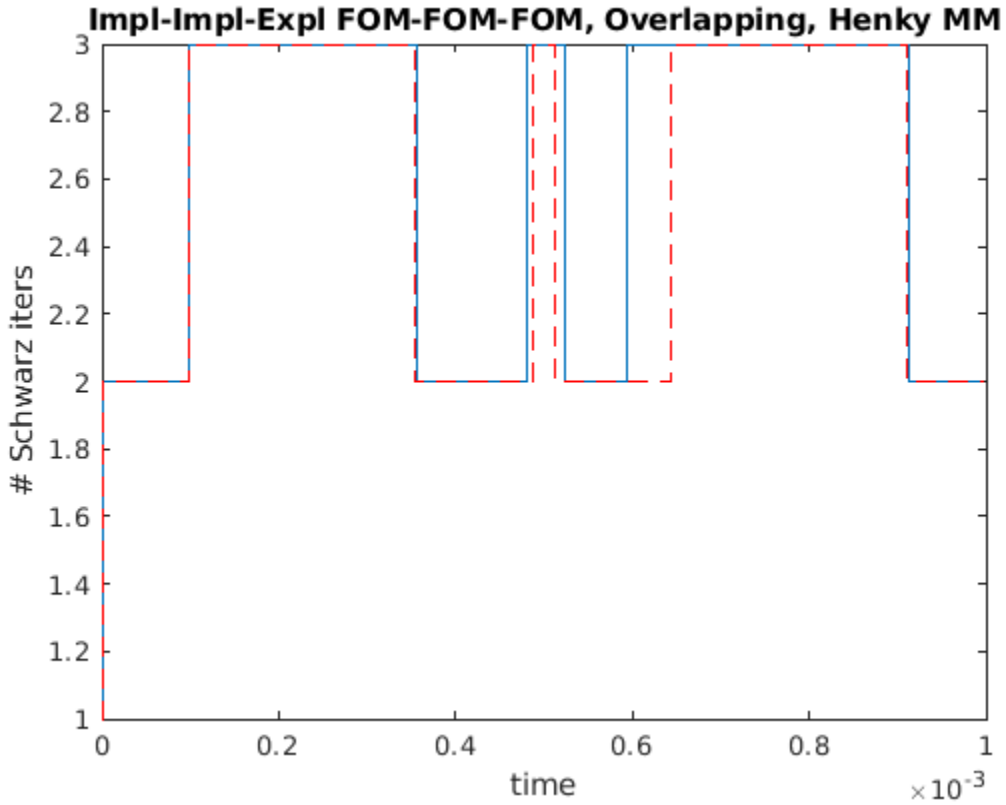

- $\Omega = [0, 0.3] \cup [0.25, 0.75] \cup [0.7, 1]$, implicit-implicit-explicit FOM-FOM-FOM coupling, dt = 1e-7, dx = 0.001.
- Solutions agree effectively to machine precision in mean square (MS) sense.
- Additive Schwarz has slightly more Schwarz iterations but is slightly faster than multiplicative.

	Additive	Multiplicative
Total # Schwarz iters	26231	25459
CPU time	1.89e3s	2.05e3s
MS difference in disp	5.3052e-13/9.3724e-13/6.1911e-13	
MS difference in velo	7.2166e-12/2.2937e-11/2.4975e-11	
MS difference in acce	2.8962e-10/1.1042e-09/1.6994e-09	

Non-overlapping Coupling, Nonlinear Henky MM, 2 Subdomains

- $\Omega = [0, 0.3] \cup [0.3, 1]$, implicit-implicit FOM-FOM coupling, dt = 1e-7, dx = 1e-3.

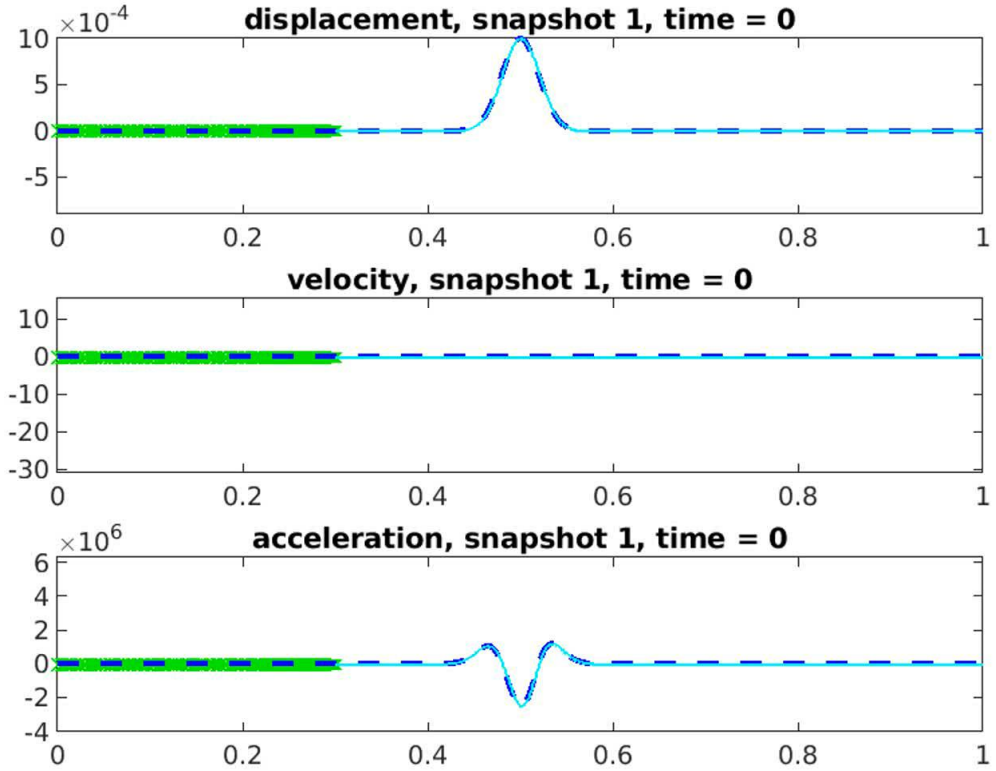

Multiplicative Schwarz

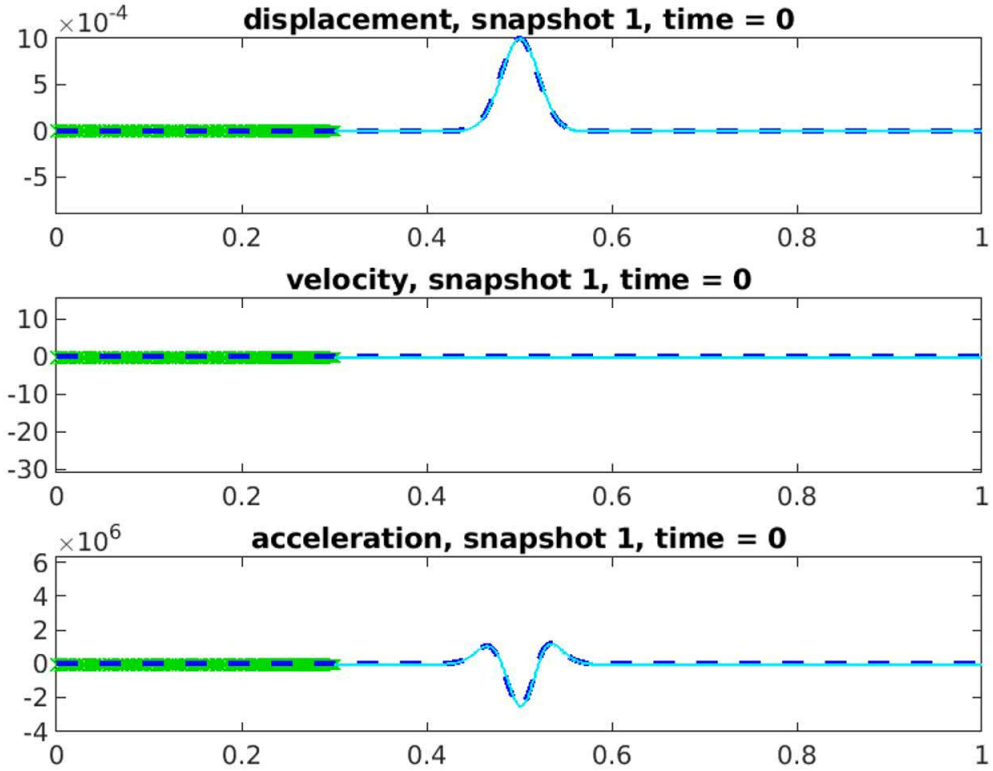

Additive Schwarz

Non-overlapping Coupling, Nonlinear Henky MM, 2 Subdomains

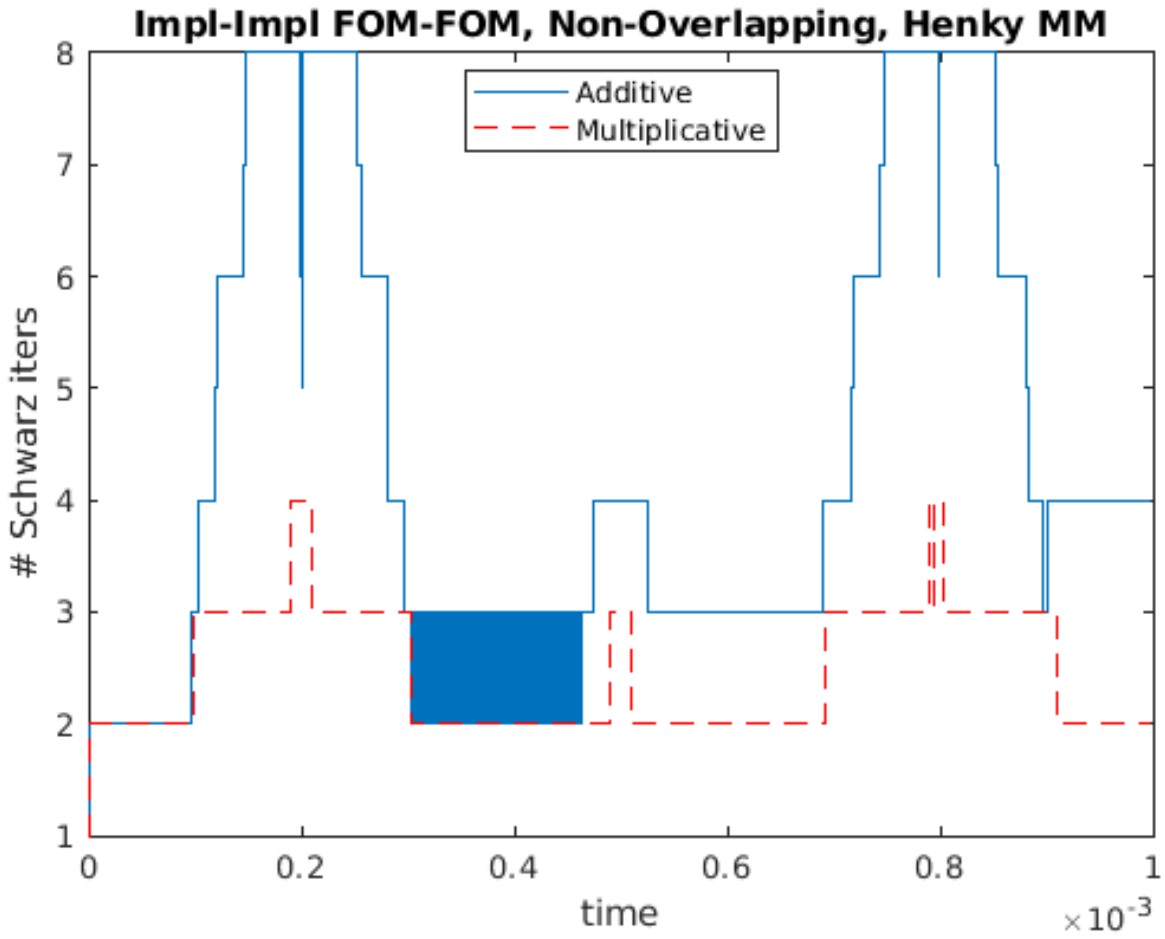

- $\Omega = [0, 0.3] \cup [0.3, 1]$, implicit-implicit FOM-FOM coupling, dt = 1e-7, dx = 1e-3.
- Additive Schwarz requires 1.81x Schwarz iterations (and 1.9x CPU time) to converge. CPU time could be reduced through added parallelism of additive Schwarz.
  - ➢ Note blue square for additive Schwarz…
- Additive and multiplicative solutions differ in mean square (MS) sense by O(1e-5).

	Additive	Multiplicative
Total # Schwarz iters	44895	24744
CPU time	1.87e3s	982.5s
MS difference in disp	4.26e-5/2.74e-5	
MS difference in velo	1.02e-5/5.91e-6	
MS difference in acce	5.84e-5/1.21e-5	

Non-overlapping Coupling, Nonlinear Henky MM, 3 Subdomains

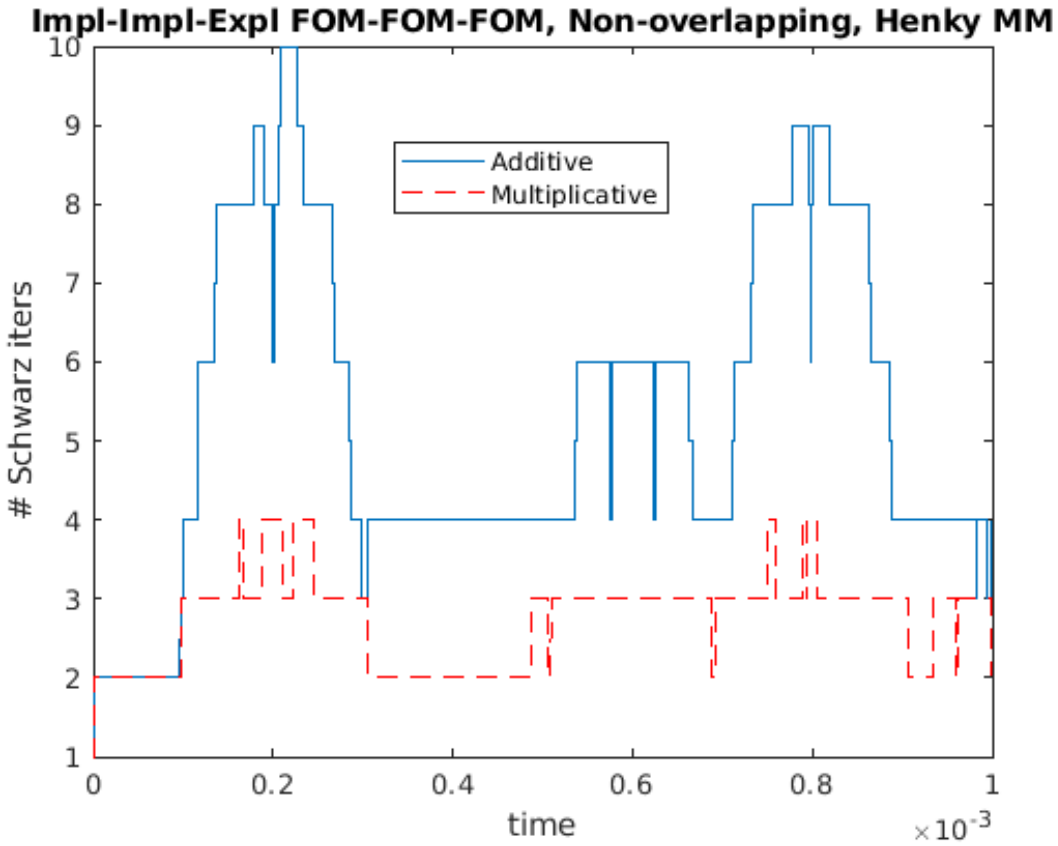

- $\Omega = [0, 0.3] \cup [0.3, 0.7] \cup [0.7, 1]$, implicit-implicit-explicit FOM-FOM-FOM coupling, dt = 1e-7, dx = 0.001.
- Additive Schwarz has about 1.94x number Schwarz iterations and is about 2.06x slower – similar to 2 subdomain variant of this problem. No "blue square".
  - ➢ Results suggest you could win with additive Schwarz if you parallelize and use enough domains.
- Additive/multiplicative solutions differ by O(1e-5), like for 2 subdomain variant of this problem.

	Additive	Multiplicative
Total # Schwarz iters	53413	27509
CPU time	5.91e3s	2.87e3s
MS difference in disp	2.8036e-05/3.1142e-05/ 8.8395e-06	
MS difference in velo	1.4077e-05/1.2104e-05/6.5771e-06	
MS difference in acce	8.7885e-05/3.2707e-05/1.3778e-05	